NUMERICAL MODELLING OF FIELD VANE SHEAR TEST IN SENSITIVE CLAY

by

© PRITAM KUNDU

A thesis submitted to the

School of Graduate Studies

in partial fulfillment of the requirements for the degree of

Master of Engineering (Civil)

Faculty of Engineering and Applied Science

Memorial University of Newfoundland

February 2022

St. John's Newfoundland and Labrador Canada

ABSTRACT

The undrained shear strength of clay is one of the key parameters in geotechnical design, which can be determined from laboratory or field tests. The disturbance of soil samples during sampling, transporting, storing and trimming could influence the laboratory test result, which could be significantly high for sensitive clay because the structure of the soil might be changed. Therefore, the field vane shear test (VST) is commonly used to determine the undrained shear strength of sensitive clay. Although the test is relatively simple, the interpretation of the VST results is challenging, as the failure mechanisms are still not well understood and cannot be observed in the field. Therefore, numerical simulation might be a viable option to examine such mechanisms. Some attempts have been made previously using Lagrangian-based finite element (FE) analysis but not could model the complete process, because large shear strains develop along the thin shear plane, which causes mesh distortion and numerical issues.

In the present study, VST is simulated using an Eulerian-based FE approach. In this approach, the Eulerian material (soil) flows through the fixed mesh; therefore, the simulation can be continued for a large penetration and rotation. A nonlinear strain-softening and strain-rate dependent soil model for the undrained shear strength of sensitive clays is incorporated in the FE simulation. The first set of simulations is performed for only one element of thickness (i.e., two-dimensional conditions) by applying rotation to a rigid vane. Three-dimensional simulations are then performed by penetrating the vane to the desired depth, followed by a rotation. The rotation initiates the formation of a rounded square-shaped failure block which turns into a circular one after the peak torque. The penetration of the vane can significantly disturb the surrounding sensitive clay and thereby reduce the maximum torque during rotation. The extent of disturbance depends on several factors, such as blade thickness, soil sensitivity, and post-peak strength degradation parameters.

ACKNOWLEDGEMENTS

First of all, I want to express my immense gratitude to Almighty God for good health throughout my research period and for giving me the opportunity to be part of Memorial University of Newfoundland.

I would like to express my utmost gratitude to my supervisor Dr. Bipul Hawlader, Professor, Memorial University of Newfoundland (MUN), Newfoundland, Canada, for his continuous guidance, valuable suggestions, motivation, and encouragement throughout the research work. I have been extremely lucky to have a supervisor like him. This thesis would not have been possible without his immense support and continuous guidance.

I would also like to express my sincere gratitude to Ripon Karmaker, Jin Chen, and Auchib Reza for their valuable advice, suggestions, and time that accelerated the progress of my research. I also gratefully acknowledge previous and current students working under Dr. Hawlader for being cooperative during different difficulties and for their continuous encouragement and knowledge sharing.

I would not have been able to have this opportunity to study at MUN without the recommendations given by Dr. G.M. Sadiqul Islam and Dr. Aftabur Rahman. I will be forever grateful to them for their support. Special thanks to Suborno Debnath, Tanmoy Sinha, and Shailen Saha for helping me with their experiences during the application and visa process. Thanks to Piash Saha and Sudipta Bhowmick for helping me with their printing resources. I am also thankful to my friends in St. John’s for their support, encouragement, and exuberant memories. Sincere gratitude to all the faculty and staff members in the Faculty of Engineering and Applied Science at MUN.

I would like to gratefully acknowledge the financial support provided by the School of Graduate Studies of MUN, Natural Sciences and Engineering Research Council of Canada (NSERC), Equinor, Petroleum Research Newfoundland and Labrador, and Mitacs for conducting this research.

Last but not least, I am greatly indebted to my parents, my younger brother, and all my family members for their endless love, constant encouragement, and spiritual support throughout this study. Without their support, I would not be able to complete my research.

This thesis is dedicated to them all.

Table of Contents

List of Figures

List of Tables

List of Symbols

B	borehole diameter
c	constant = $= (1 - s_{\mathrm{uR}}/s_{\mathrm{u0}})e^{-6}$
d_1	target location for vane rotation
D	vane diameter
D_{e}	effective vane diameter
e	vane blade thickness
E_{u}	undrained Young's modulus
f_1	strain-softening factor
f_2	strain-rate factor
H	vane height
H_{e}	effective vane height
i_{B}	angle of taper at the bottom of the vane
i_{T}	angle of taper at the top of the vane
n	coefficient depends on shape of shear stress distribution on the horizontal surface
N	normalized penetration resistance
PI	plasticity index
r	radial distance from the centerline on the horizontal surface
R	vane radius
S_{t}	sensitivity = $s_{\mathrm{u0}}/s_{\mathrm{uR}}$
s_{u}	mobilized undrained shear strength
s_{u0}	s_{u} before strain softening and at $\dot{\gamma}_{\mathrm{ref}}$
$s_{\mathrm{u,ref}}$	undrained shear strength at $\dot{\gamma}_{\mathrm{ref}}$

s_{uh}	maximum value of shear stress on the horizontal surface
s_{uld}	s_u at large displacements
$s_{u(r)}$	mobilized undrained shear stress at distance r
s_{uR}	s_u mobilized in shear band at considerable shear displacement
s_{uv}	maximum value of shear stress on the vertical surface
s_{uy}	undrained shear strength at a very low strain rate
t_{FE}	thickness of the finite element
t_z	thickness (one element thickness) of element for 2D condition
T	Torque
T_h	torque carried by the horizontal surface
T_{max}	maximum torque
T_v	torque carried by the cylindrical surface
v_x	velocity along x-axis
v_y	velocity along y-axis
v_z	velocity along z-axis
α	perimeter ratio
β	soil parameter for strain-rate effect in power-law model
γ	total unit weight of soil
γ^p	engineering plastic shear strain
$\dot{\gamma}$	strain rate
$\dot{\gamma}_{ref}$	reference shear strain rate
δ	plastic shear displacement
δ_{95}	δ at which s_u reduced by 95% of ($s_{u0} - s_{uR}$)
δ_{ld}	δ at large displacements

ε_q^p equivalent plastic shear strain

η soil parameter for strain-rate effect in additive power-law model

θ rotation angle

μ soil parameter for strain-rate effect in semi-logarithmic model

ν_u undrained Poisson's ratio

σ_e von Mises stress

σ_{y0} yield strength

Chapter 1: Introduction

1.1 General

The stress–strain behaviour of soil depends on dissipation of the excess pore water pressure during loading. Generally, analyses are performed for drained and undrained conditions, although partially drained conditions might govern many designs. The undrained shear strength is one of the important parameters in geotechnical engineering design for clays. Laboratory and field tests are performed to estimate the value of this parameter. In the laboratory, direct shear, triaxial, and direct simple shear tests are performed on reconstituted and undisturbed soil specimens. However, testing on reconstituted soil is not an option for sensitive clays because the soil structure will be destroyed. Also, to find the soil profile, the samples should be collected and tested from different depths, which is generally expensive. The collection of high-quality undisturbed soil samples from the field is always a concern, and it is challenging for sensitive clays because the soil sample becomes disturbed and might not maintain the exact clay structure in the field (Baligh et al. 1987). Sample disturbance might reduce the undrained shear strength significantly (La Rochelle et al. 1973). The impact and extent of the sample disturbance depend on several factors, such as sampling procedures, soil property (e.g., sensitivity and plasticity index), and sampling depth. The sample disturbance is caused not only during the sampling and transportation to the laboratory but also due to trimming during specimen preparation (Hvorslev 1949; La Rochelle and Lefebvre 1971; Karlsrud and Hernandez-Martinez 2013). La Rochelle and Lefebvre (1971) have shown that sampling causes a significant reduction of undrained shear strength, as shown in Fig. 1.1. The disturbance could be more for sensitive clays (Gylland et al. 2016).

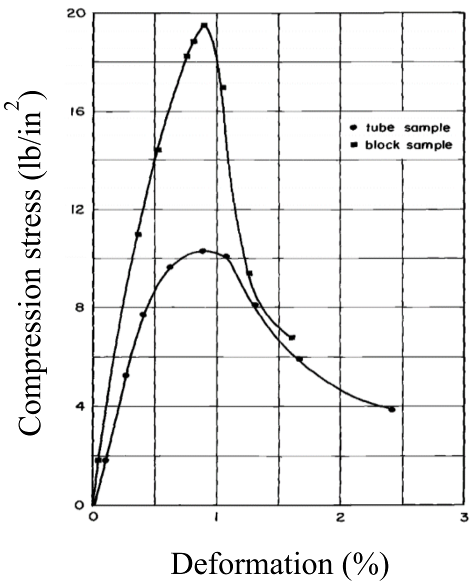

Figure 1.1: Stress-strain curves from unconfined compression tests on block and tube samples of sensitive Champlain clay (La Rochelle and Lefebvre 1971)

Many geotechnical problems involve large deformation (e.g., landslides and pile installation). However, such a large strain cannot be applied in typical laboratory tests. Typically, a maximum of approximately 20% shear strain could be applied in direct simple shear and triaxial tests in undrained conditions (Lunne et al. 2006). The shear strain could be several hundred percent along the failure planes in a landslide or in soil elements near the pile during installation. Significantly large post-peak shear strength degradation (strain softening) occurs under such large strains. The triaxial or direct simple shear tests cannot capture the whole range of post-peak failure behaviour. Ring shear tests could be performed to understand behaviour in the soil at larger strain levels. Stark and Contreras (1996) reported a ring shear test on sensitive Drammen clay, but the test was stopped at a displacement of less than 60 mm, which is small compared to that required to reach the completely remoulded state. Moreover, the ring shear test apparatus is not available in most geotechnical laboratories, and the specimen preparation is difficult, especially for sensitive clays.

A safe and economical geotechnical design depends on the proper estimation of soil parameters. The disturbance during sampling is a major factor, and the tests on disturbed soil cannot give the actual shear strength in the field. Therefore, field tests, such as the cone penetration test and field vane shear test (VST), are generally performed to determine the undrained shear strength of clay. The VST is widely accepted, and is one of the commonly used field tests to characterize sensitive clay soil. The test is very simple, but the interpretation of the results is not straightforward. Estimation of undrained shear strength from a vane shear test involves some uncertainties, which might come from different sources, such as progressive failure, strain rate, anisotropy, disturbance due to penetration, shear stresses' distribution on the failure surfaces, strain level, and failure geometry (Chandler 1988). The test gives only the torque (i.e., overall response); therefore, the effects of these factors cannot be identified easily without doing tests for varying conditions. Also, it is not possible to investigate the actual mechanisms involved in the test, which could be better explored from numerical simulations.

The vane shear test is performed below a pre-bored hole. The vane is first penetrated into the soil to approximately 5 times of the borehole diameter and then rotated at a constant angular velocity. The test causes large deformation of the soil around the vane and large shear strain development along the failure zones. Finite element (FE) modelling of such large deformation is very challenging. Also, the penetration disturbs the surrounding soil (i.e., shear strength reduction), depending upon sensitivity. Most of the FE simulations of vane shear tests have been conducted using Lagrangian-based FE modelling techniques, which cannot handle the large deformations due to mesh distortion issues (Donald et al. 1977; Matsui and Abe 1981; De Alencar et al. 1988; Griffiths and Lane 1990; Gylland et al. 2012; Kouretzis et al. 2017; Henneseid 2018). Some attempts have also been made to incorporate large deformations, such as the analyses using an

Arbitrary Lagrangian-Eulerian formulation by modelling the soil as a non-Newtonian fluid (Pérez-Foguet et al. 1999), and preliminary analyses using a Coupled Eulerian-Lagrangian (CEL) approach (Ansari et al. 2014; Gupta et al. 2016). However, many issues related to highly sensitive clays have not been investigated in these studies. Moreover, the effects of disturbance have not been simulated in the previous numerical studies. In the present study, a large deformation FE modelling technique is developed to examine the mechanisms involved in the test and quantify the effects of various factors on interpreted undrained shear strength of sensitive clay from vane shear test results.

1.2 Rationale

Laboratory tests for undrained shear strength of sensitive clay are difficult, and sample disturbance could significantly affect the results. However, the field vane shear test is one of the widely used in-situ tests to determine the undrained shear strength, especially for soft sensitive clays. The test is relatively simple and less expensive, but proper interpretation is needed. Understanding the soil failure mechanisms during the tests could explain the uncertainties involved in the interpretation. Finite element simulations with advanced numerical approaches, incorporating appropriate soil models, provide further insights into the mechanisms. The following are some of the challenging issues in numerical modelling: (i) modelling of large deformation without numerical issues due to mesh distortion; (ii) modelling of strain-softening behaviour, as it is one of the major properties of sensitive clay; and (iii) modelling of strain rate effect, as the undrained shear strength of clay increases with the rate of shearing. The Lagrangian-based FE methods may suffer mesh distortion and non-convergence when simulating large deformation problems (Griffiths 1999). Moreover, most of the FE programs do not have any built-in soil models that can be directly used to model sensitive clay behaviour. Therefore, some special techniques, such as the development of user subroutines, are necessary to incorporate the strain-softening and strain-rate dependent soil behaviour. In the present study, the vane shear tests are simulated, addressing these issues.

1.3 Objectives

This study aims to understand the mechanisms involved in the vane shear test in soft-sensitive clays. A numerical modelling technique is developed using the CEL approach available in Abaqus FE software, where the soil is modelled as an Eulerian material, which allows simulating large deformations during penetration and rotation of the vane. The followings are the main objectives of this research:

- Develop two and three-dimensional large deformation FE models for field vane shear test.
- Implement a soil model considering the post-peak degradation of undrained shear strength of sensitive clay.
- Identify the effects of strain softening and strain rate on field vane shear strength.
- Identify the failure geometry, progressive formation of failure planes, and mobilized shear stresses and strains; and
- Investigate the effects of disturbance due to penetration of the vane.

1.4 Outline of the thesis

The thesis consists of five chapters. The outline is as follows:

Chapter 1 highlights the background, rationale of the current study, and objectives of the research work.

Chapter 2 contains a comprehensive literature review. The literature review covers the studies mainly related to the behaviour of sensitive clay and factors affecting the field vane shear test. The findings from field, laboratory, and numerical simulations are discussed. Moreover, the limitations of previous studies are summarized in this chapter.

Chapter 3 presents two-dimensional FE modelling of the field vane shear test in sensitive clay. The failure geometry, progressive formation of failure planes, and mobilized shear stresses are investigated in this chapter. A part of the work presented in chapter 3 has been published as: Kundu, P., Hawlader, B. and Karmaker, R. 2021. “Two-dimensional finite element modelling of field vane shear test in sensitive clay.” *74th Canadian Geotechnical Conference*, Niagara, ON, Canada, paper no-516.

Chapter 4 presents the effects of disturbance due to penetration of the vane on the undrained shear strength of sensitive clay. The penetration of a rigid vane and the subsequent rotation are simulated. Some simulations are performed only for rotation to quantify the effects of penetration. A parametric study is performed to show the effects of several factors that affect soil disturbance due to penetration.

Chapter 5 summarizes the outcomes of the research. The limitations of the present study and recommendations for future research are also discussed in this chapter.

Chapter 2: Literature Review

2.1 Introduction

The field vane shear test (VST) is one of the widely used methods of determining the in-situ undrained shear strength of soft clay because of its simplicity and the difficulties involved in collecting undisturbed soil samples from the field for laboratory tests. It was first developed in 1919 in Sweden and has been used extensively worldwide since the 1940s (Chandler 1988). The peak and residual undrained shear strength and sensitivity of soft clay can be determined from the vane shear test results. A vane shear test is also preferable, as the test is relatively simple and a shear strength profile with depth can be developed in a cost-effective way. However, the interpretation of the results is difficult, as the result might be affected by several factors, such as the strain rate effect, anisotropy, mobilized stress distribution, and disturbance due to penetration. Several studies were dedicated to investigate the effects of these factors, which include experimental works and numerical analyses. This chapter provides a brief overview of the behaviour of sensitive clay, factors affecting the test results, and numerical modelling of the vane shear test.

2.2 Behaviour of sensitive clay

Many researchers studied the behaviour of sensitive clays in onshore and offshore environments (Tavenas et al. 1983; Thakur 2007). For example, an intensive geological and geotechnical investigation was carried out in the Norwegian Sea during the Ormen Lange gas field development, where different types of sediments of varying sensitivities were found. The sediments in this area have been classified into two groups: relatively strong insensitive or slightly sensitive glacial clays and weak marine and/or glaciomarine sensitive clays (Kvalstad et al. 2005). Soft sensitive clay is a term generally used to represent marine clay deposits. Marine clays have a higher clay content, plasticity index, liquidity index, and higher water content than glacial clays. The marine clays are very sensitive as compared to the glacial clay (Kvalstad et al. 2005; Lunne and Andersen 2007) and show higher strain-softening behaviour during undrained loading than glacial clays (Fig. 2.1). Marine clays are generally normally consolidated to lightly overconsolidated, and the behaviour is very similar to onshore sensitive clay (Locat et al. 2015; Kvalstad et al. 2005). Offshore marine/glaciomarine clays are generally less sensitive (DeGroot et al. 2007). For marine clay, rapid post-peak degradation of shear strength first occurs because of a rapid increase in pore water pressure immediately after the peak, due to structural breakdown. At large strains, the strength reduction occurs relatively slowly. However, for glacial clays, the post-peak degradation of shear strength could occur for limited strain-softening behaviour at a large strain (Kvalstad et al. 2005).

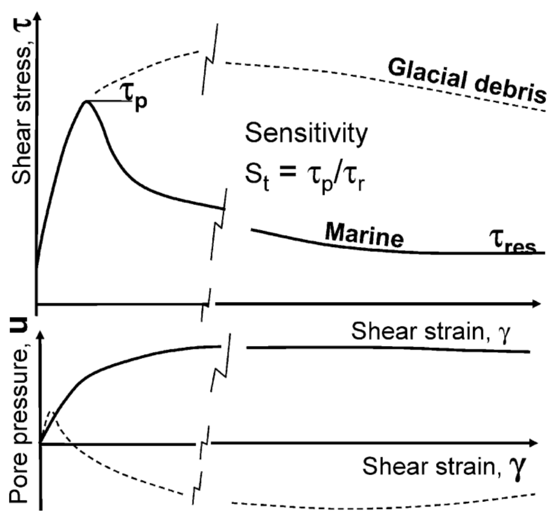

Figure 2.1: Typical stress-strain development for marine clay and glacial debris (Kvalstad et al. 2005)

2.2.1 Strain-softening behaviour of sensitive clays

Sensitive clays in eastern Canada and quick clays in Scandinavia exhibit strain-softening behaviour under undrained loading conditions, indicating that these types of soil tend to lose strength quickly when subjected to excessive shear loading, which is the main cause of progressive failure (e.g., large-scale landslides). The strain-softening behaviour of sensitive clay can be viewed as the collapse after reaching the peak resistance. Therefore, in sensitive clays, many small to large-scale landslides occur rapidly under undrained conditions. In addition to other tests, the vane shear tests are widely used to evaluate the stability of the landslide. Note that elasto-plastic soil models cannot simulate this behaviour, as strain-softening is not considered.

Thakur et al. (2014) showed that shear-induced pore pressure causes post-peak shear strength reduction in soft sensitive clay instead of the reduction of the strength parameters (c' and ϕ'). Figure 2.2 schematically shows the response of sensitive clay under undrained loading. Thakur et al. (2014) identified two stages in the strain-softening process. At the first stage, a rapid increase in excess pore water pressure occurs due to structural breakdown within a shear strain level of 10–20%. In the second stage, the residual state is reached at a large strain level.

Tavenas et al. (1983) conducted tests on a typical Eastern Canadian sensitive soil sample and showed that normalized shear strength, which can be defined by the remolding index (I_r), decreases with an increase in strain energy (w_N). Quinn et al. (2011) found that post-peak degradation of undrained shear strength from small to large strain levels might not be linear in all cases. Based on some realistic assumptions, Quinn et al. (2011) plotted the results with respect to relative displacement (δ), as shown in Fig. 2.3. They proposed that shear displacement can better represent the post-peak softening behaviour than shear strain, because shear strain is mainly concentrated in the shear band.

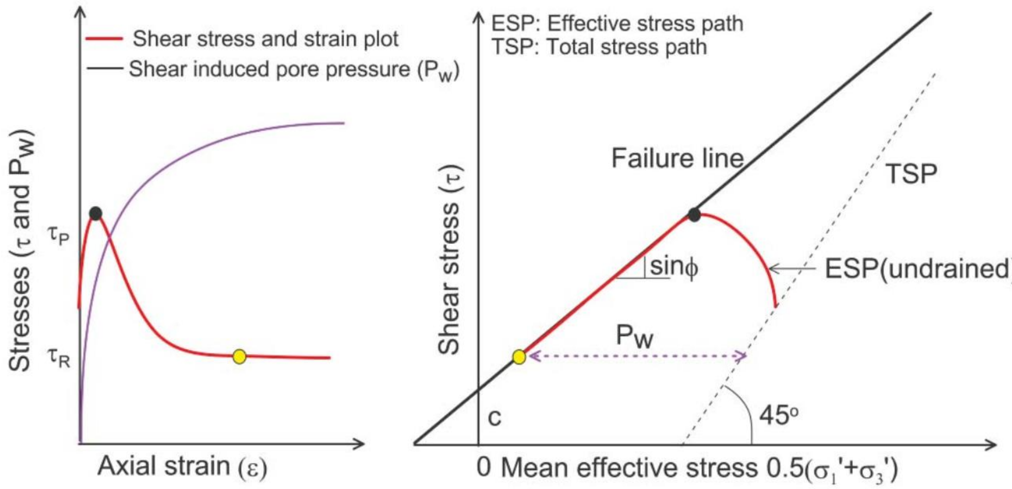

Figure 2.2: Undrained behaviour of soft sensitive clays within laboratory strain level (Thakur et al. 2014)

Tavenas et al. (1983) conducted four types of special tests, namely, impact on a rigid surface, impact from falling objects, extrusion through a narrowing tube, and shear reversals in a large shear box, and showed that the remoulding index decreases with strain energy (Fig. 2.3(a)). Quinn et al. (2011) reanalyzed these data and plotted shear strength degradation (s_u/s_{u0}, where s_{u0} and s_u are the peak and mobilized undrained shear strength) as a function of shear displacement (δ) (Fig. 2.3(b)).

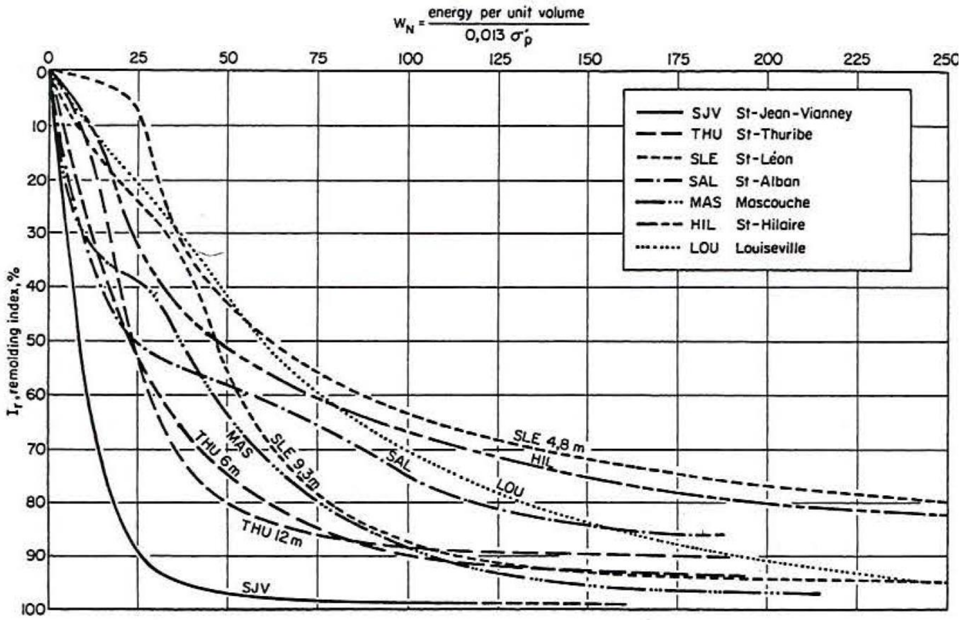

(a)

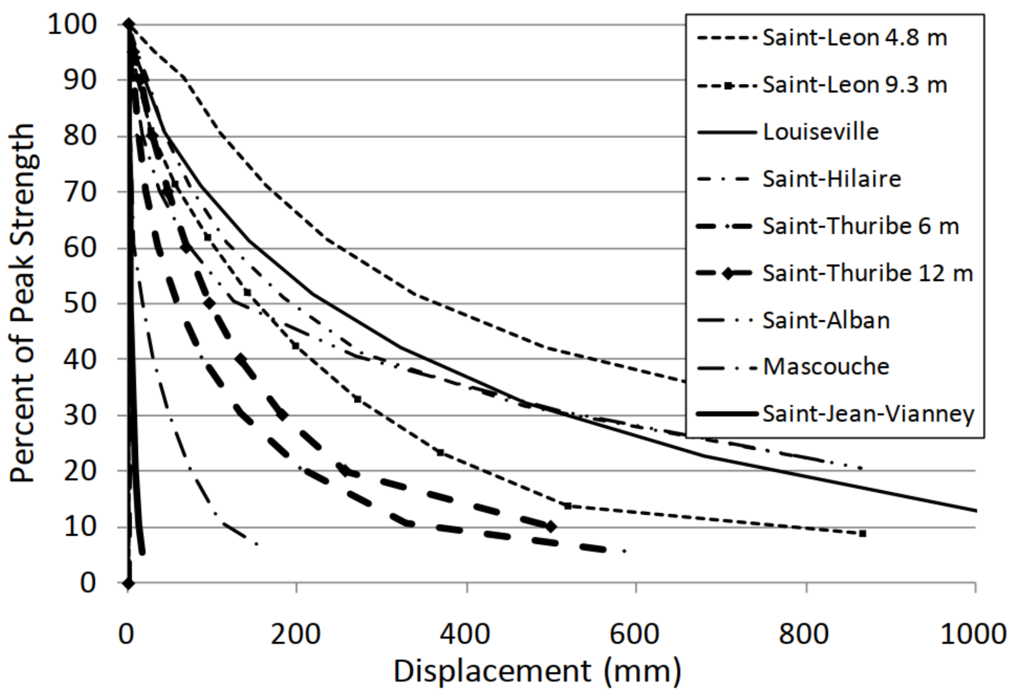

(b)

Figure 2.3: Undrained shear strength degradation in sensitive clays: (a) variation of remoulding index with strain energy (Tavenas et al. 1983); (b) shear strength reduction with plastic strain (Quinn et al. 2011)

The following are the key features of this s_u/s_{u0} vs δ plot (Fig 2.3(b)): (i) s_u decreases rapidly at the beginning and at a slower rate at large strains in a nonlinear form; (ii) the rate of reduction of s_u for all clays is not the same but depends upon soil type (e.g., sensitivity). Dey et al. (2015) proposed a relationship between mobilized s_u and δ, as shown in Fig. 2.4, where an exponential relationship, originally by Einav and Randolph (2005) for mobilized s_u and plastic shear strain, is used for the initial rapid reduction of s_u. At large strains, s_u reduces slowly, which has been modelled using a linear degradation of s_u.

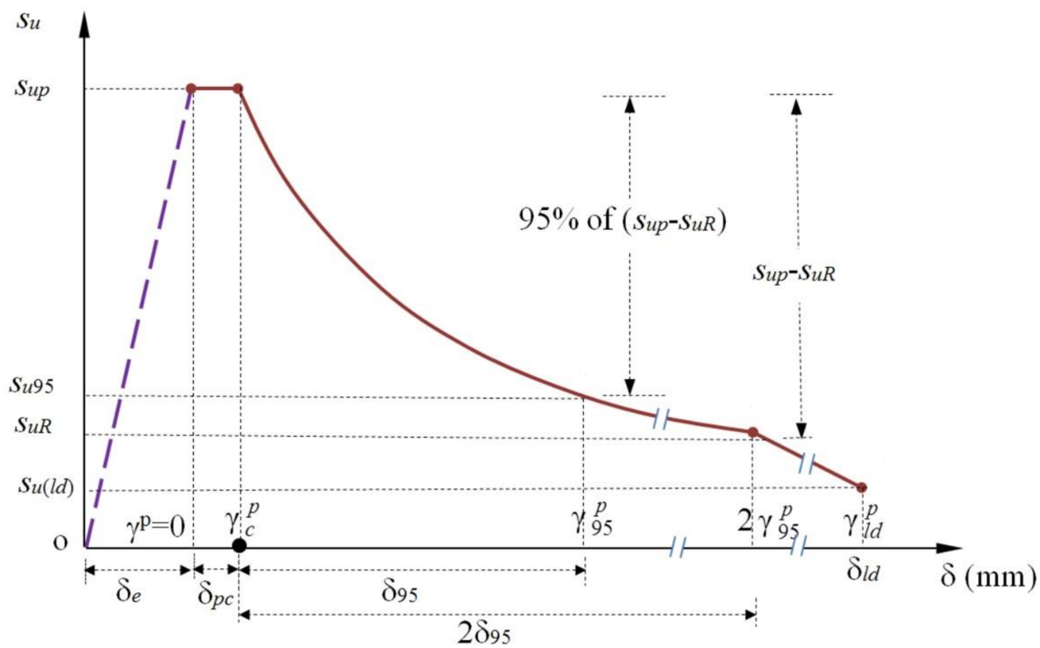

Figure 2.4: Post-peak shear strength degradation model (Dey et al. 2015)

2.2.2 Strain-rate effects of sensitive clays

In general, the undrained shear strength of clay increases with the shear strain rate (Crawford 1959, 1963, 1965; Conlon 1966). Sensitive clays also show strain-rate dependent behaviour. For example, a series of triaxial tests on Norwegian sensitive clays shows a significant increase in peak resistance with the loading rate (Fig. 2.5). Similarly, the post-peak strength degradation and excess pore water pressure generation are also dependent on the shearing rate.

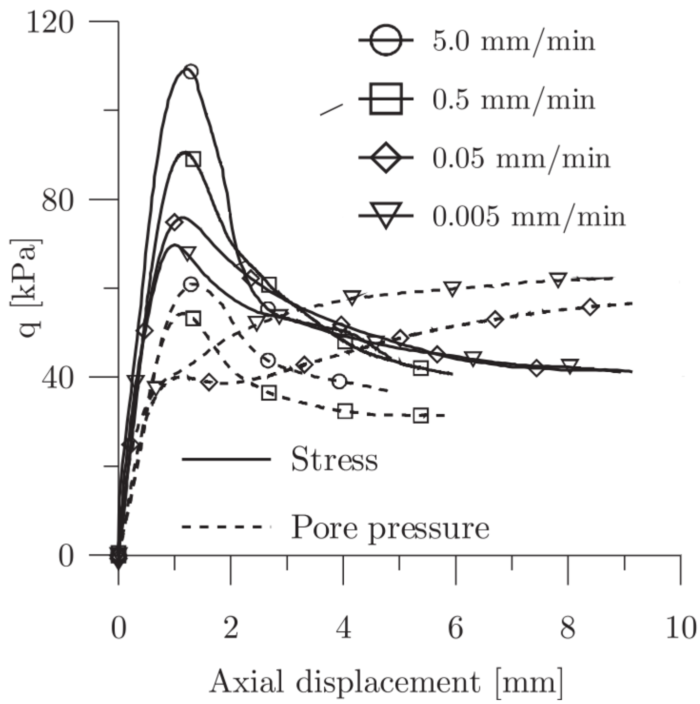

Figure 2.5: Strain rate effect from triaxial test (Gylland 2012)

Similarly, in vane shear tests, the undrained shear strength increases with the rotation rate, as reported by Cadling and Odenstad (1950) for Swedish clays for rotation rates of 6 to 60 deg/min, and by Wiesel (1973) for Swedish plastic clays for rotation rates of 0.0002 to 200 deg/min.

Soil remoulding can also play a role in loading rate effects on shear strength. When sensitive clays are in remolded condition, they behave like fluids with a very low undrained shear strength. It is well known that the strain rate effect of non-Newtonian fluid is different from that of typical clays.

Therefore, using a rate-dependent undrained shear strength model is preferable to capture the soil behaviour from the intact state to highly remoulded fluidized material.

For soil, the relation between s_u and $\dot{\gamma}$ is normally modelled using semi-logarithmic, power-law, and hyperbolic-sine functions as:

$$s_u = \left[1 + \mu \log\left(\frac{\dot{\gamma}}{\dot{\gamma}_{ref}}\right)\right] s_{u,ref} \tag{2.2}$$

$$s_u = \left(\frac{\dot{\gamma}}{\dot{\gamma}_{ref}}\right)^{\beta} s_{u,ref} \tag{2.3}$$

$$s_u = \left[1 + \frac{\mu}{\ln(10)} \sin^{-1}\left(\frac{\dot{\gamma}}{\dot{\gamma}_{ref}}\right)\right] s_{u,ref} \tag{2.4}$$

where $s_{u,ref}$ is the undrained shear strength at the reference strain rate ($\dot{\gamma}_{ref}$) (Graham et al. 1983); μ (= 0.05–0.2) is the rate of strength increase per decade and β (= 0.05–0.1) is the model parameter of the power-law model (Zhu and Randolph 2011).

Zhu and Randolph (2011) proposed an "additive power-law model" that combines the Herschel–Bulkley model (fluid-mechanics approach) with the power-law model (geotechnical approach) to capture the response from intact to fluidized remoulded soil. Their proposed model includes both the characteristics of soil and fluid as follows:

$$f_2 = 1 + \eta \left(\frac{\dot{\gamma}}{\dot{\gamma}_{ref}}\right)^{\beta} \tag{2.5}$$

where η is a viscous property, and β is the shear-thinning index.

Further discussion of strain softening and strain rate effects is provided in the following chapters.

2.3 Vane shear test device and procedure

A vane shear test device consists of four flat metal blades or plates, fixed at a 90° angle to each other, and a rod connecting the blades. The height (*H*) to diameter (*D*) ratio is usually two, and the typical thickness of the blade is 2 mm. The area ratio, defined as the ratio of the cross-section area of the vane to the circular area of the rotating vane expressed as a percent, should be less than 10%, according to ASTM D2573 (2018). The device is pushed into the soil at the desired depth, and then a constant rotation rate of 6 or 12 deg/min is applied by rotating the rod. The penetration depth beyond the end of the borehole is usually 4*B* to 5*B* (where *B* is the diameter of the borehole). It is important to avoid any rotation while penetrating the vane into the soil. During rotation, torque is measured, and from the measured torque, undrained shear strength is calculated based on some simplified equations. Then the vane is rotated 5 to 25 revolutions rapidly, based on the soil properties, to measure the remoulded undrained shear strength. Figure 2.6 shows the dimensions of the commonly used vane.

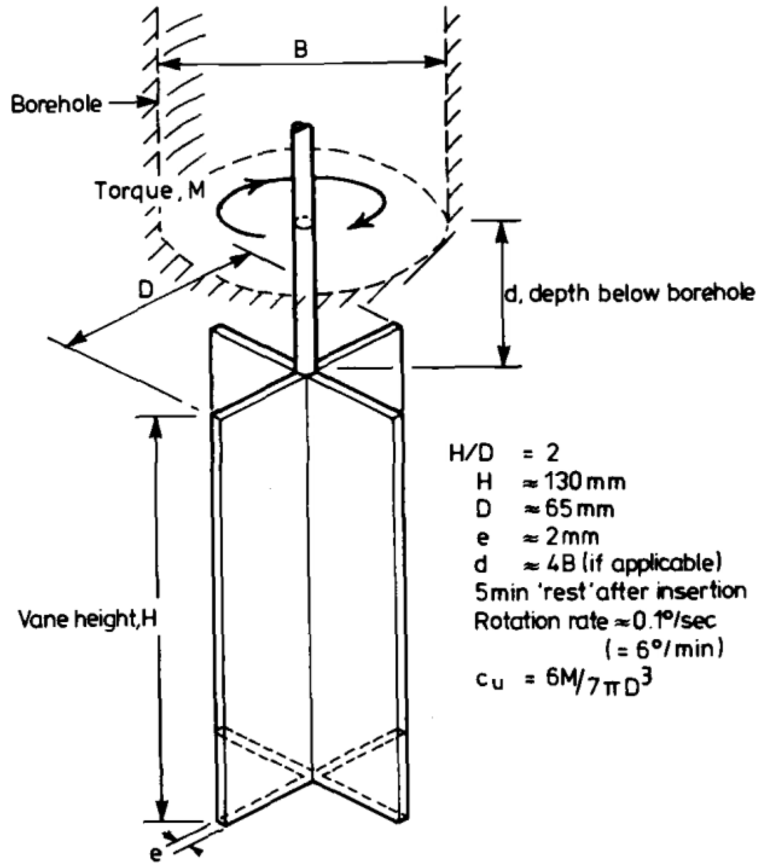

Figure 2.6: Vane shear tests and typical dimensions (Chandler 1988)

2.4 Factors affecting field vane shear test

To obtain the shear strength from the measured torque, a simple formula is used that correlates the torque at failure and shear strength. This formula is based on several assumptions. Several factors influence the measured undrained shear strength: (a) disturbance due to vane insertion; (b) rate of rotation of the vane; (c) progressive formation of the failure block (d) anisotropy of the soil; (e) non-uniform stress distribution; (f) the time interval between vane insertion and rotation; and (g) thickness of the blade.

Some assumptions are made to develop the relationship between torque and undrained shear strength, as shown in Table 2.1 (Chandler 1988; Chini et al. 2015).

When determining the shear strength from the shear vane test, a simple formula is used that correlates the torque at failure and shear strength. This formula is based on several assumptions. For those assumptions, the interpretation of the undrained shear strength is more complicated than the simplified and idealized formula. There are a number of factors that influence the measured undrained shear strength, as follow: (a) disturbance due to vane insertion; (b) rate of vane rotation; (c) progressive failure; (d) anisotropy of soil; (e) non-uniform stress distribution; (f) the time interval between vane insertion and rotation; and (g) influence of blade thickness.

There are some general assumptions that are made to convert the torque into undrained shear strength (Chandler 1988; Chini et al. 2015) which are given in Table 2.1:

Table 2.1: General assumptions in vane shear test

Assumptions	Remarks
Vane insertion causes negligible disturbance	In reality, vane insertion might cause significant soil disturbance and decrease in s_u (La Rochelle et al. 1973; Kimura and Saitoh 1983)
Cylindrical failure surface	A rounded square-shaped failure surface forms initially, which changes to a cylindrical one at larger rotations (Gylland et al. 2012, 2013)
Stress distribution along the failure surface is uniform	On the horizontal surfaces, mobilized shear stress distribution is not uniform (Menzies and Merrifield 1980; Donald et al. 1977)
Diameter of the failed block is the same as the vane diameter	Some studies found a larger shear surface diameter than the vane diameter (Skempton 1948; Roy and Leblanc 1988; Pérez-Foguet et al. 1999)
Soil is isotropic and homogeneous	Clay behaves anisotropically, especially the soft sensitive clay (Donald et al. 1977)
No progressive failure	Failure surface forms progressively with rotation of the vane (Donald et al. 1977; De Alencar et al. 1988; Griffiths and Lane 1990)
Minimal consolidation occurs before or during the application of vane rotation	High pore pressure is generated during vane insertion, and the pore pressure change is smaller during vane rotation (Kimura and Saitoh 1983)

Further details of these assumptions will be discussed in the following sections.

2.4.1 Influence of vane insertion

The disturbance caused by vane insertion has been discussed by several researchers (Cadling and Odenstad 1950; Flaate 1966; La Rochelle et al. 1973; Kimura and Saitoh 1983). Vane insertion leads to disturbance of soil structure and displacement of the soil particles. Cadling and Odenstad (1950) suggested that the disturbance could be assessed by

$$\alpha = 4e/\pi D \tag{2.6}$$

where α is the perimeter ratio, e is blade thickness, and D is vane diameter. Figure 2.8 shows a schematic diagram of the disturbance caused by the vane.

Figure 2.7 is the diagrammatic representation of the disturbance effect caused by vane insertion. As an alternative to the area ratio, the perimeter ratio can also express the disturbance effect.

According to a study by La Rochelle et al. (1973), the insertion of the vane in highly sensitive marine clays could result in significant strength reductions; therefore, vane blades should be kept as thin as possible to minimize soil disturbance. They carried out four tests with the same height and diameter (H = 95 mm and D = 47.5 mm) but different blade thicknesses ranging from 1.6 to 4.7 mm at Saint-Louis site. Figure 2.8 shows that the undrained strength decreases significantly with the perimeter ratio, because an increase in blade thickness results in an increase of the horizontal cross-sectional area and causes more disturbance of the soil mass.

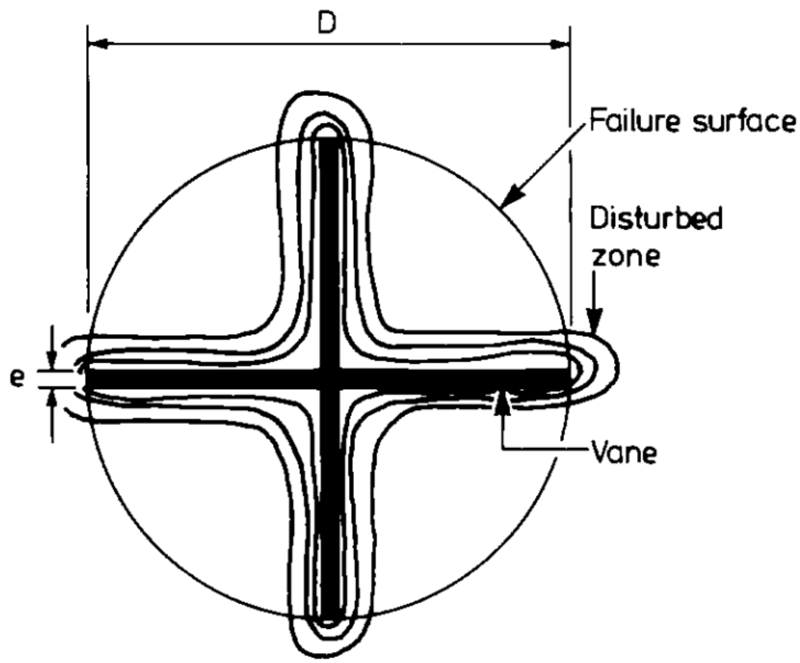

Figure 2.7: Disturbance caused by the vane insertion (Cadling and Odenstad 1950, La Rochelle et al. 1973 and Chandler 1988)

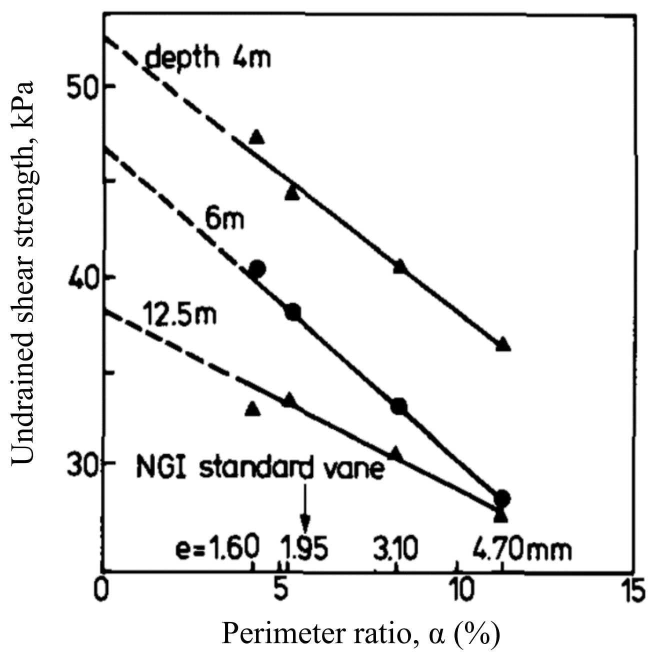

Figure 2.8: Effect of vane blade thickness on measured undrained shear strength (La Rochelle et al. 1973)

La Rochelle et al. (1973) found an average increase in shear strength of 15% in Saint-Louis and 11% in Saint-Vallier clays if extrapolated to zero blade thickness vane from the result with a blade thickness of 1.95 mm. The higher disturbance effect found for Saint-Louis may be due to the higher sensitivity of the clay. Flaate (1966) reported that the clay in one layer might stick to the vane and thus increase the area ratio of the vane for tests at other depths, which can also cause some unknown degree of disturbance.

Roy and Leblanc (1988) carried out field and laboratory tests with different thicknesses of blades. They also found a linear relationship between blade thickness and disturbance. A certain amount of clay disturbance was caused by the vane insertion, and the measured shear strength varied depending on the clay properties and thickness of the blade.

Kimura and Saitoh (1983) conducted laboratory tests to evaluate the disturbance effect due to the insertion of the vane. They pushed the vane into the soil and measured the torque at different consolidation times (maximum 240 min). To measure the extent the disturbance due to vane insertion, they also conducted the test where torque was measured free from disturbance due to vane insertion (the vane was inserted into the soil after applying the preconsolidation pressure, and then final consolidation was carried out keeping the vane in the soil). A significant disturbance in the soil caused by vane insertion, resulting in a reduction in shear strength, is found from the tests, as shown in Fig. 2.9, where the ratio of shear strength to the vertical consolidation pressure (c_u/p) with plasticity index (I_p) is plotted.

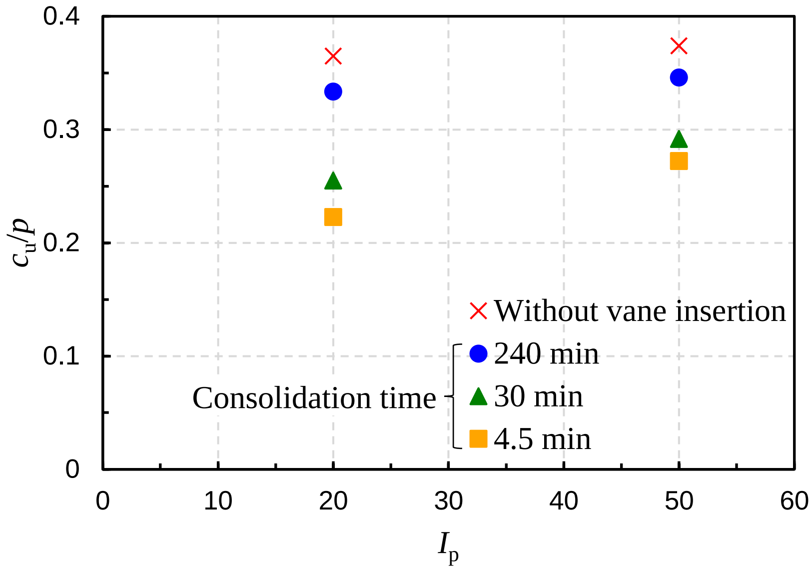

Figure 2.9: Penetration and consolidation effects on shear strength for two soils of varying plasticity index (after Kimura and Saitoh 1983)

2.4.2 Consolidation time

The time interval between the end of penetration and the start of rotation should not be more than five minutes (Chandler 1988; ASTM D2573 2018). Torstensson (1977) found no significant increment in strength when the waiting time was less than 10 min, while a 20% increase in strength was obtained in the case of more than 24 hours of waiting time. The waiting period has a very significant effect on shear strength, which also depends on the type of soil (Fig. 2.10).

Kimura and Saitoh (1983) performed laboratory tests on two soils having the plasticity index (I_p) of 50 and 20. They found that the ratio of shear strength to the vertical consolidation pressure (c_u/p) for an elapsed time of 240 min increased about 20% and 45% for soils with I_p of 50 and 20, respectively, compared to the ratio for the elapsed time of 4.5 min.

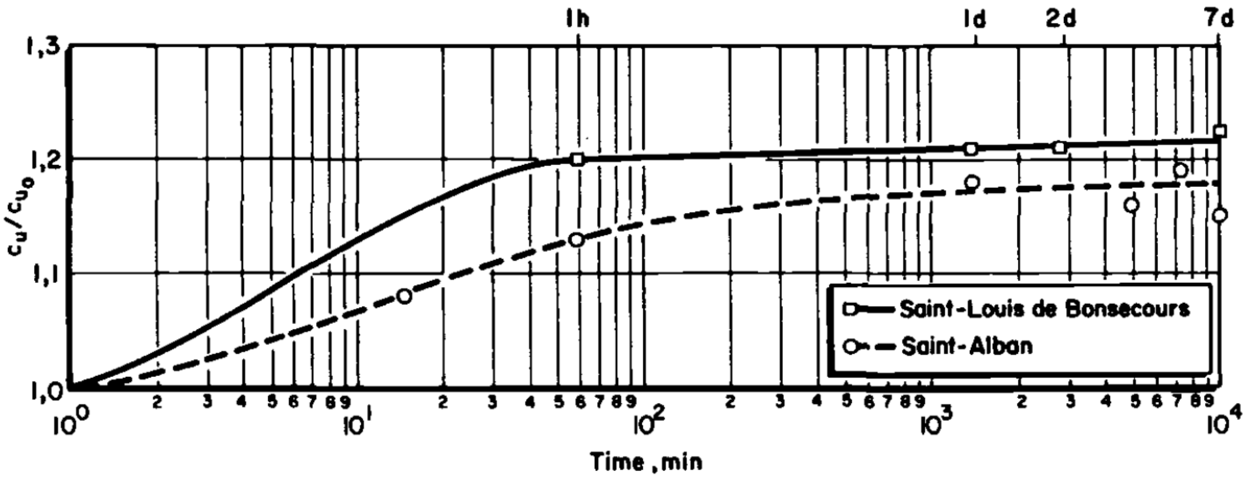

Figure 2.10: Consolidation effect on the undrained shear strength (Roy and Leblanc 1988)

2.4.3 Stress distribution

In the field test, rectangular vanes are the most commonly used vane. In the traditional method of interpretation, it is assumed that the shear stress distribution on both the cylindrical (vertical) and top and bottom (horizontal) surfaces is rectangular (i.e., uniform). This assumption has been reexamined by a number of researchers (Donald et al. 1977; Menzies and Merrifield 1980; Wroth 1984; Griffiths and Lane 1990).

Donald et al. (1977) have performed a three-dimensional FE analysis using a linear elastic constitutive model and found an almost parabolic-shaped stress distribution on the horizontal surfaces. On the vertical surface, significantly higher shear stresses were found at the ends than at the centre of the vane. The findings of Donald et al. have been verified by Menzies and Merrifield (1980). They carried out a number of experiments with a 120 mm diameter and 240 mm height rectangular vane in dense, dry, fine Leighton Buzzard sand in the laboratory and in over-consolidated, saturated, brown London clay in the field. They plotted equivalent shear stress distributions along the horizontal and vertical surfaces of the vane, as shown in Fig. 2.11.

From these investigations, it appears that the uniform stress distribution on the cylindrical vertical surface is reasonable, but the stress distributions on the horizontal surfaces are very different from the commonly assumed uniform distribution. For strain-softening material, the decrease in strength after the peak will result in non-uniform strength distribution around the vane. Therefore, the determination of the undrained shear strength becomes difficult (De Alencar et al. 1988).

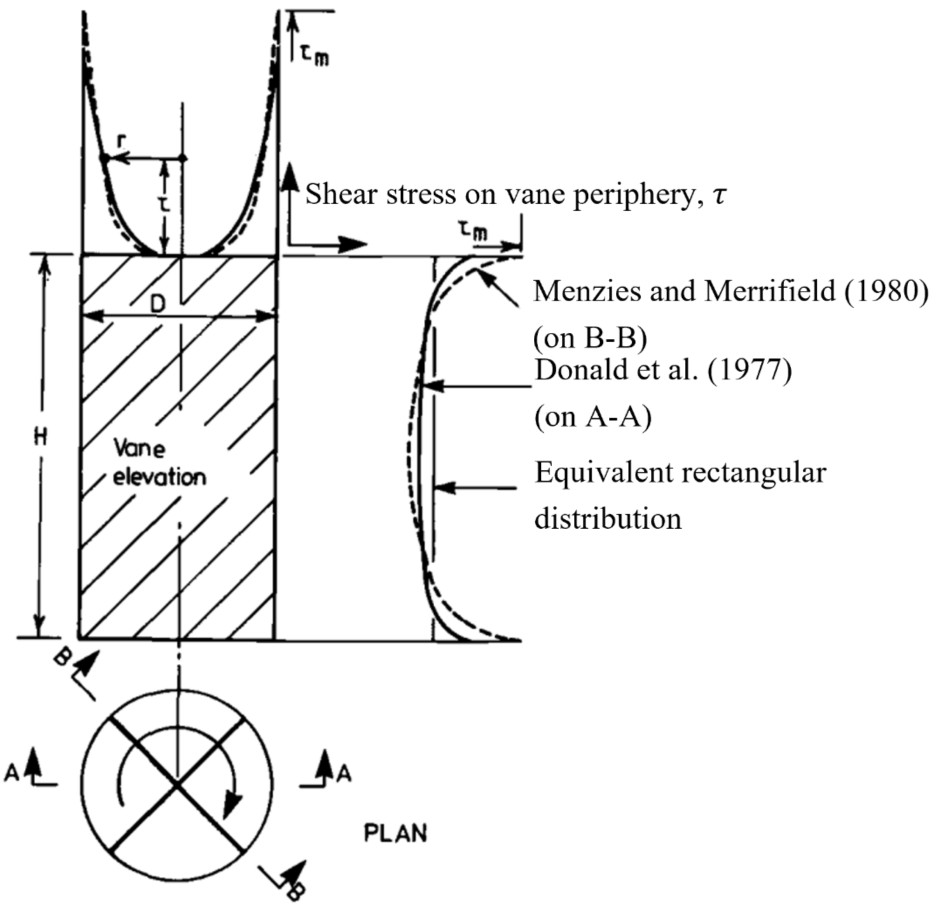

Figure 2.11: Shear stress distribution on the vertical and horizontal surfaces (Chandler 1988)

Wroth (1984) developed an expression assuming the following shear stress distribution on the horizontal surface:

$$\frac{s_{\mathrm{u(r)}}}{s_{\mathrm{uh}}} = \left[\frac{r}{D/2}\right]^n \tag{2.7}$$

where *r* is the radial distance from the centerline on the horizontal surface, *D* is the diameter of the cylindrical failure surface, $s_{\mathrm{u(r)}}$ is the mobilized undrained shear stress at distance *r*, s_{uh} is the maximum value of shear stress that occurs simultaneously along the cylindrical surface and *n* is a coefficient which depends on the shape of shear stress distribution on the horizontal surface. Different types of shear stress distribution and the value of *n* are shown in Table 2.2.

Integrating Eq. (2.7), the torque carried by the horizontal surface (T_{h}) is calculated as $T_{\mathrm{h}} = \pi D^3 s_{\mathrm{uh}}/ p_{\mathrm{n}}$, where $p_{\mathrm{n}} = 2(n + 3)$ is a factor that depends on the horizontal shear stress distribution, as shown in Table 2.2. Similarly, the torque carried by the cylindrical surface is $T_{\mathrm{v}} = \pi D^2 H s_{\mathrm{uv}}/2$.

For a typical vane of $H/D = 2$, $T_{\mathrm{v}} = \pi D^3\ s_{\mathrm{uv}}$. Hence the ratio between these torques is:

$$\frac{T_{\mathrm{h}}}{T_{\mathrm{v}}} = \frac{s_{\mathrm{uh}}}{s_{\mathrm{uv}}}\frac{1}{p_n}$$

For the conventional uniform shear stress distribution on the horizontal surface, $n = 0$ and $p_{\mathrm{n}} = 6$ give $T_{\mathrm{h}}/T_{\mathrm{v}} = 1/6$. Menzies and Merrifield (1980) showed that, for London clay $n \cong 5$ and $p_{\mathrm{n}} = 16$, which gives $T_{\mathrm{h}}/T_{\mathrm{v}} = 1/16$. This implies that the vertical surface carries 94% of the total resistance, while it is 86% if one assumes uniform stress distribution on the horizontal surface.

Table 2.2: End shear stress distribution for rectangular vanes (Silvestri and Aubertin 1988)

Type	Pattern	n	P_n
Uniform	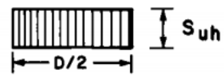	0	6
Parabolic		1/2	7
Triangular		1	8
Square power		2	10
Cubic power	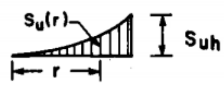	3	12
Fourth power		4	14
Bessel function (Cassan, 45)		–	6.77
Trapezoidal	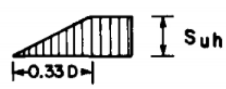	–	6.48
Strain-softening		–	7.27

2.4.4 Shear rate

Shear strength is directly proportional to the rate of shearing or rate of loading for both field and laboratory tests (Bjerrum 1972; Chandler 1988; Roy and Leblanc 1988). The higher the rate of shearing, the higher the shear strength. The typical rotation rate of the vane is 0.1°/s (Chandler 1988; ASTM D2573 2018), and failure is reached in 30–60 s. The time to failure is substantially shorter than that in full-scale or laboratory tests. For laboratory tests, the time required to reach the failure could vary from a few minutes to several hours, and it could be even higher for full-scale field failure. Therefore, in order to be comparable to laboratory testing or field failures, a correction for the rate effect is required.

The undrained shear strength increases with the rotation rate of the vane (Cadling and Odenstad 1950; Wiesel 1973; Torstensson 1977). Due to the differences in strain rates in field tests and laboratory tests, it is important to take into account the strain rate effect when determining the shear strength parameter for design purposes. Due to the strain rate effect, the vane test strength is not as conservative as laboratory testing (higher observed shear strength because of the high strain rate). This is critical in circumstances where vane test results determine the geotechnical parameter. Einav and Randolph (2005) reported an increase in peak strength by 5–20 % for each log cycle increase in strain rate. Cheng (1981) observed that undrained shear strength increased initially with strain rate from the static state, but it reached a maximum value with increasing strain rate, as shown in Fig. 2.12, with variations in water content.

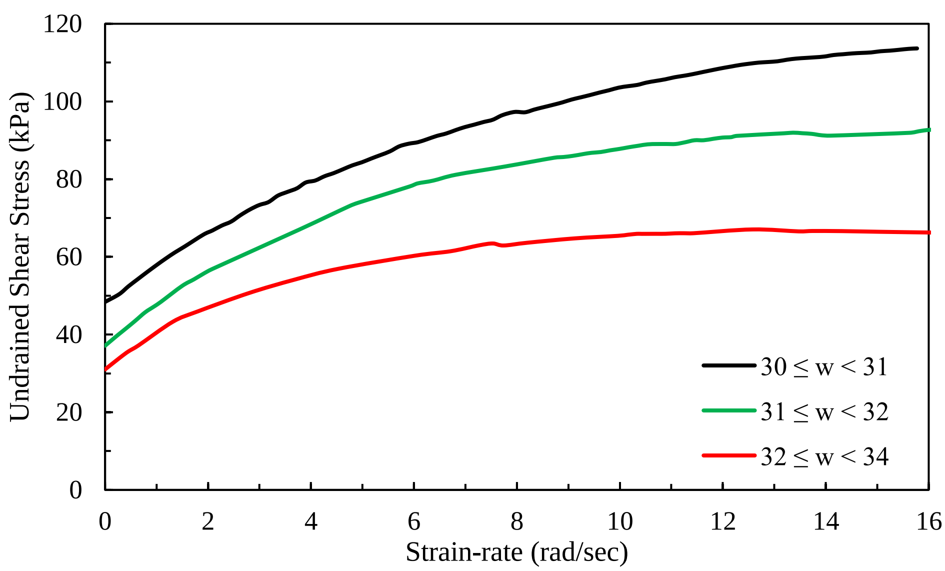

Figure 2.12: Relationship between undrained strength and strain-rate (after Cheng 1981)

2.4.5 Progressive failure

It is commonly assumed that the shear strength is uniformly mobilized on the cylindrical failure surface without any progressive failure during the rotation of the vane. However, sensitive clay is very susceptible to progressive failure because of the strain-softening behaviour, resulting in non-uniformity in stress and strain conditions (Rismyhr 2017). Progressive failure initiates from the edge of the vane blade, where the clay is more intensely strained than the rest of the shared zone (La Rochelle et al. 1973). From the numerical simulation, Griffiths and Lane (1990) observed that not all shear strains will reach their maximum simultaneously, due of the progressive failure of the soil surrounding the vane. They found that soil close to the vane blade fails first, rather than the soil in the middle of the vane, as shown in Fig. 2.13. Figure 2.13 also shows that the shear stress mobilizes more rapidly in an element near the vane than an element at 45º from the blade, although they are at the same radius.

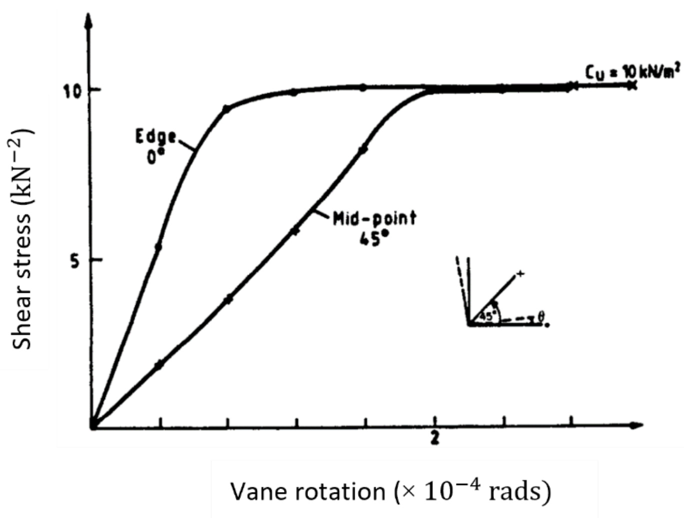

Figure 2.13: Shear stress mobilization (Griffiths and Lane 1990)

2.4.6 Failure geometry

The geometrical shape of the failure surface around the vane is very important for interpreting the shear strength. A circular failure surface is commonly assumed to be formed during vane rotation. However, Gylland et al. (2013) conducted field tests on sensitive clay and found a rounded square shape of the failure surface when the peak shear strength was mobilized. They observed a trend of outward and inward minor shear band formations in the front and back of the vane blade, respectively. They also found very small particle reorientation near the blade tip at the pre-peak regime and a non-smooth shear zone, composed of complex shear surfaces of micrometer thickness, at the post-peak regime. With further rotation, a thicker shear band emerges in the front and back of the vane blades.

Wilson (1964) experimentally found that the failure geometry is not circular but almost a square shape, from the start of rotation up to the mobilizing of maximum torque. At the post-peak condition and also at considerable deformations, the failure surface becomes circular. He also observed cracks close to the edge of the vane blades at the early stage of deformation, due to diagonal tension.

Roy and Leblanc (1988) found a rounded square failure surface during the initial stage of rotation, changes to the circular shape at 45º rotation, and a completely defined failure surface formed at 90º rotation. They found the failure surface to be approximately 5% larger than the vane diameter, which is consistent with the observation of Skempton (1948) and Keentok et al. (1985). An increase in diameter of the failure surface leads to a direct decrease in the undrained shear strength (5% increase in the failure surface decreases the undrained shear strength by approximately 16%) and thus overestimates the strength.

Gylland et al. (2012) conducted a two-dimensional FE analysis using Plaxis and found a rounded square failure prior to mobilizing the peak resistance. They also observed that soil adjacent to the blade tip reaches maximal strength first and subsequently softens; however, the soil elements far from the blade tip remain in the hardening regime, as shown in Figs 2.14(a) and 2.14(b).

Cadling and Odenstad (1950) did some field and laboratory tests to observe the failure geometry during vane rotation. Field tests on clay and laboratory tests on clay and sand were performed. A wetted tissue-paper sheet with a pattern on it was used to observe the failure geometry in the laboratory, and circular failure surfaces were found in all cases.

De Alencar et al. (1988) conducted a two-dimensional FE analysis using an elasto-plastic and strain-softening soil model and found a circular failure surface. Griffiths and Lane (1990) also conducted 2D FE analysis and found a circular failure mode, as shown in Fig. 2.14(c). Pérez-Foguet et al. (1999) performed 2D FE analysis and found a circular failure surface of a radius of 1–1.01 times the vane radius.

Martinez and Frost (2017) found that the number of vane blades affects the shape of the failure surface. They found that a vane of two blades creates an elliptically shaped failure surface, and eight blades create an almost circular failure surface. However, there is no significant change in the failure surface perimeter and magnitude of the shear stress.

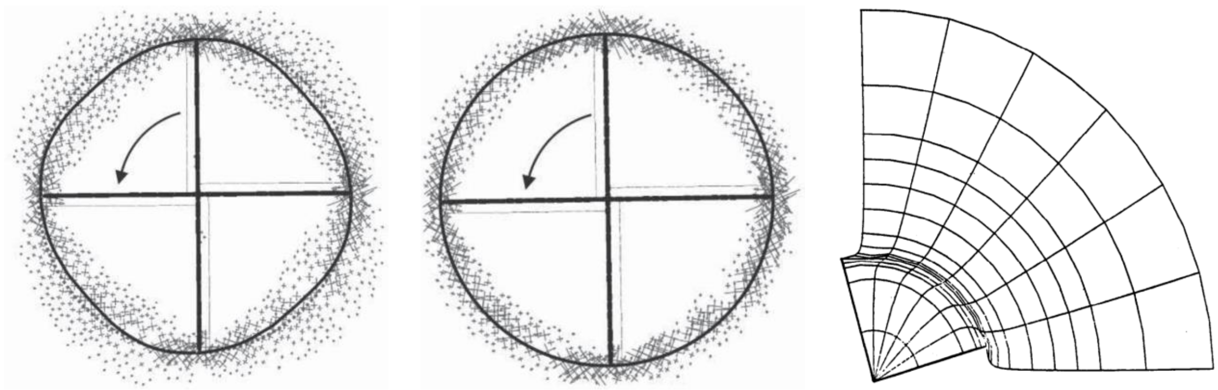

(a) (b) (c)

Figure 2.14: Failure geometry: (a) at the peak; (b) at the residual state (Gylland et al. 2012); (c) FE simulation (Griffiths and Lane 1990)

2.4.7 Soil anisotropy

In the conventional analysis, it is assumed that the soil is isotropic (i.e., the shear strength in the vertical and horizontal directions are equal). However, many clays show anisotropic behaviour, and the strength varies with the loading direction, as shown in Fig. 2.15.

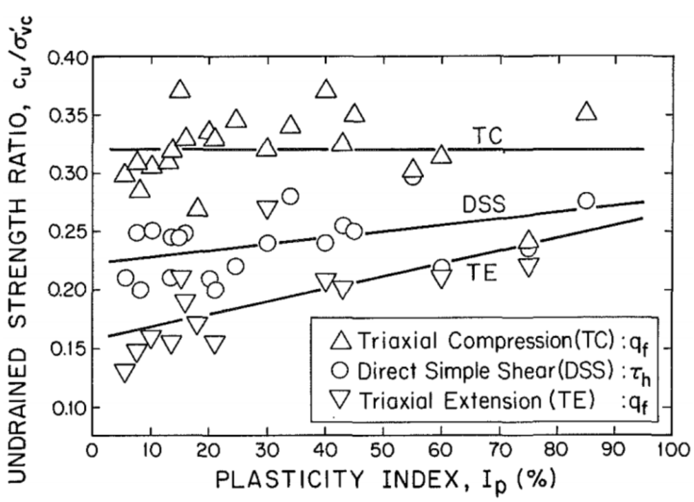

Figure 2.15: Effect of shearing mode on undrained shear strength (Ladd 1991)

In this figure, the undrained strength ratio obtained from the triaxial compression, triaxial extension, and direct simple shear are plotted with respect to the plasticity index. There is a difference in the measured value of strength among all three tests because of different loading directions. The difference of shear strength for these three modes of shearing decreases with the increase of plasticity index, which means the soil is more isotropic.

Anisotropic shear strength from VST has been reported in several studies (Aas 1965, 1967; Silvestri and Aubertin 1988). Aas (1965) investigated strength anisotropy in normally consolidated to overconsolidated clays, using vanes of different height to diameter ratios, and reported that the ratio of undrained shear strength in the horizontal and vertical direction is close to 1, and for normally consolidated clay, it varies from 1.5 to 2. Aas (1967) found that undrained shear strength obtained from the VST is dependent on the in situ failure plane's effective normal stress.

Silvestri and Aubertin (1988) carried out a field investigation to observe the possible anisotropic nature of the undrained shear strength of sensitive clay using rectangular (H/D varied between 0.5 and 2) and diamond-shaped vanes (angle with respect to the horizontal is varied between 30º and 60º). The results obtained from the test indicate that the undrained shear strength in the horizontal plane (s_{uh}) is greater than the vertical plane (s_{uv}) because of the anisotropy, and they found s_{uh}/s_{uv} varies between 1.14 and 1.41. They suggested that both inherent anisotropy and stress-induced anisotropy affect the behaviour. The orientation of the soil structure at the micro-level is referred to as inherent stress anisotropy, and different horizontal and vertical stresses cause stress-induced anisotropy. Therefore, for the correct measurement of undrained shear strength, anisotropy should be included when measuring from the VST, because a major portion of the torque comes from the contribution of the cylindrical vertical surface.

2.5 Previous numerical modelling

In addition to field or lab tests, some numerical studies are also available in the literature. Different software packages (e.g., Abaqus, PLAXIS, SAP) with different soil constitutive models (e.g., Mohr-Coulomb, Non-Newtonian fluid model, Tresca soil model, and Hardening soil model) have been used in these analyses. The available numerical studies are discussed in this section, and a summary is presented in Table 2.3.

Donald et al. (1977) conducted three-dimensional FE simulations using SAP software with a linear elastic soil model. A rigid vane was rotated by applying rotational displacements. FE simulations show a parabolic stress distribution in the horizontal plane and, in the vertical plane, significantly higher stresses are found at the ends than at the center.

De Alencar et al. (1988) developed a hyperbolic strain-softening soil model to simulate the post-peak soil behaviour and conducted two-dimensional and three-dimensional FE simulations. They found that the peak torque depends not only on the peak and residual strength but also on the post-peak softening rate. For a high softening rate, the stress is distributed in a non-uniform way around the vane; the effect is more pronounced for high strain-softening clay. They found that at a high strain-softening rate, the yield zone propagates faster and results in a lower peak value at a smaller rotation angle (ranging between 1º to 2º). They also found progressive failure around the vane.

Griffiths and Lane (1990) conducted two-dimensional FE simulations considering strain-softening and the anisotropic behaviour of soil. The mobilized shear stress on the horizontal and vertical surfaces up to the failure was calculated and compared with the analytical solutions. In the two-dimensional FE analysis, they applied displacement boundary conditions from zero (at the center) to maximum (at the blade tip) to the appropriate boundary nodes. They found that, due to the progressive nature of the failure of soil having strain-softening behaviour, soil elements close to the vane reach the failure first, and the failure progresses gradually with rotation. They also performed some three-dimensional analyses to calculate shear stress mobilization on the horizontal surface. They did not model the actual vane in their three-dimensional analysis; instead, they replaced the vane with a cylinder of stiff material and rotated it into the soil. For elastic analysis, the shape of shear stress distribution includes a corner peak and rapid fall in stresses away from the edge. For elastoplastic materials, the maximum shear stress develops first at the edge, and further rotation changes the shear stress distribution close to a constant value in the horizontal plane when the peak torque is developed. However, in the vertical plane, the shear stress distribution is almost uniform.

Pérez-Foguet et al. (1999) conducted a two-dimensional FE analysis using the Arbitrary Lagrangian-Eulerian (ALE) formulation to overcome some of the difficulties of traditional FE analysis related to strain localization. The soil was modeled as a non-Newtonian fluid, and simulations were performed with different vane sizes and rotational velocities. The inertial effect becomes significant at a high angular velocity, but viscous force dominates at a low angular velocity, and inertial force is negligible. They examined the shear stress distributions on the failure surface and demonstrated how the constitutive model affected shear band development. They also concluded that the fluid mechanics approach is suitable for interpreting the results of VST in soft materials.

Gylland et al. (2012) conducted a two-dimensional numerical simulation using Plaxis to study the failure geometry of VST in soft sensitive clay. Their experimental results supported the findings of numerical analysis. In their analysis, they discussed the failure geometry, which has already been discussed above.

Ansari et al. (2014) simulated the penetration and subsequent rotation of a vane in soil using the Coupled Eulerian-Lagrangian (CEL) approach in Abaqus. They implemented a rate-dependent Tresca soil model considering strain-softening effects. They investigated the dependency of the undrained shear strength on the rate of shearing and the softening response. They rotated the vane up to 20º, but did not discuss the penetration effects. They also found the non-uniform formation of a shear band that extends initially in front of the blade, and at 20° rotation the shear band also extends behind the blade.

Rismyhr (2017) conducted two-dimensional and three-dimensional numerical simulations using Plaxis 2D and 3D and discussed the effects of anisotropy, strain rate, and progressive failure. Using several material models (Mohr-Coulomb, Geofuture, and NGI ADP), the effects of progressive failure, strain rate, and strength anisotropy were examined. A point load was applied at the tip of the vane blade in the two-dimensional simulation, and a line load at the end of the vane blade in the three-dimensional simulation, to rotate the vane. Numerical simulations showed a rounded square failure surface when strain-softening was considered; however, the failure surface is circular for non-softening soil. The effects of strain rate were investigated by varying the time to failure for each simulation and it was found that a correction for strain rate should be included. The shear strength increases by 3–4% for every 10% increase in the plasticity index, and the effect of anisotropy also needs to be considered. The peak torque was attained at a rotation of about 0.5º.

Henneseid (2018) investigated the strain-softening behaviour of soft clay using Plaxis 2D. The simulations were performed with the hardening soil model (HS) and the unified enhanced soft clay creep model (UESCC) to investigate the failure modes, local drainage effects, excess pore pressure, and torque for various rotation rates. A circular failure surface forms when the HS model was used; a rounded square failure was observed for the UESCC model. In the case of the HS model, a slight increase in maximum torque was observed when the rotation rates became very low, and a relatively higher post-peak degradation occurred for a higher rotation rate. In the case of the UESCC model, higher rates resulted in higher maximum torque and exhibited a steeper decrease after maximum torque.

Table 2.3: Summary of previous numerical studies

Reference	Method and FE software	Constitutive Model and Factor considered	Remarks
Donald et al. (1977)	3D SOLID SAP	Linear elastic	Rotated the vane by rotational displacement and presented elastic stress distribution in the vertical and horizontal surfaces.
Matsui and Abe (1981)	2D	Strain-hardening elasto-plastic	Investigated excess pore pressure and effective and total normal stress distribution at different angular velocities.
De Alencar et al. (1988)	2D SAFE	Strain-softening model	Observed the stress distribution on the horizontal plane at radial and peripheral directions.
Griffiths and Lane (1990)	2D and 3D	Strain-softening and anisotropy	Did 2D and 3D FE analysis to observe the share stress distribution in the horizontal and vertical planes, considering different soil models: elastic, elastoplastic, softening, and anisotropy.
Pérez-Foguet et al. (1999)	2D ALE	Non-Newtonian fluid	Analyzed the shear stress distributions on the failure surface and presented the dependence of shear band formation on the constitutive model selected.
Gylland et al. (2012)	2D Plaxis	Hardening Soil model	Observed rounded square failure geometry at pre-peak and peak conditions and circular at residual condition.

Ansari et al. (2014)	3D Abaqus CEL	Tresca soil model considering the rate and softening	Did 3D for the penetration and subsequent rotation of vane, but did not provide any details about the penetration effect.
Gupta et al. (2016)	3D Abaqus CEL	Mohr-Coulomb constitutive model	Modelled only rotation of the vane and observed the shear stress distribution is almost constant on the vertical plane and on the middle part of the horizontal vane blade.
Taiani et al. (2016)	3D Plaxis	Mohr– Coulomb constitutive model	Disturbance due to vane insertion was not considered in their analysis. They introduced anisotropy by dividing the soil volume into three different horizontal layers. They found stress concentration occurs near the vane tip.
Kouretzis et al. (2017)	2D	Standard Tresca isotropic failure criterion with tension cut-off	Demonstrated that vane shear strength is analogous to direct simple shear conditions in the vertical plane at normal stress and equals the horizontal effective stress at a given depth.
Rismyhr (2017)	2D and 3D Plaxis	Mohr-Coulomb, Geofuture, and NGI ADP material model	Simulated vane rotation in 2D and 3D conditions and found that correction factors are needed for strain rate effects and anisotropy.
Henneseid (2018)	2D Plaxis	HS and UESCC model	Performed numerical simulation and observed the effect of failure modes, local drainage effects, excess pore pressure, and rate effect for different soil models.

2.6 Large deformation finite element modelling

The penetration of vane and subsequent rotation causes large deformation of the surrounding soil. One of the difficulties associated with the numerical analysis of the vane test is dealing with large deformations that occur in the failure area. Most of the FE models have been developed based on Lagrangian formulation, where mesh points coincide with material points, move together simultaneously, and result in a non-convergency when simulating large deformation problems (Griffiths 1999). Significant mesh distortion occurs in these types of FE models, especially around the failure planes (Griffiths and Lane 1990). These types of FE formulation become more complex when dealing with large deformation analysis in soft sensitive clay, as strain localization occurs. In the Eulerian formulation, the mesh is fixed as the background, and the material flows through the fixed mesh (Fig. 2.26). An Eulerian-based FE approach is used in the present study.

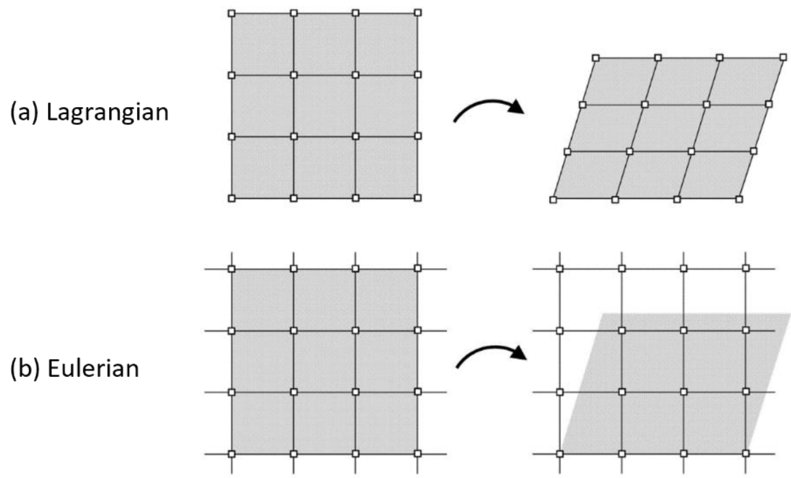

Figure 2.16: Finite element modelling approaches: (a) Lagrangian; and (b) Eulerian (Yerro 2015)

2.7 Summary

Vane shear tests in sensitive clays show different responses than those in non- to low-sensitive clays. The failure of soil occurs progressively, and the shape of the rotating soil block might be different depending upon sensitivity, which could affect the torque and interpreted undrained shear strengths. The literature review reveals some two- and three-dimensional FE analyses on VST have been developed progressively over the last few decades. However, there is still significant room for improvement and new research by incorporating the missing segments, and especially models of penetration and subsequent rotation using large deformation FE analysis, the effect of strain-softening, strain rate, progressive failure and the effect of penetration disturbance, which are the focus of the current study. Most of these numerical studies focused on the peak strength but did not examine the post-peak response. Moreover, the studies on highly sensitive clays are very limited. Some experimental results show that penetration of the vane prior to the rotation could influence the results, and the effect of disturbance could be significant for highly sensitive clays. These issues have been examined in the present study through large deformation finite element simulations using an Eulerian-based FE modelling technique.

Chapter 3: Two-Dimensional Finite Element Modelling of Field Vane Shear Test in Sensitive Clay

3.1 Abstract

The field vane shear test is one of the widely used methods to determine the in-situ undrained shear strength of soft sensitive clay. The rotation of the vane generates large shear strains around the failure plane. Large deformation finite element simulation of the field vane shear test is presented in this study. The effects of strain rate and strain softening on undrained shear strength are considered in the soil model. The simulation is performed over a large rotation, up to 90°, and the post-peak degradation of torque with rotation is shown for varying sensitivities and shear strength degradation rates. The simulation results show the formation of a rounded square-shaped failure plane for a rotation when the maximum torque is mobilized; however, the shape of the failure plane changes to a circular one at large rotation. A softening model with an exponential reduction followed by gradual degradation of the undrained shear strength can simulate the pattern of post-peak degradation of torque measured in vane shear tests in sensitive clays.

3.2 Introduction

The vane shear test is one of the widely used in-situ test methods for the estimation of undrained shear strength (s_u) of soft clay and clayey silt. The test is relatively simple; however, the estimation of s_u from the measured torque (T) involves uncertainties. Previous studies investigated the effects of several factors, including the disturbance caused by vane insertion (Cadling and Odenstad 1950; Kimura and Saitoh 1983), the time interval between insertion and rotation and drainage conditions (Flaate 1966; Kimura and Saitoh 1983; Roy and Leblanc 1988), soil anisotropy (Donald et al. 1977; Kouretzis et al. 2017), progressive failure (Donald et al. 1977; De Alencar et al. 1988;

Griffiths and Lane 1990), rate of vane rotation (Pérez-Foguet et al. 1999), non-uniform stress distribution around the vane (Donald et al. 1977; Menzies and Merrifield, 1980), and failure geometry (Griffiths and Lane 1990; Gylland et al. 2013). The field vane (FV) shear test is also a widely used method for characterizing low plastic sensitive clays.

Two key factors might significantly affect the vane shear test results and their interpretation, namely the rate of shearing and strain softening. The field vane shear tests are generally conducted at a faster rate of rotation so that the developed excess pore water pressure does not dissipate during the tests (i.e., undrained condition). The maximum shear strain rate is higher in the FV shear test than that of typical laboratory element tests. For example, the standard rate of rotation of FV of 0.1°/s might give the maximum shear strain rate of 0.05 s^{-1}, while it is very low (~3×10^{-6} s^{-1}) in the typical undrained triaxial tests (Einav and Randolph 2006; Boukpeti et al. 2012). It is well-known that the undrained shear strength of clay increases with the shear strain rate. Several researchers conducted vane shear tests for varying rotation rates. For example, Biscontin and Pestana (2001) conducted a large number of vane shear tests on a high plastic (PI = 75) lightly cemented bentonite-kaolinite mixture. Tests were conducted for a wide range of rotation rates, including the tests at a rotation rate of approximately three orders higher than the standard rotation rate, to capture possible rates for seismic or storm-wave events. It has been shown that the rate effect increases at higher shearing rates. Comparing two sets of vane shear test data conducted previously, Chandler (1988) showed that while high plastic clays show a continuous decrease in s_u with decreasing shear strain rate up to ~0.00002 %/min, the low plastic sensitive clay shear strength does not decrease for rotation rates below the standard vane shear test rate.

For strain-softening, low plastic sensitive clay might behave differently from highly plastic clays. Figure 3.1 shows the measured torque normalized by the peak value (T_{max}) for tests on two types of soil. Kimura and Saitoh (1983) conducted the tests on highly plastic (*PI* = 47.8%) Kawasaki clay, while the test conducted by Gylland et al. (2013) was on low plastic (*PI* = 5%) highly sensitive Scandinavian quick clay. For Kawasaki clay, the shear strength gradually decreases with rotation. However, for sensitive clay, a rapid reduction of shear strength occurs first, and then a gradual decrease in s_u occurs.

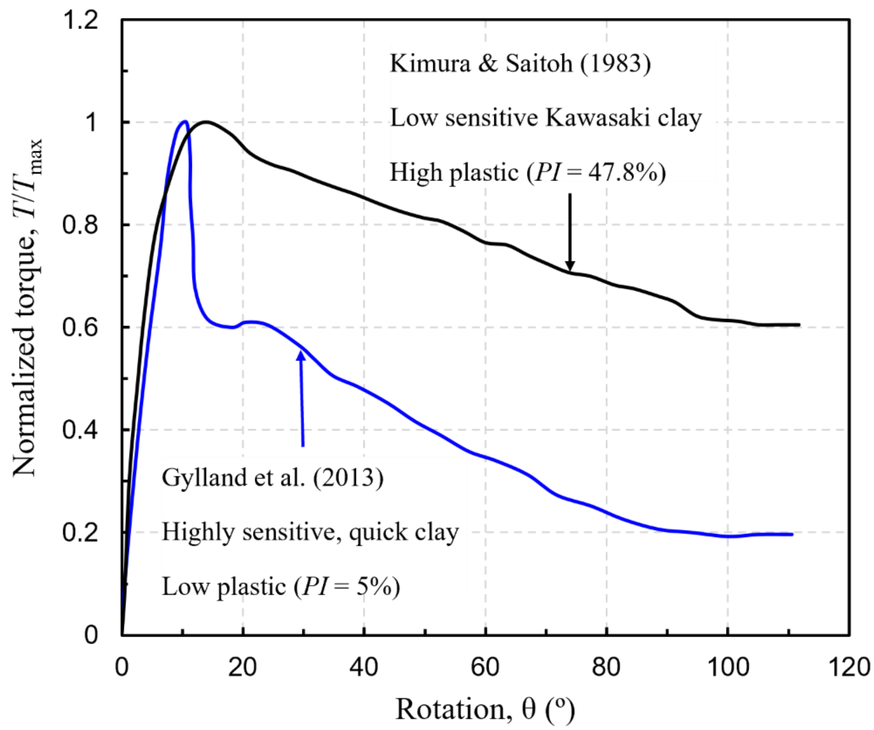

Figure 3.1: Vane shear tests on highly plastic and low plastic sensitive clays

The effects of strain rate and strain-softening cannot be directly measured in the FV shear tests. Finite element (FE) modelling could provide further insights into the mechanisms and better interpretation of the test results. Most of the FE simulations of vane shear tests have been conducted using Lagrangian-based FE techniques, which cannot handle the large deformation due to mesh distortion issues (Donald et al. 1977; Matsui and Abe 1981; De Alencar et al. 1988; Griffiths and Lane 1990; Gylland et al. 2012; Kouretzis et al. 2017; Henneseid 2018). Some attempts have also been made to incorporate large deformations, such as the analyses using an Arbitrary Lagrangian-Eulerian formulation by modelling the soil as a non-Newtonian fluid (Pérez-Foguet et al. 1999), and preliminary analyses using a Coupled Eulerian-Lagrangian (CEL) approach (Ansari et al. 2014; Gupta et al. 2016).

The objective of this chapter is to simulate the vane shear test using a CEL approach, incorporating appropriate models for strain rate and strain softening. The failure geometry, progressive formation of failure planes, and the mobilized shear stresses and strains are investigated.

3.3 Problem statement

Only three-dimensional analysis can be performed using the present CEL approach. Therefore, for modelling the in-plane strain condition of a horizontal section of the vane, the analysis is performed with only one element of thickness (t_z) of 2 mm in the out-of-plane direction (z-direction in Fig. 2). A 65-mm diameter (D) vane is considered. The modelling is performed for a wished-in-place condition (i.e., without considering insertion effects).

3.4 Finite element modelling

The Coupled Eulerian-Lagrangian (CEL) approach available in Abaqus FE software is used. The FE mesh used in the numerical modelling is shown in Fig. 3.2. A dense mesh is used near the tip of the vane, where a significant amount of soil deformation is expected due to the rotation of the vane. A varied mesh distribution that increases with radial distance is used to reduce the computational time. Analyses are also carried out with a larger soil domain and using finer mesh than the one shown in Fig. 2; however, no significant change in the result is found.

The FE model is comprised of three parts: soil, vane, and void. The soil is modelled as an Eulerian material, and the vane is modelled as a Lagrangian rigid body. In the Eulerian formulation, the mesh is fixed at the background, and the material flows through the fixed mesh without causing any numerical issue related to mesh distortion (Dey et al. 2015; Karmaker and Hawlader 2018; Karmaker et al. 2019; Wang et al. 2020). The Eulerian Volume Fraction (EVF) is used for defining and tracking the flow of material during analysis. For an element, EVF = 0 represents no soil in that element (void), while EVF = 1 represents an element entirely filled with soil. EVF is between 0 and 1 for an element partially filled with soil.

The soil is modelled using EC3D8R elements in the software, which are 8-node linear brick, reduced integration, and hourglass control elements. The vane is modelled using C3D8R, which is also 8-node linear brick, reduced integration, and hourglass control elements. The vane is defined as a rigid body with a reference point at the center.

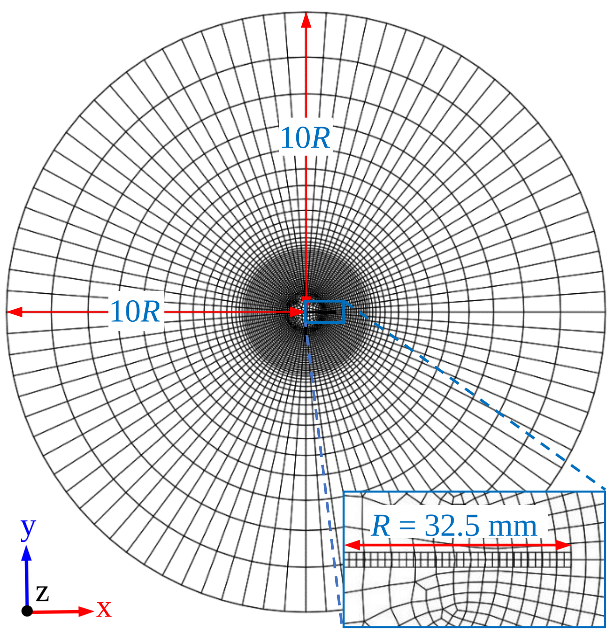

Figure 3.2: Finite element mesh

Zero-velocity boundary condition (i.e. $v_z = 0$) is used in the out-of-plane direction (i.e. no soil movement occurs in the z-direction). At the outer cylindrical surface, zero-velocity boundary conditions are used for all three directions (i.e. $v_x = v_y = v_z = 0$).

Undrained analysis is performed by giving the yield strength (σ_y) adopting the von Mises yield criterion ($\sigma_\mathrm{y} = 2s_\mathrm{u}$) as a function of strain rate and strain softening. A frictionless interface condition between soil and vane is used. The vane is rotated with respect to the reference point at a constant angular velocity.

3.5 Constitutive modelling of soil

Under the undrained loading condition, sensitive clays show significant strain-softening behaviour. Strain-softening behaviour has many practical implications, such as large-scale landslides. In the present study, the mobilized undrained shear strength (s_u) of the sensitive clay is modelled as:

$$s_\mathrm{u} = f_1 f_2 s_\mathrm{uy} \tag{3.1}$$

where f_1 is a strain-softening factor, f_2 is a strain-rate factor and s_uy is undrained shear strength at a very low strain rate.

The strain-softening factor (f_1) has been defined in previous studies as a linear and exponential function of accumulated plastic shear strain or plastic shear displacement (δ) (Locat et al. 2013; Dey et al. 2016; Wang et al. 2020). Eq. (3.2) is used in this study for the strain-softening factor, which consists of a rapid exponential degradation followed by a slower linear degradation and finally remains constant at large strains.

$$f_1 = \begin{cases} \dfrac{s_\mathrm{uR}}{s_\mathrm{u0}} + \left(1 - \dfrac{s_\mathrm{uR}}{s_\mathrm{u0}}\right) e^{-3\delta/\delta_{95}} & \text{if } 0 \le \delta < 2\delta_{95} \\ \dfrac{s_\mathrm{uR}}{s_\mathrm{u0}} - \dfrac{s_\mathrm{uR} - s_\mathrm{uld}}{s_\mathrm{u0}} \dfrac{\delta - 2\delta_{95}}{\delta_\mathrm{ld} - 2\delta_{95}} + c & \text{if } 2\delta_{95} \le \delta < \delta_\mathrm{ld} \\ \dfrac{s_\mathrm{uld}}{s_\mathrm{u0}} + c & \text{if } \delta > \delta_\mathrm{ld} \end{cases} \tag{3.2}$$

where s_{u0} is the peak undrained shear strength at the reference shear strain rate $(\dot{\gamma}_{ref})$ before softening; s_{uR} is the value of s_u at a sufficiently large value of δ; δ_{95} is the value of δ at which 95% reduction of $(s_{u0} - s_{uR})$ occurs; s_{uld} is the value of s_u at the completely remoulded state at a very large value of δ; and $c = (1 - s_{uR}/s_{u0})e^{-6} \approx 0$. Further information about these strain-softening equations is available in previous studies (Dey et al. 2015; Dey et al. 2016; Wang et al. 2020).

The shearing resistance around the failure plane (rounded square and circular, as discussed in the following sections) is governed by the stresses on that vertical plane. The mode of failure at this surface is similar to the direct shear or closely analogous to simple shear conditions (Wroth 1984; Chandler 1988). Assuming a simple shear condition, plastic shear strain (γ^p) can be calculated as $\gamma^p = \delta/t_{FE}$, where t_{FE} is the thickness of the finite element. The equivalent plastic shear strain (ε_q^p) is calculated as $\varepsilon_q^p = \gamma^p/\sqrt{3}$. Now, using the input parameters δ_{95} and δ_{ld} (Table 3.1), the post-peak shear strength degradation curve (Eq. (3.2)) can be defined as a function of ε_q^p, which is used in the subroutine to provide the variation of s_u with the development of plastic shear strain. In the present study, the characteristic length is considered as t_{FE}.

For strain-rate effects, an "additive power-law model" proposed by Zhu and Randolph (2011) is used. This model combines the Herschel–Bulkley model (fluid-mechanics approach) with the power-law model (geotechnical approach) to capture the response from intact to fluidized remoulded soil.

$$f_2 = 1 + \eta \left(\frac{\dot{\gamma}}{\dot{\gamma}_{ref}}\right)^{\beta} \tag{3.3}$$

where η and β are soil parameters, and the value of these parameters is taken based on previous studies (Randolph et al. 2012; Wang et al. 2020). At the reference strain level (i.e., $\dot{\gamma} = \dot{\gamma}_{\mathrm{ref}}$), $s_{\mathrm{uy}} = s_{\mathrm{u0}}/(1 + \eta)$.

For low plastic sensitive clays, the shear strength does not decrease at very low strain rates; instead, it shows some increase in strength because of excess pore water pressure dissipation for a very slow rate of rotation of the vane (Roy and Leblanc 1988). Therefore, in the present study, $f_2 = 1$ is used for $\dot{\gamma} \leq \dot{\gamma}_{\mathrm{ref}}$. In the FE program, $\varepsilon_{\mathrm{q}}^{\mathrm{p}}$ is called in each time increment, and $\dot{\gamma}$ is calculated as $\dot{\gamma} = \sqrt{3}\Delta\varepsilon_{\mathrm{q}}^{\mathrm{p}}/\Delta t$, where Δt is a time interval.

Standard field vane tests are generally conducted at a 0.1°/s rotation rate. However, the FE simulations are performed at a 240 times faster rate (24°/s) to save computational cost. Therefore, the $\dot{\gamma}$ obtained from FE is divided by 240 to calculate f_2 using Eq. (3.3).

Table 3.1: Geotechnical parameters used in analysis

Parameters	**Value**
Total unit weight, γ (kN/m$^{3)}$	16.7
Peak undrained shear strength, s_{u0} (kPa)	30
Remoulded undrained shear strength, s_{uR} (kPa)	17.64
Large displacement undrained shear strength, s_{uld} (kPa)	1
Undrained Young's modulus, E_{u} (MPa)	9.0
Undrained Poisson's ratio, ν_{u}	0.49
Reference shear strain rate, $\dot{\gamma}_{\mathrm{ref}}$	0.05
δ_{95} (m)	0.005
δ_{ld} (m)	0.055
η	0.5
β	0.1

3.6 Results

In the following sections, the discussion is mainly focused on the variation of torque (T) with rotation (θ), shear stress and strain distributions, and soil failure patterns.

3.6.1 Torque for idealized elastic-plastic clay

To validate the numerical modelling technique, a simulation is performed first with a simple elastic perfectly plastic soil model, and the results compared with an analytical solution, which is commonly used for estimation of s_u from the measured torque. Figure 3.3 shows that the torque increases with rotation and then remains constant at T_{max}.

It is commonly assumed that the rotation of the vane creates a cylindrical failure surface. The maximum torque required to overcome the shear resistance at this cylindrical surface (T_{max}) is $0.5\pi D_e^2 t_z s_u$ where D_e is the diameter of the failure zone. Generally, the diameter of the vane (D) is used for D_e. However, as will be shown later, the strain concentration in FE analysis occurs in the soil elements outside the tip of the vane. Also, the integration point of a finite element is at the center of the element; therefore, the FE calculated torque could be better compared to the calculated value, with D_e equal to the diameter of the vane, plus the thickness of one element around the tip (~ 2 mm in this simulation), which gives D_e = 67 mm. Figure 3 shows the calculated maximum torque using this expression multiplied by $2/\sqrt{3}$ to incorporate the plane strain failure mode during shearing. The FE calculated T_{max} matches the analytical value with D_e = 67 mm.

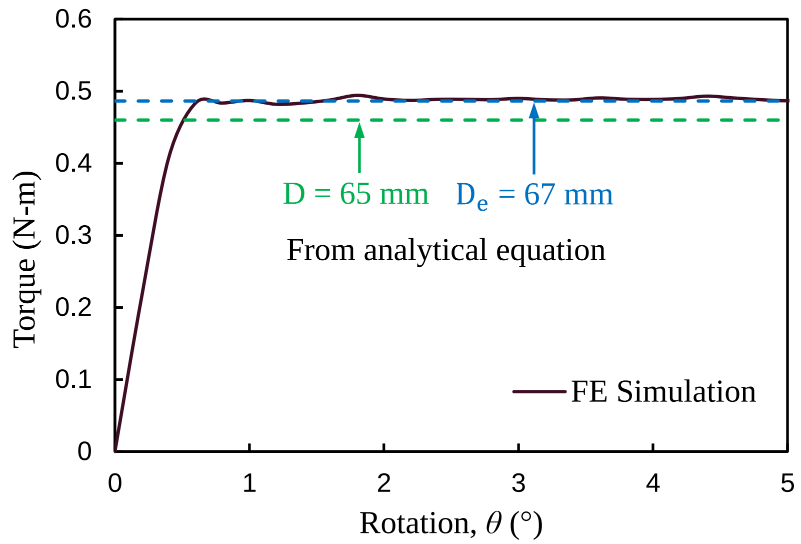

Figure 3.3: Torque for elastic perfectly plastic soil

3.6.2 Post-peak response

Figure 3.4 shows the calculated torque where the effects of strain softening and strain rate on s_u are implemented using Eqs. (3.2) and (3.3), respectively. The results are shown only from the peak because the pre-peak response also depends on soil disturbance, due to the insertion of the vane. The results of a vane shear test are also presented in Fig. 3.4 to show the post-peak shear strength degradation pattern.

Several approaches have been proposed to incorporate strain-softening effects on s_u and its influence on the overall response of geotechnical problems such as sensitive clay slope failure. For example, brittleness (D'Elia et al. 1998; Fornes and Jostad 2017) and remoulded energy (Tavenas et al. 1983; Thakur et al. 2015) have been used to define how much shear strain is necessary to reduce the strength from the peak value by a certain amount. In the present study, two parameters, S_t and δ_{95}, control the rate of shear strength degradation during the rapid reduction phase of s_u ($\delta \leq \delta_{95}$ in Eq. (3.2)). Vane shear tests in sensitive clays also show a rapid reduction of torque immediately after the peak, within a few degrees of rotation, followed by a slower reduction phase over a large rotation (Gylland et al. 2013; Thakur et al. 2015). Note that, in Eq. (3.2), S_t represents the ratio between the shear strength at the peak and after the rapid reduction phase (not the completely remoulded shear strength). Therefore, to examine the effects of post-peak shear strength degradation curve on torque, three simulations are performed for varying S_t and δ_{95}. Two simulations (Cases 1 and 3 in Fig. 3.4) are performed with S_t = 5 and only an exponential shear strength degradation curve (i.e., first equation of Eq. (3.2)), while the other simulation (Case 2) for S_t = 1.7 is performed with exponential, followed by linear degradation of shear strength (i.e. all three equations in Eq. (3.2)).

Figure 3.4 shows that for a given S_t (= 5), a lower value of δ_{95} (= 0.01 m) rapidly reduces T/T_{max} to 0.2 within 20° rotation, while it takes more than 90° rotation when δ_{95} = 0.05 m is used. However, when two levels of degradation (exponential and then linear) are used, a quick reduction of torque, followed by gradual reduction, similar to that reported from vane shear tests (i.e. Gylland et al. 2013) are found. This implies that using only a linear or an exponential strain-softening curve may not be able to simulate the response reported from vane shear tests on highly sensitive clays.

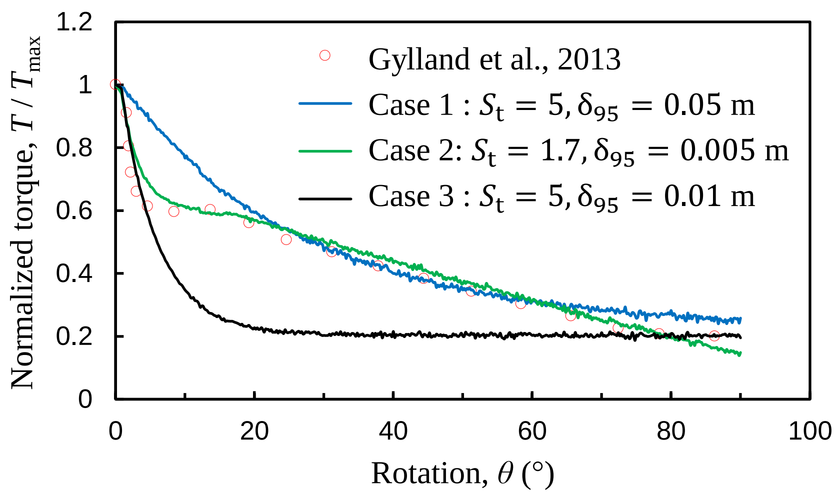

Figure 3.4: Torque for three different strain-softening behaviour

A lower δ_{95} (= 0.005 m) could reasonably match the initial segment, and a higher δ_{95} might give a similar trend at large rotation. However, when two levels of degradation (exponential and linear) are considered, they better match the test results. Note that the mechanisms of strain-softening are different at different strain levels. For example, structural breakdown immediately after the peak increases the pore water pressure and causes a rapid reduction of shear strength, while particle rearrangement could be the primary cause of strength reduction at large strains. For practical applications, the strength reduction rate at different strain levels might be equally important. For example, the formation of shear bands during progressive failure of a slope would be governed by the rapid reduction of shear strength after the peak, while the mobility of the debris depends on strength degradation at large strains.

3.6.3 Shear stress distribution

Figure 3.5 shows the variation of von Mises stress (σ_e) with radial distance (r) measured from the center (intersection of the vane blades) for θ_1 = 45° and 15° from the initial horizontal position of the vane blade (see inset of Fig. 3.5). This simulation is performed with an elastic perfectly plastic soil model (Fig. 3.3). To obtain the value of σ_e, a path has been created, and the stress of soil elements around that path is extracted. As there are a limited number of elements around the path near the center (see inset of Fig. 3.5), the exact value of σ_e could not be obtained. In any case, σ_e is small in these elements and is well below the yield strength; therefore, it does not have a significant effect on the interpretation of the mechanisms. It is also to be noted that the computational cost is high for this type of large deformation finite element analysis. Therefore, the analysis is not performed with very fine mesh near the center; instead, the stress distribution is shown from a certain radial distance.

Figure 3.5 shows that, for a given rotation of the vane, σ_e increases with radial distance and is maximum near the tip of the blades. Also, σ_e increases with rotation; however, after $\theta \approx 0.6°$, the stress distribution does not change with further rotation. At this stage, σ_e at $r = R$ is equal to the yield strength. The maximum torque is mobilized at this rotation, as shown in Fig. 3.3. Note that, in the field, the rotation required to attain the maximum torque is typically higher than that of the simulation results, which might be due to, inter alia, disturbance of the soil during insertion of the vane. However, numerical simulations conducted in previous studies also found the peak at lower rotations (Griffiths and Lane 1990; Rismyhr 2017; Henneseid 2018). For $\theta_1 = 15°$, the shear stress increases quickly as compared to that of $\theta_1 = 45°$ because these elements are closer to the horizontal blade.

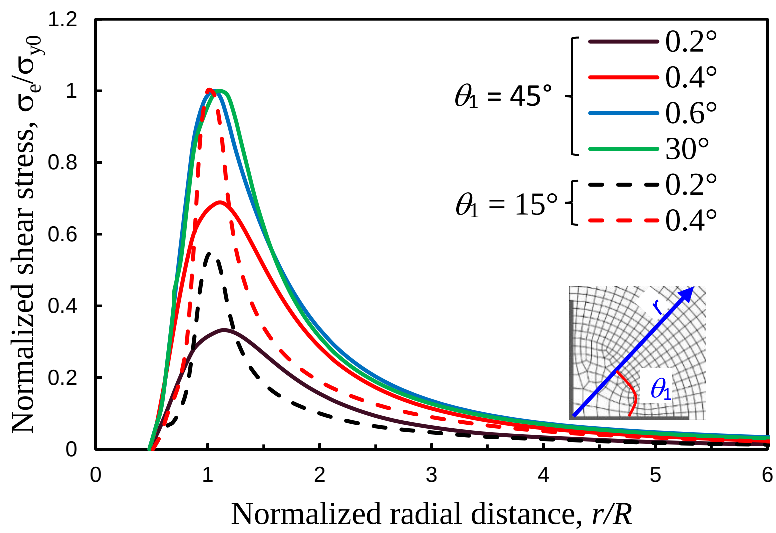

Figure 3.5: Shear stress distribution with radial distance for elastic perfectly plastic soil model

Figures 3.6(a) and 3.6(b) shows the variation of σ_e for $\theta_1 = 45°$ when strain-softening and strain rate effects are considered. Similar to Fig. 3.5, σ_e increases with rotation and becomes maximum at a rotation of approximately 0.6°. At this stage, the maximum σ_e is equal to the yield strength.

With further rotation, plastic shear strain starts to develop and strain softening occurs in the soil elements around $r = R$, which reduces the shear strength. Therefore, σ_e reduces with rotation. For a lower value of δ_{95}, more degradation in shear strength is observed.

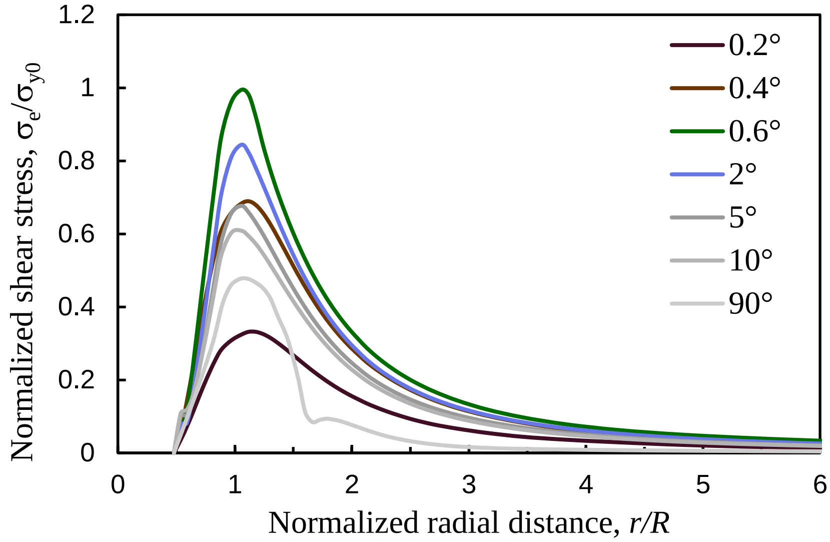

(a)

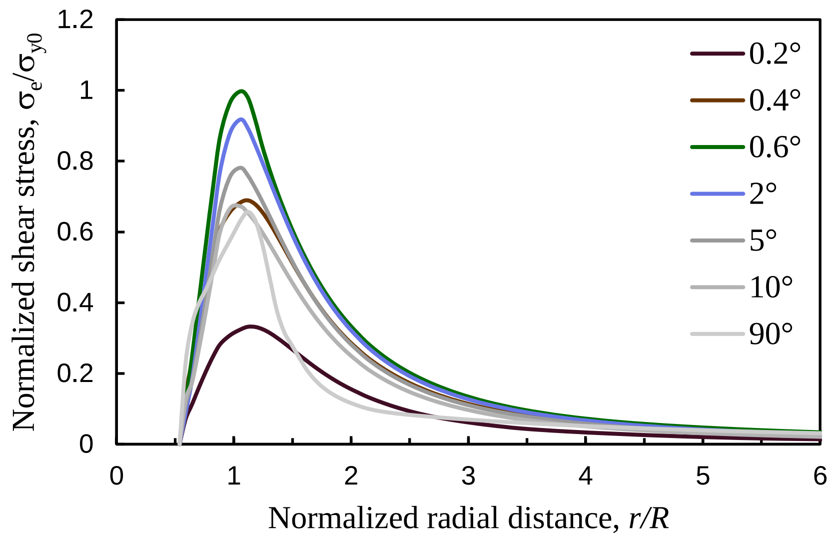

(b)

Figure 3.6: Shear stress distribution with radial distance for soil model with strain rate and strain softening effects (a) δ_{95} = 0.005 m; (b) δ_{95} = 0.01 m

3.6.4 *Development of plastic shear strain*

Figure 3.7 shows the development of equivalent plastic shear strain ($\varepsilon_{\mathrm{q}}^{\mathrm{p}}$) with rotation of the vane for Case 3 in Fig. 3.4. The failure initiates from the tip of the blade and propagates circumferentially. In the beginning, strain concentration mainly occurs in a small zone around the tip. With rotation, the zone of plastic shear strain extends over a larger distance along the circumference both in the front and back of the tip. At $\theta \approx 0.6°$, a complete failure plane of rounded-square shape is formed. The maximum torque ($T_{\max}$) is mobilized at this rotation. With further rotation, post-peak shear strength degradation occurs, and the rounded square shape failure plane becomes circular. The shear strain mainly concentrates in a narrow zone. Once the circular failure plane is developed, shear strain generates only in this zone without any noticeable change in shear strain outside this zone. In other words, the failed cylindrical soil block simply rotates with rotation of the vane. The simulation was stopped after 90° rotation of the vane, although it could be continued without any numerical issues. It is to be noted that the Lagrangian-based FE method cannot simulate such large deformation because of significant mesh distortion (De Alencar et al. 1988; Griffith and Lane 1990).

Attempts have also been taken previously to identify the shape of the failure plane with rotation of the vane, which has been used to examine the mechanisms of shear band formation and their effects on the interpretation of shear strength. Some studies supported the idealization of cylindrical failure geometry for low-sensitive and soft clays (Cadling and Odenstad 1950; Arman et al. 1975). However, highly sensitive clays (Roy and Leblanc 1988; Gylland et al. 2013), even reconstituted kaolin (Chandler 1988) and illite-clay (Veneman and Edil 1988), show the formation of failure geometry similar to those shown in Fig. 3.8. Gylland et al. (2013) conducted a microscopic analysis of the failure zone at different rotation levels and showed that minor shear bands form initially from the tip of the blade, which leads to the formation of a rounded square-shaped failure plane first. With further rotation, a thicker shear band forms with reorientation of the particles, and a cylindrical failure geometry is observed. In the present FE analysis, although micro-level shear surface formation could not be simulated, the overall response and failure geometry could be successfully modelled.

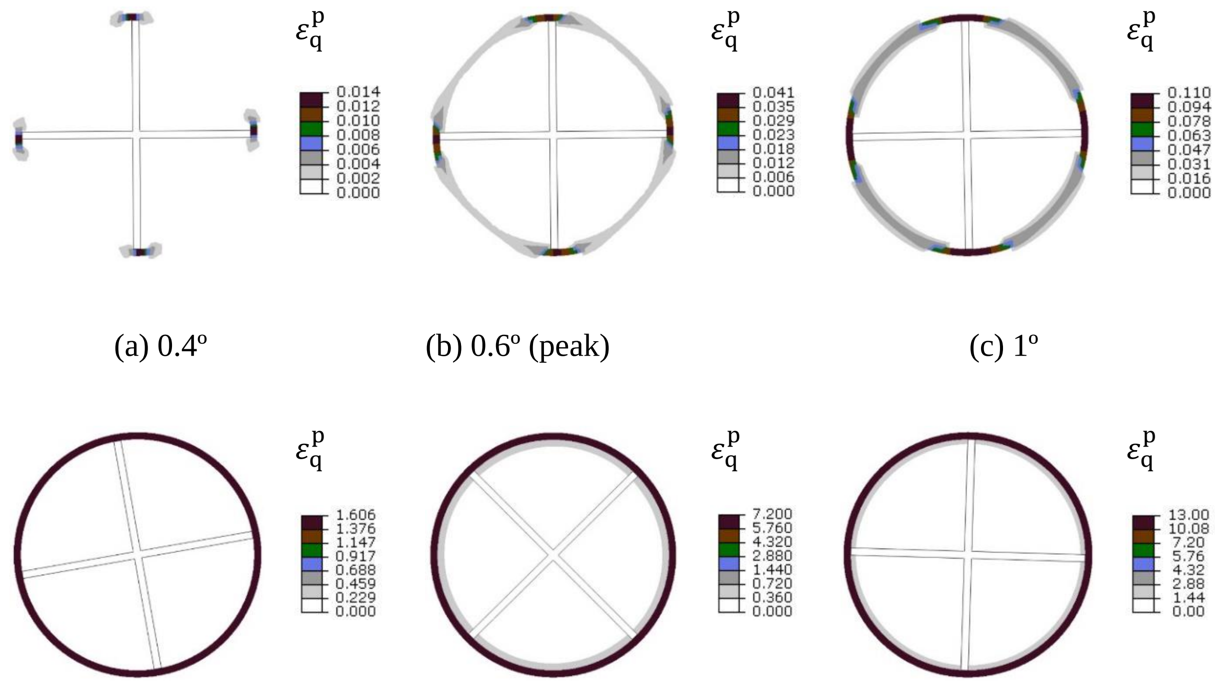

(a) 0.4º (b) 0.6º (peak) (c) 1º

(d) 10º (e) 45º (f) 90º

Figure 3.7: Formation of failure planes during rotation for soil model with strain rate and strain softening effects

3.7 Progressive failure mechanisms

The progressive failure mechanisms during the rotation of the vane are shown in Figs. 3.8 and 3.9. These figures show the von Mises stress (σ_e) distribution along a circular path drawn from the tip of the vane. Figure 3.8 shows the variation of σ_e/σ_{y0} for the elastic perfectly plastic soil model, where $\sigma_{y0} = 2s_{u0}$. At the beginning of rotation, shear stress is maximum ($\sigma_e = 0.8\sigma_{y0}$) near the tip of the four blades. When the vane is rotated to 0.4°, the von Mises stress in some elements near the tip reaches the yield strength ($\sigma_e/\sigma_{y0} = 1$). When the rotation is 0.6°, all the elements along this circular path reach the yield strength and a complete failure plane forms. For further rotation, σ_e at this failure plane remains at σ_y as the elastic perfectly plastic soil model is used.

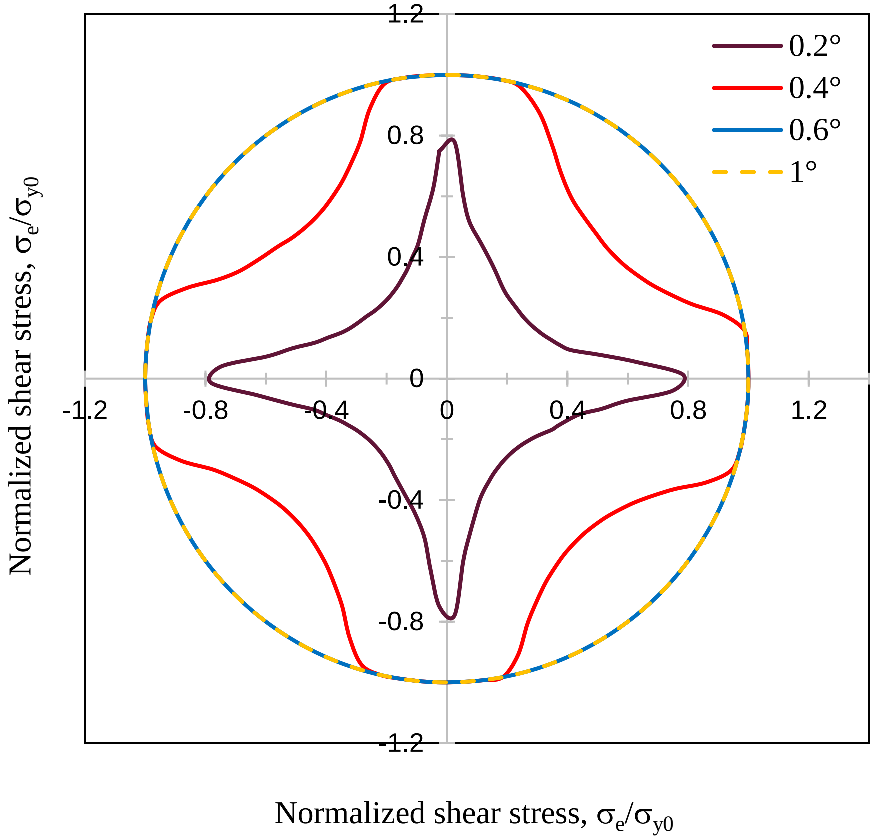

Figure 3.8: von Mises stress distribution along the circular path from the tips of the vane blade for elastic perfectly plastic soil model

Figures 3.9(a) and 3.9(b) show the variation of σ_e for strain-softening and the strain-rate dependent soil model. Similar to Fig. 3.8, σ_e increases quickly near the tip of the vane. When the vane rotates to approximately 0.6°, a complete failure plane is formed, and $\sigma_e \approx \sigma_{y0}$ in all the elements along this circular path. Further rotation decreases the von Mises stress of the sensitive clay because of post-peak shear strength degradation. The reduction of σ_e starts to occur near the tip of the vane blades. The rate of reduction is more pronounced for a higher softening rate (i.e., lower value of δ_{95}), as shown in Fig. 3.9(a).

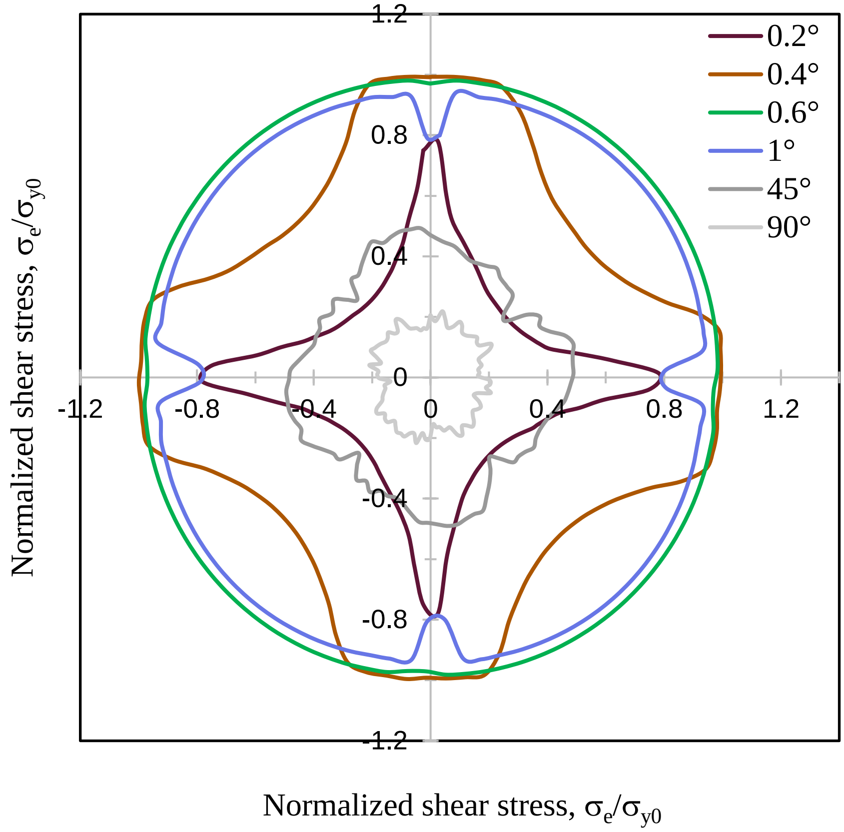

(a)

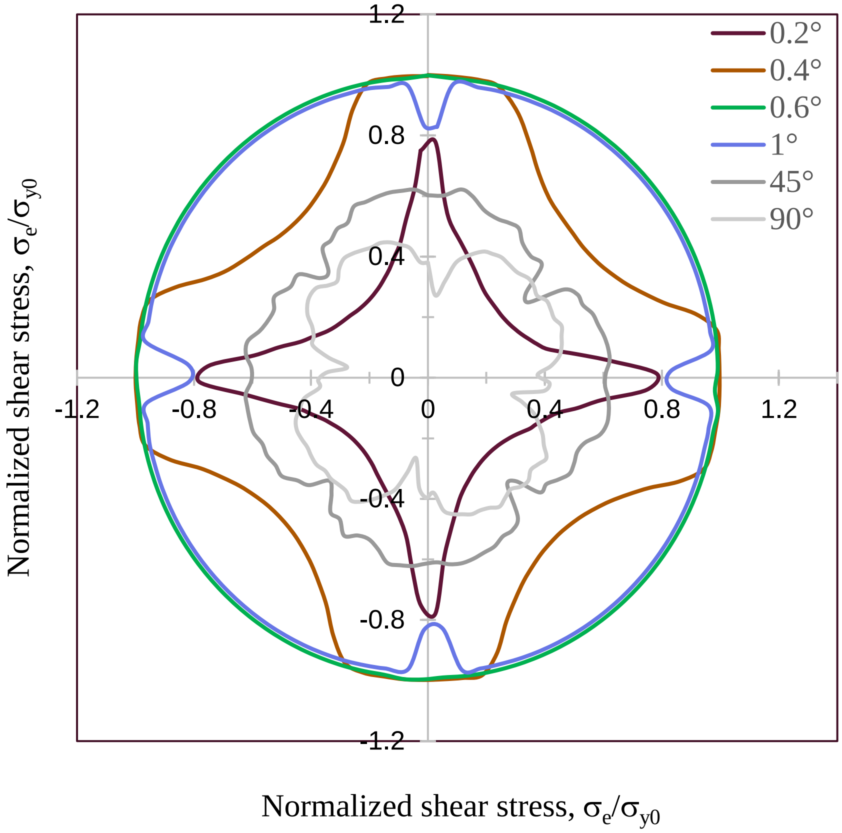

(b)

Figure 3.9: von Mises stress distribution along the circular path from the tips of the vane blade:

(a) δ_{95} = 0.005 m; (b) δ_{95} = 0.01 m

3.8 Summary

This chapter presents large deformation finite element modelling of vane shear tests in soft sensitive clay. Experimental results show that the undrained shear strength of soft clay is highly dependent on the shearing rate. Also, the tests on sensitive clays show a rapid reduction of undrained shear strength with shearing. These two key factors, strain-rate and strain-softening effects on undrained shear strength, are incorporated in the soil model. The soil is modelled as an Eulerian material that can simply flow through the mesh without causing any numerical issues related to mesh distortion, as encountered in typical Lagrangian-based finite element modelling.

The simulation results show the formation of failure planes similar to those observed through close examination of the soil block at different stages of the vane shear tests in sensitive clay. The failure initiates with the formation of a rounded square-shaped soil block and then changes to a circular one at large deformation when considerable reduction of shear strength occurs in the soil elements around the failure planes. The softening model used in this study can simulate the post-peak degradation of torque, as observed in tests in sensitive clays.

Finally, the simulations are performed only for a thin section of the vane. Also, insertion of the vane and strength anisotropy might affect the overall response.

Chapter 4: Modelling of Penetration and Subsequent Rotation of Vane Shear Tests in Sensitive Clay

4.1 Abstract

The penetration of a vane prior to rotation could disturb the surrounding soil, depending upon the sensitivity and dimensions of the vane. Both penetration and rotation cause large soil deformation. The present study aimed to develop a numerical modelling technique using a Coupled Eulerian-Lagrangian (CEL) approach to investigate penetration effects on the undrained shear strength. A rigid vane is penetrated into the clay under the quasi-static condition and then rotated to obtain the torque–rotation relationship. The effects of strain rate and strain softening on undrained shear strength are considered in the numerical simulations. In addition, some simulations are performed only for rotation to quantify the effects of penetration on shear strength. The effects of blade thickness on soil disturbance and undrained shear strength are investigated. Based on simulated stresses and strains' distributions, the potential reasons behind the variation of calculated shear strength are discussed. A parametric study is also carried out to investigate the effects of soil properties on calculated torque.

4.2 Introduction

The main advantage of the field vane test (FVS) is that it provides an almost direct assessment of the in-situ undrained shear strength (s_u). However, the strength calculation of s_u from the measured torque involves some simplified assumptions. There are several sources of uncertainties in calculated s_u based on FVS tests, including the test procedure, methods of interpretations, and type of vane used. The level of uncertainties might also vary with soil type; for example, the effects of soil disturbance on s_u might be higher for sensitive clays.

The undrained shear strength is calculated from the measured torque (T), which is a function of s_u at the failure surfaces that form due to the rotation of the vane. Generally, it is assumed that a uniform shear stress distribution occurs at the vertical and horizontal surfaces. However, some researchers have re-examined this assumption and showed that the assumption of uniform shear stress distribution on the vertical surface is quite reasonable (Donald et al. 1977; Menzies and Merrifield 1980; Griffiths and Lane 1990). However, the distribution of shear stress on the horizontal surfaces (top and bottom) is very different from the commonly assumed uniform shear stress distribution. Three types of variation of shear stress on the horizontal surfaces is assumed: uniform, triangular and parabolic. Other types of shear stress distribution at the top and bottom surfaces were also reported in some studies (Silvestri and Aubertin 1988). Also, for low plastic sensitive clay, which has strain-softening behaviour, the stress distribution is different from highly plastic clays (Thakur et al. 2014). In this case, the post-peak shear strength degradation results in non-uniform stress distribution along the failure planes because the failure planes form progressively. Therefore, the strain and mobilized shear strength are not the same. This type of non-uniform strength distribution makes the calculation of s_u more difficult for sensitive clays (De Alencar et al. 1988). Unfortunately, the variation of strength or stress cannot be measured in the field; therefore, the numerical analysis provides further insights into the process.

Another important factor of the field vane shear test is the soil disturbance caused by vane insertion. Kimura and Saitoh (1983) conducted laboratory tests to investigate the effect of disturbance due to vane insertion on measured shear strength. They also investigated the effect of elapsed time between vane insertion and the start of the rotation and reported an increase in the ratio of shear strength to the vertical consolidation pressure (c_u/p) with the increase of time interval between vane insertion and the start of the rotation (t_i). They reported that the c_u/p, for a sufficiently long elapsed time (240 min) increases by about 45%, by 20% for soil with plasticity index (*PI*) of 20, and 50 respectively than for the short elapsed time (4.5 min). They also did the laboratory test without any penetration of vane to investigate the reduction in measured shear strength due to disturbance caused by vane insertion and found an increase in the ratio of about 10% and 8% for soil with *PI* of 20 and 50, respectively than for the longer time interval (240 min). They found high pore pressure development during vane penetration, and the generation of pore pressure is very small during vane rotation.

The penetration of the vane during the test could cause large deformation of the surrounding soil. La Rochelle et al. (1973) found that vane insertion causes a breakdown of bond in the clay particles and increases the pore pressure, therefore giving lower strength. We cannot measure the amount of disturbance from the field or laboratory at the time of penetration. However, from numerical simulation, the change of stress state during penetration can be measured.

The shaft might have some effect due to friction resulting from surrounding soil that presses against the shaft. The friction might be avoided by using a casing around the shaft that prevents direct contact between the shaft and the surrounding soil, although there might be some friction between the shaft and the casing. There are different categories of vane, but it is very difficult to eliminate the soil-shaft and any internal friction completely (Ortigão and Collet 1988). The torque sensor and measuring device should be placed as close to the vane as possible for the most accurate measurement of torque (Selänpää et al. 2017).

There is no way to investigate or measure the actual mechanisms involved in the test while conducting it in the field or laboratory. The penetration of vane during the test could cause disturbance of the adjacent soil, which could be more significant for sensitive clay. Numerical simulation is the best way to observe and identify the mechanisms involved in the test. There is no finite element (FE) analysis available in the literature that discusses any penetration effect of the vane shear test. The test involves large deformation of the surrounding soil. So, the large deformation FE modelling technique is necessary for modelling such large deformation problems. Therefore, the effect of penetration disturbance for the vane shear test in sensitive clay has been observed in the present study.

4.3 Problem statement

Vane tests are generally carried out below the base of a borehole. The vane is pushed below the bottom of the borehole, usually about 5*B*, where *B* is the borehole diameter (ASTM D2573), to ensure that the vane is in undisturbed soil and the in-situ stresses are not affected by the drilling of the borehole. For a typical borehole diameter, which is larger than the vane diameter (*D*), a considerably large penetration is necessary, which could disturb the surrounding soils, especially for sensitive clays. As discussed before, such a large penetration cannot be modelled using traditional FE programs because of significant mesh distortion. Also, modelling of such large penetration, even with the currently used Eulerian-based FE, is computationally expensive. Therefore, to reduce the computational costs, the vane is initially placed at a certain height above the target location, d_1 ($< 5B$), as shown in Fig. 4.1. Most of the analyses are performed for $d_1 = 2D$; however, some analyses are performed with larger d_1 to investigate the effects of larger penetration distance on test results. The vane is then penetrated vertically at a constant velocity to the targeted depth and then rotated at a constant angular velocity. FE modelling is also performed only for the vane rotation without any penetration, to study the effect of penetration. In the present study, the vane is rotated up to 90º, although it could be continued without any numerical issues. The geometry of the vane used in numerical simulations is shown in Table 1. For these dimensions, the vane area ratio (the ratio of the cross-section area of the vane to the circular area of the rotating vane) is 9% (less than 10% as recommended by ASTM D2573).

Table 4.1: Vane geometry used in FE simulation

Vane height, H (mm)	130
Vane diameter, D (mm)	65
Blade thickness, t_b (mm)	2
Shaft diameter above the vane, mm	10
Shaft diameter at the center of the vane, mm	6

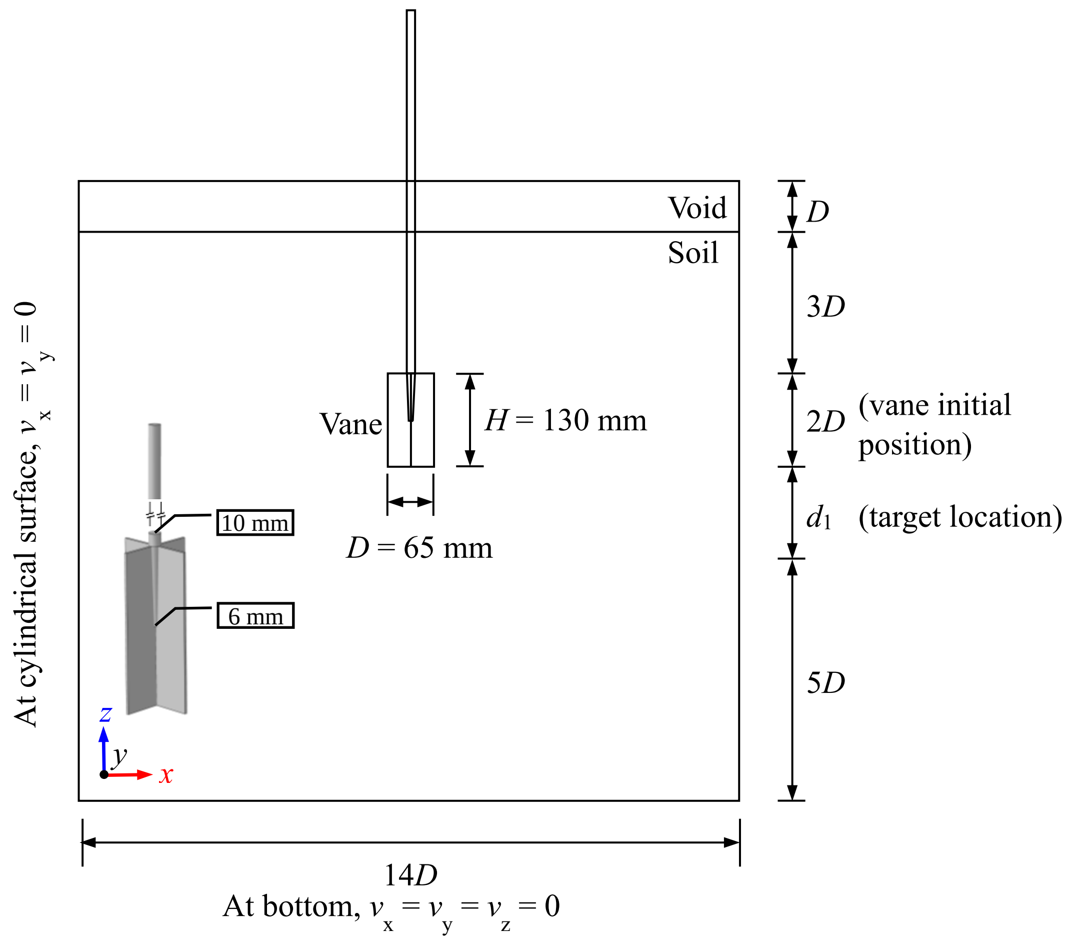

Figure 4.1: Details of FE modelling

4.4 Finite element modelling

The Coupled Eulerian-Lagrangian (CEL) approach available in Abaqus FE software is used for large deformation FE simulations. Most of the analyses were conducted for rectangular vanes; however, some analyses were conducted to show the effects of bottom tapering of the vane. For FE modelling of a rectangular vane, the shaft and vane are created separately, as shown in Figs 4.2(a) and 4.2(b), and are placed in position and then merged to model the complete vane as a unit body. The shaft is modelled as a cylinder-shaped deformable body, and then the bottom face is extruded up to the middle of the vane by using the 'draft angle' option available in the software. Then the shaft and vane are merged, and the intersecting boundaries are removed to make a unit rigid body with respect to a reference point, as shown in Fig 4.2(c). To model the tapered vane, the same procedure is followed as for the rectangular vane (Figs 4.2(a)–4.2(c)). However, the tapering portion of the vane blade is created separately and placed under four vane blades. Finally, a pyramid-shaped deformable part is created and attached at the very bottom of the joint of four tapering portions of vane blade (Fig. 4.2(d)). Then all the parts are merged, and the intersecting boundaries are removed to make a unit rigid taper vane with respect to a reference point. After that, the vane is placed in the targeted position in the soil domain, and further analyses are performed, as discussed below.

The FE mesh used in the numerical modelling is shown in Fig. 4.3. A dense mesh is used near the tip of the vane, where a significant amount of soil deformation is expected, due to the penetration and rotation of the vane. The boundaries are placed sufficiently far from the vane: the vertical (cylindrical) boundary at $7D$ from the center of the vane and the bottom horizontal boundary at $5D$ from the bottom of the vane during rotation. Analyses are also carried out with a larger soil domain, but no significant change in the result is found.

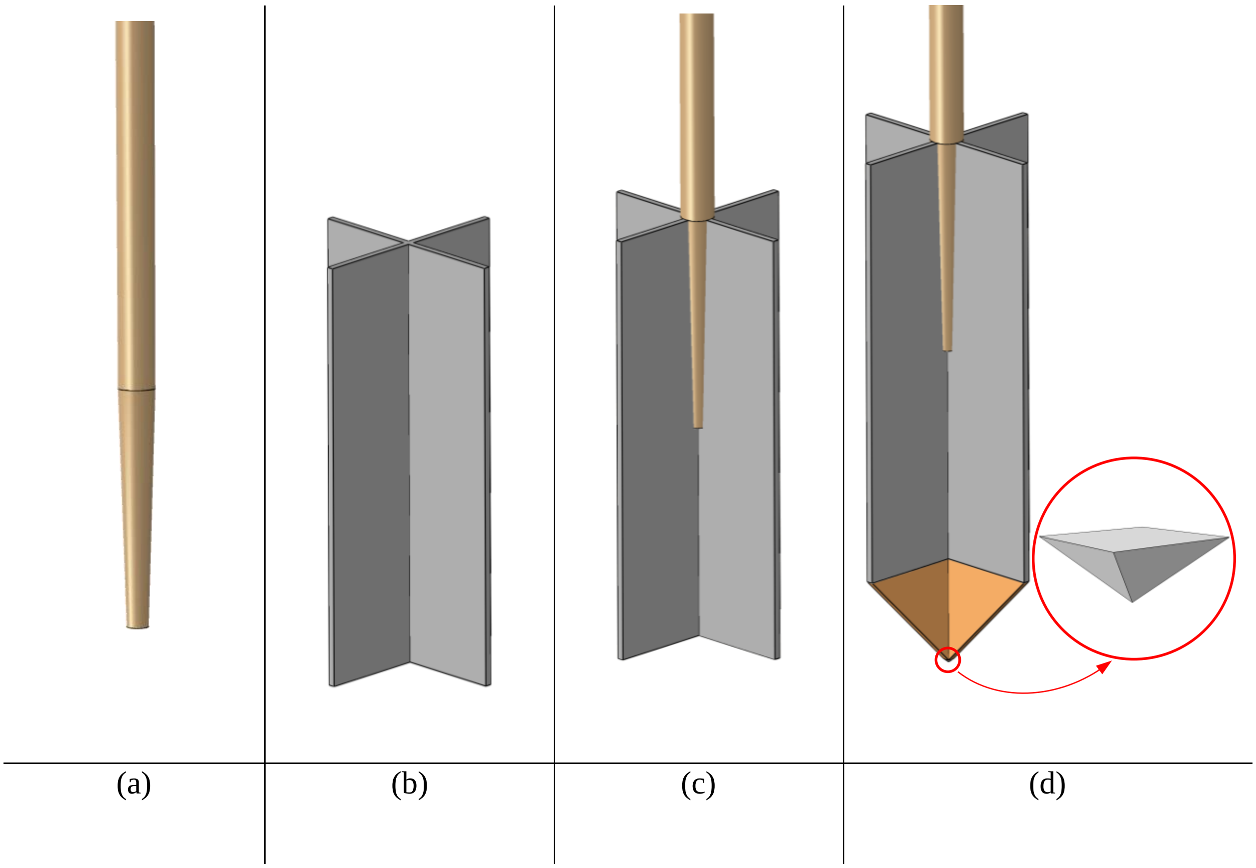

Figure 4.2: Modelling of the vane

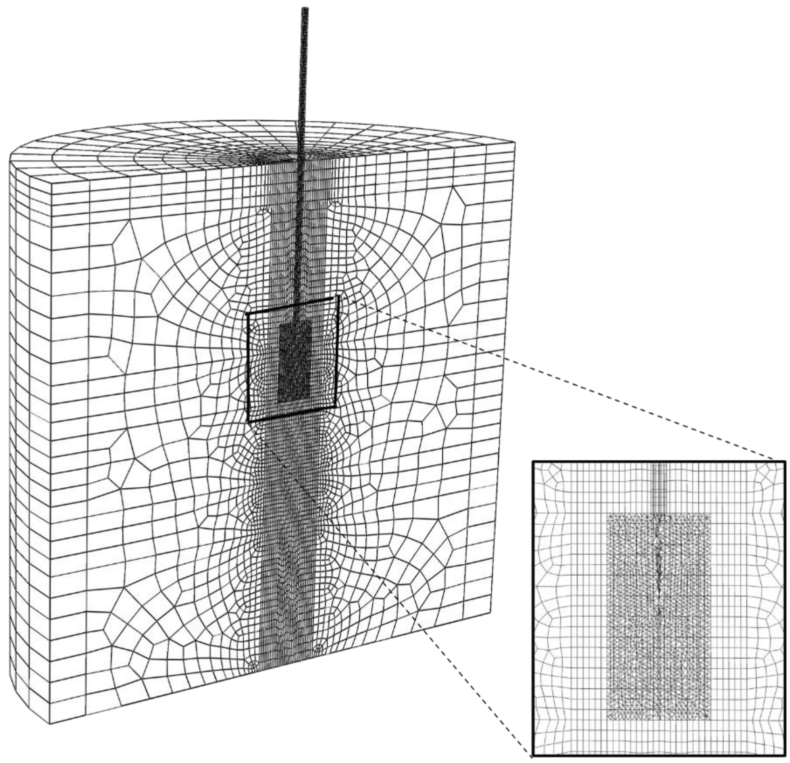

(a)

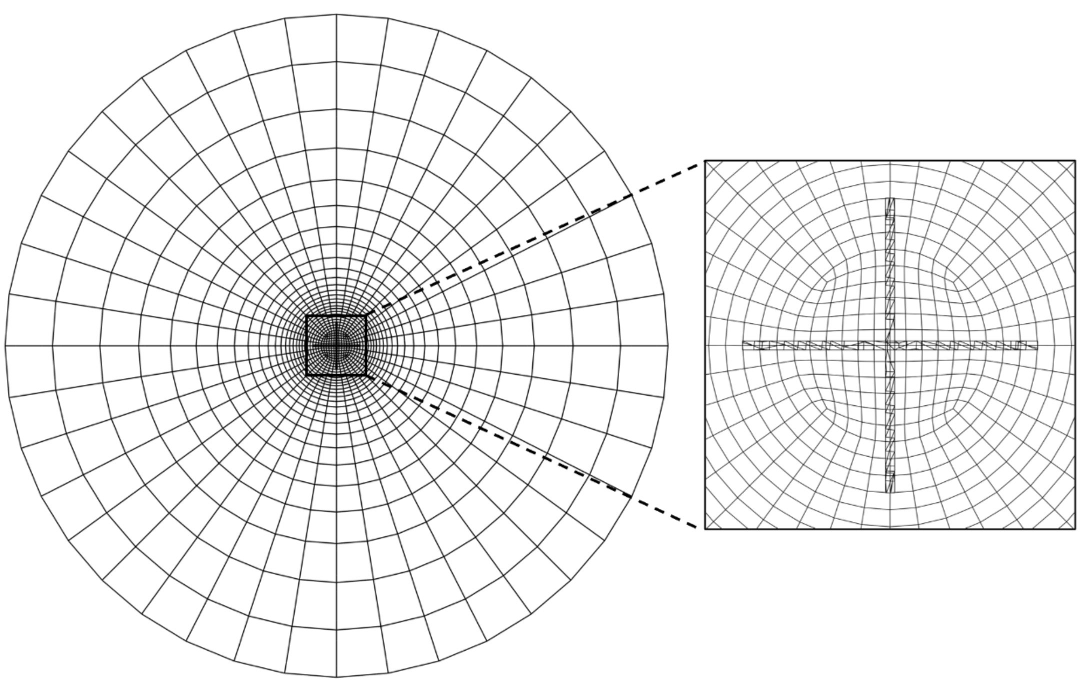

(b)

Figure 4.3: Finite element mesh (a) vertical section, (b) horizontal section

The FE model is comprised of three parts: soil, vane, and void. The soil is modelled as an Eulerian material, and the vane is modelled as a Lagrangian rigid body. In the present FE program, the Eulerian material (soil) can flow through the fixed mesh without causing numerical problems associated with mesh distortion. Further details on Eulerian-based FE modelling and the use of CEL for large deformation analysis (e.g., landslides, pipeline penetration, and pile jacking) are available in previous studies (Benson 1992; Qiu et al. 2012; Dey et al. 2015, 2016; Dutta et al. 2015; Karmaker and Hawlader 2018; Karmaker et al. 2019; Islam et al. 2019; Wang et al. 2019, 2020).

The Eulerian Volume Fraction (EVF) is used to define and track the flow of material during analysis. For an element, EVF = 0 represents no soil in that element (void), while EVF = 1 represents an element entirely filled with soil. EVF is between 0 and 1 for an element partially filled with soil.

The soil is modelled using EC3D8R elements in the software, which are 8-node linear brick, reduced integration, and hourglass control elements. The vane is modelled using C3D8R, which are also 8-node linear brick, reduced integration, and hourglass control elements. The vane is defined as a rigid body with a reference point.

At the bottom of the domain, zero velocity boundary conditions are applied in all three directions (i.e., $v_{\mathrm{x}} = v_{\mathrm{y}} = v_{\mathrm{z}} = 0$). Zero velocity boundary conditions in the x and y directions (i.e., $v_{\mathrm{x}} = v_{\mathrm{y}} = 0$) are also applied to the vertical cylindrical boundary. An undrained analysis is performed by giving the yield strength (σ_{y}), adopting the von Mises yield criterion ($\sigma_{\mathrm{y}} = 2s_{\mathrm{u}}$) as a function of strain rate, and strain softening. A frictionless interface condition between soil and vane is used.

The vane is penetrated and rotated by giving penetration and angular velocities at the reference point. The FE analysis consists of three steps of loading: gravity, penetration, and rotation.

4.5 Geotechnical parameters

Table 4.2 shows the geotechnical parameters used in this study. The clay is modelled as an elastic-plastic material with the strain-rate and strain-softening dependent undrained shear strength. The von Mises yield criterion is adopted unless otherwise mentioned. The elastic behaviour is modeled using the undrained Young's modulus and Poisson's ratio. All the details about constitutive modelling of soil, including post-peak softening, have already been discussed in Chapter 3.

Table 4.2: Geotechnical parameters used in the analysis

Parameters	Values
Total unit weight of soil, γ (kN/m$^{3)}$	16.7
Peak undrained shear strength, s_{u0} (kPa)	30
Remoulded undrained shear strength, s_{uR} (kPa)	17.64
Large displacement undrained shear strength, s_{uld} (kPa)	1
Undrained Young's modulus, E_{u} (MPa)	7.5
Undrained Poisson's ratio, ν_{u}	0.49
Reference shear strain rate, $\dot{\gamma}_{\mathrm{ref}}$ (/s)	0.05
δ_{95} (m)	0.03
δ_{ld} (m)	1.2
η	0.5
β	0.1

4.6 FE simulation results

4.6.1 Vane shear tests in elastic-plastic clay

To validate the numerical modelling technique, a simulation is performed first with a simple elastic–perfectly plastic soil model and the results compared with an analytical solution which is commonly used for estimation of s_u from the measured torque. Figure 4.4 shows that the torque increases with rotation and then remains constant at T_{max}.

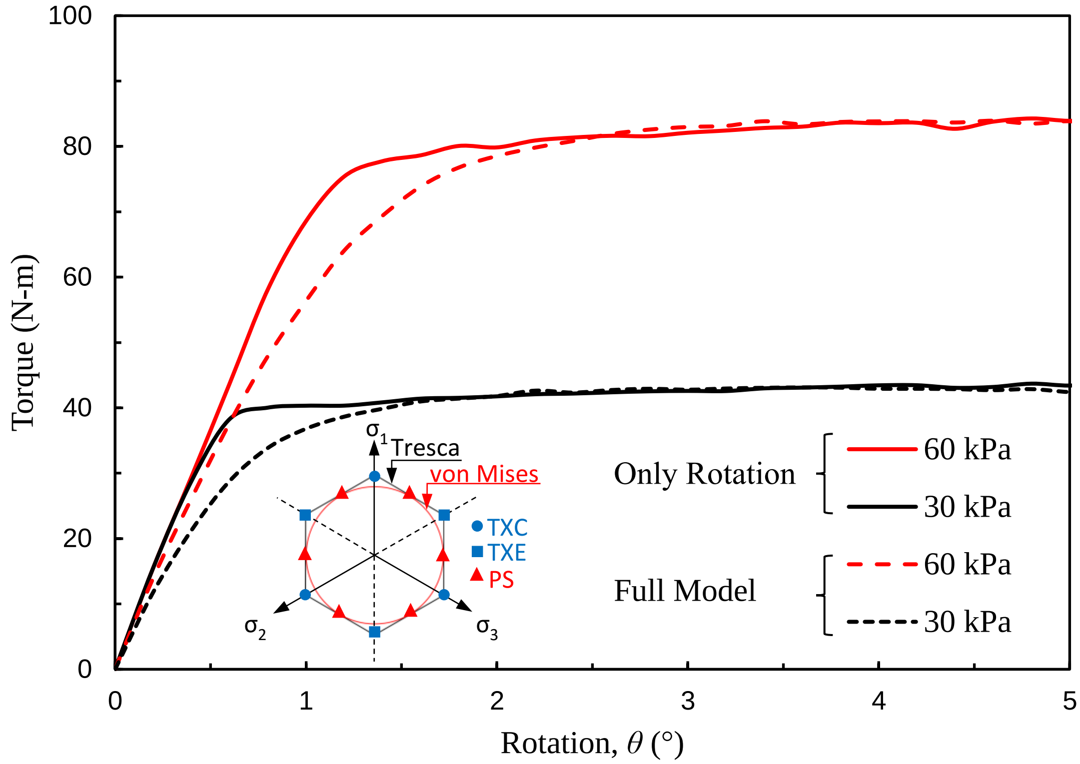

Figure 4.4: Torque for elastic perfectly plastic soil

It is common practice to assume uniform mobilized shear strength on the cylindrical rupture surface. However, for the top and bottom surfaces of the soil cylinder, the following three types of distribution of s_u are assumed:

a) Triangular: The mobilized shear strength is zero at the center and increases linearly to the maximum value at the periphery,

b) Uniform: A constant s_u, like that at the periphery, is mobilized over the whole area, and

c) Parabolic: The shear strength is zero at the center and maximum at the periphery, and mobilized s_u varies parabolically.

For these three distributions, the maximum torque (T_{max}) is related to the shear strength and dimension of the vane as:

$$T_{max} = \pi s_{\text{u\_vane}} \left(\frac{D_e^2 H_e}{2} + \frac{D_e^3}{8} \right) \tag{4.1}$$

$$T_{max} = \pi s_{\text{u\_vane}} \left(\frac{D_e^2 H_e}{2} + \frac{D_e^3}{6} \right) \tag{4.2}$$

$$T_{max} = \pi s_{\text{u\_vane}} \left(\frac{D_e^2 H_e}{2} + \frac{3D_e^3}{20} \right) \tag{4.3}$$

where $s_{\text{u\_vane}}$ is the undrained shear strength estimated from the vane shear test. In these equations, D_e and H_e represent the "effective" diameter and height of the vane, respectively. In FE analysis, the calculation is performed using the effective dimension because the failure occurs through the element (integration point) next to the blade. In this study, D_e and H_e are calculated by adding one element of thickness (i.e., half of element thickness from both sides) to the diameter and height of the vane, respectively. In this simulation, D = 65 mm, and H = 130 mm. The element thickness near the tip of the blade is ~3.75 mm, and immediately above and below the vane is ~6.5 mm, which gives D_e = 68.75 mm and H_e = 136.5 mm.

Figure 4.4 shows that the torque (T) increases with rotation (θ), reaches the maximum at $\theta \sim 2°$, and then remains constant. One key observation is that the torque increases slowly with rotation for the cases when the vane was penetrated first and then rotated, as compared to that of only rotation cases. However, in both cases, the same value of maximum torque is found. Kimura and Saitoh (1983) also found the maximum torque appeared at a slightly larger rotation angle when the vane was penetrated before rotation was applied.

The von Mises and Tresca failure criteria are commonly used to model the undrained behaviour of clay. When the yield strength is defined using the Tresca failure criterion, it basically defines s_u in triaxial condition (the same for triaxial compression (TXC) and triaxial extension (TXE)), as shown in the inset of Fig. 4.4. However, most of the elements near the cylindrical rupture surface are close to the plain strain (PS) condition (shown by the triangle in the inset of Fig. 4.4). In other words, to mobilize similar s_u on the ruptured surface, a higher value of s_u should be given when modelling with Tresca criteria, which is $2/\sqrt{3}$ times the value of s_u used in FE modelling with von Mises criteria. When an analysis is performed with Tresca criteria with $\sigma_y = 2[(2/\sqrt{3}) \times 30$ kPa] and $2[(2/\sqrt{3}) \times 60$ kPa], exactly the same torque–rotation curves shown in Fig. 4.4 are obtained. This implies that the elements which are in PS conditions primarily control the torque–rotation relationship, and the von Mises yield criteria with the inscribed circle could be used to simulate this. The use of von Mises criteria has some advantages in defining the strain-softening using this software because of its simplicity in the calculation of accumulated plastic shear strain, as discussed in the following sections.

Using Eqs. (4.1)–(4.3), $T_{\max}$ is calculated with $s_{\mathrm{u\_vane}} = (2/\sqrt{3}) \times 30$ kPa and $(2/\sqrt{3}) \times 60$ kPa is calculated, which give $T_{\max}$ of 39.4–40.8 kN-m and 78.7–81.7 kN-m, respectively, for these two shear strengths. These values are comparable to the FE calculated values in Fig. 4.4.

De Alencar et al. (1981) conducted a two-dimensional FE simulation, which gives the torque only from the cylindrical surface. Compared with the analytical solution ($T_{\max} = \pi s_{\mathrm{u\_vane}} D_e^2/2$ for a unit height of the vane derived from Eq. (4.1)), they showed that the Tresca criterion underestimates and von Mises (circumscribed) criterion overestimates the FE calculated value. This discrepancy has been clarified from the present simulations. That is, if the three-dimensional simulation is performed with an actual height of the vane with a Tresca or inscribed von Mises criterion, the FE calculated maximum torque matches the analytical solution, provided $s_{\mathrm{u\_vane}}$ is considered for the triaxial condition. In other words, based on measured torque in the field, the calculated $s_{\mathrm{u\_vane}}$ using Eqs. (4.1)–(4.3) represents the strength in the triaxial condition, not in plane strain conditions.

4.6.2 *Vane shear tests in sensitive clay*

Sensitive clays show a significant strain-softening behaviour during undrained loading. Strain softening could disturb the soil and affect torque–rotation behaviour. In addition, the rate of shearing could affect undrained shear strength behaviour. The effects of strain rate and strain softening are investigated in this section.

The mobilized undrained shear strength (s_{u}) of the sensitive clay is modelled as:

$$s_{\mathrm{u}} = f_1 f_2 s_{\mathrm{uy}} \tag{4.4}$$

where f_1 is a strain-softening factor, f_2 is a strain-rate factor and s_{uy} is undrained shear strength at a very low strain rate, which are described by the following equations:

$$f_1 = \begin{cases} \dfrac{s_{\mathrm{uR}}}{s_{\mathrm{u0}}} + \left(1 - \dfrac{s_{\mathrm{uR}}}{s_{\mathrm{u0}}}\right) e^{-3\delta/\delta_{95}} & \text{if } 0 \leq \delta < 2\delta_{95} \\ \dfrac{s_{\mathrm{uR}}}{s_{\mathrm{u0}}} - \dfrac{s_{\mathrm{uR}} - s_{\mathrm{uld}}}{s_{\mathrm{u0}}} \dfrac{\delta - 2\delta_{95}}{\delta_{\mathrm{ld}} - 2\delta_{95}} + c & \text{if } 2\delta_{95} \leq \delta < \delta_{\mathrm{ld}} \\ \dfrac{s_{\mathrm{uld}}}{s_{\mathrm{u0}}} + c & \text{if } \delta > \delta_{\mathrm{ld}} \end{cases} \tag{4.5}$$

$$f_2 = 1 + \eta \left(\frac{\dot{\gamma}}{\dot{\gamma}_{\mathrm{ref}}}\right)^{\beta} \tag{4.6}$$

The details of these equations have been discussed in Chapter 3.

Figure 4.5 shows the calculated torque where the effects of strain softening and strain rate on s_u are implemented using Eqs. (4.5) and (4.6), respectively. Other soil parameters used in these simulations are shown in Table 4.2. The simulations are performed only for rotation and penetration followed by rotation. Note that in both cases, three-dimensional modelling is performed. In both cases, the torque reduces after the peak value (T_{max}). Figure 4.5 shows that T_{max} is 39.6 kN-m and 25.6 kN-m for the only rotation and full model (penetration plus rotation), respectively, which implies that soil disturbance due to penetration reduces the T_{max} by 35% (= (39.6-25.6)/39.6). The value of T_{max} for the full model is approximately 65% of that in rotation-only cases, which is because of soil disturbance due to penetration. Further details on soil disturbance in terms of plastic shear strain generation are provided in the following sections. At a large rotation (e.g., θ = 90°), FE calculated torque is almost the same for both cases, because the mobilized strength on the cylindrical rupture surface is almost the same at this stage. The rotation could be continued without any numerical issues; however, it is not performed, for two reasons:

(i) even in the field, the fully remoulded shear strength conditions do not develop, even after a number of rotations, and (ii) response at this strain level is not the focus of the present study.

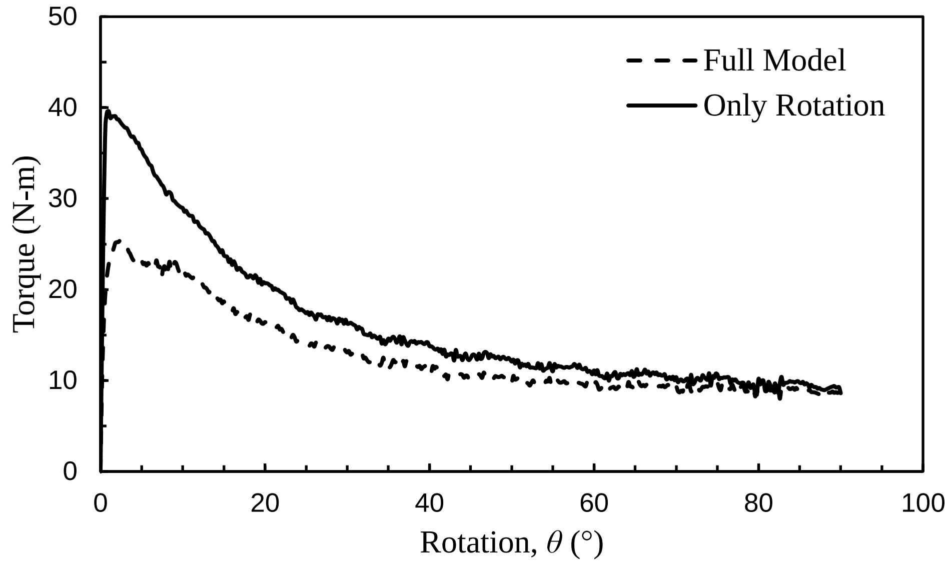

Figure 4.5: Torque for strain-softening behaviour

The percentage of decrease in maximum torque due to penetration disturbance also depends on the initial undrained shear strength of the soil. Figure 4.6 shows that the percentage of decrease in maximum torque due to penetration reduces with an increase in the initial undrained shear strength of the soil. The penetration induced disturbance effects on T_{max} reduces for larger s_{u0}.

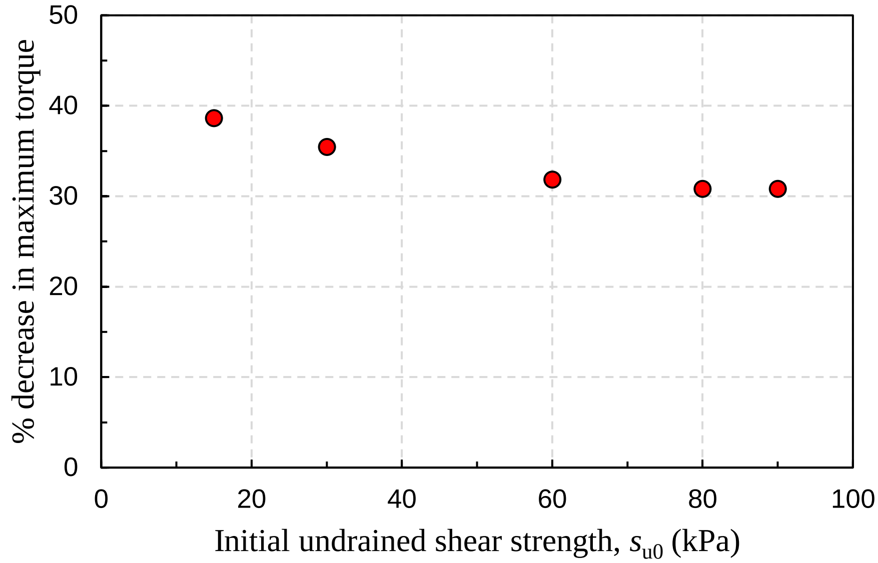

Figure 4.6: Effect of initial undrained shear strength maximum torque

4.6.3 Effect of blade thickness

Figure 4.7 shows the calculated maximum torque and torque at a sufficiently large rotation, both for the full model and only rotation cases. For the full model, the maximum torque decreases with an increase in blade thickness. It has been assumed in previous studies that an extrapolation of the results to the zero-blade thickness provides an estimation of undrained shear strength without any disturbance effect caused by vane insertion (La Rochelle et al. 1973; Chandler 1988; Cerato and Lutenegger 2004). The shear strength at the zero-blade thickness is called "zero disturbance" shear resistance. These studies found an approximately linear relationship between the blade thickness or perimeter ratio and the maximum undrained shear strength. The present FE simulations also show a linear relationship. An approximately 12% increase in the maximum torque at zero blade thickness, compared to that of 2 mm blade thickness (perimeter ratio, α = 3.9% and s_{u0}/s_{uR} = 5), is found, while the increase is 19% for s_{u0}/s_{uR} = 10.

The only rotation model calculates significantly higher maximum torques than that of the full model. As an example, for 2-mm blade thickness, the only rotation model calculates $T_{\max}$ = 39.6 N-m while it is 25.6 N-m for the full model. This implies that the penetration of the vane has a significant influence on the maximum torque in the tests in sensitive clays.

La Rochelle et al. (1973) found an increase in undrained shear strength of about 15% for the Saint-Louis site and 11% for the Saint-Vallier site when they were extrapolated to zero-blade thickness. Roy and Leblanc (1988) found an approximate increase in undrained shear strength of about 6.5% and 9% higher than the standard vane in the Saint-Alban and Saint-Louis sites, respectively. They also found that disturbance varies not only with blade thickness but also with clay types. La Rochelle et al. (1973) have used a larger perimeter ratio vane and found more disturbance for the Saint-Louis site than that reported by Roy and Leblanc (1988).

The maximum torque is almost independent of blade thickness for the only rotation model (Fig. 4.7). Figure 4.7 also shows that, at a large rotation (90°), the calculated torque is almost the same for both models (only rotation and full model), and is independent of blade thickness. As significant remoulding occurs at this rotation level and there is no significant difference in mobilized shear strength of the severely remoulded soil, therefore, an almost similar torque is calculated for all the cases.

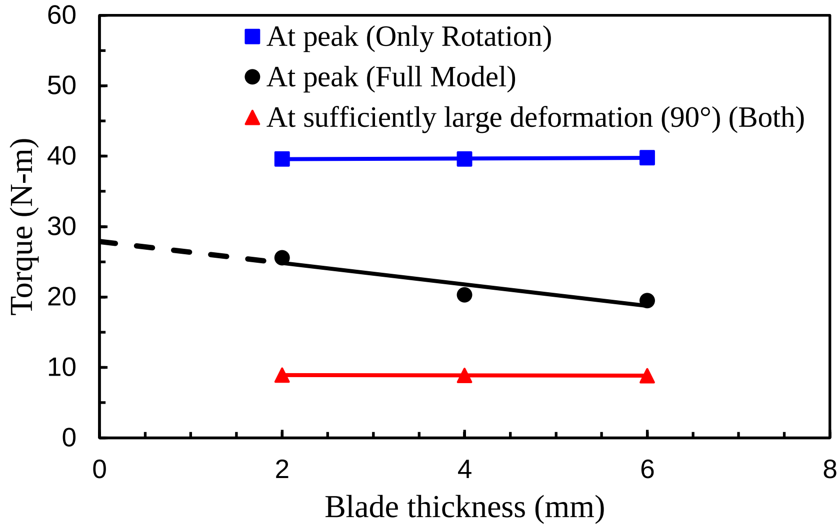

Figure 4.7: Effect of blade thickness on peak and residual torque

4.6.4 Effect of sensitivity (s_{u0}/s_{uR})

Figure 4.8 shows the effects of s_{u0}/s_{uR} on the maximum torque and the torque at sufficiently large rotation (90°). For the only rotation model, the maximum torque is almost the same, independent of s_{u0}/s_{uR}. However, in the full model, the maximum torque also decreases with an increase in s_{u0}/s_{uR}. The higher the value of s_{u0}/s_{uR}, the higher the shear strength degradation during penetration, which influences the mobilized torque during rotation. Therefore, smaller torque is calculated even in the pre-peak state of rotation in the full model. At large rotations, the soil becomes highly remoulded, and no significant difference in torque is found for the only rotation and full model simulations. However, the calculated torque at this stage is higher for lower s_{u0}/s_{uR}. Note that the rotation does not cause extremely large shear displacements (e.g., δ_{ld} in Eq. (4.5)); therefore, the torque is still dependent on s_{u0}/s_{uR}.

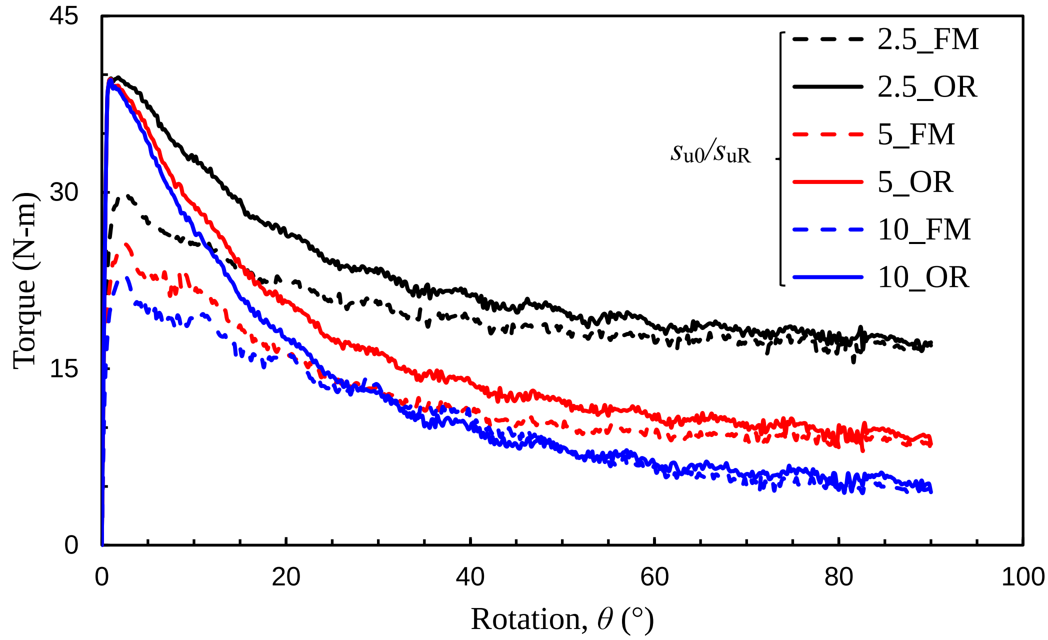

Figure 4.8: Effect of s_{u0}/s_{uR} on peak and post-peak response

4.6.5 Effect of penetration depth

In the field, the vane is normally penetrated to 5 times the diameter of the borehole. However, numerical simulation of such penetration depth will be computationally very expensive, as fine mesh has to be used to model the soil around the thin blades. Figure 4.9 shows the torque-rotation graphs for 65 mm, 130 mm, and 260 mm ($d_1 = D$, 2D, and 4D as shown in Fig. 4.1) penetrations prior to rotation. In the case of 65-mm penetration, the maximum torque is considerably higher because of less disturbance during penetration. However, for the 130-mm and 260-mm penetrations, the calculated torque is almost the same. This implies that the soil disturbance around the vane would be similar if it penetrates a sufficiently large distance. Therefore, all the simulations in this study are performed with 130 mm penetration.

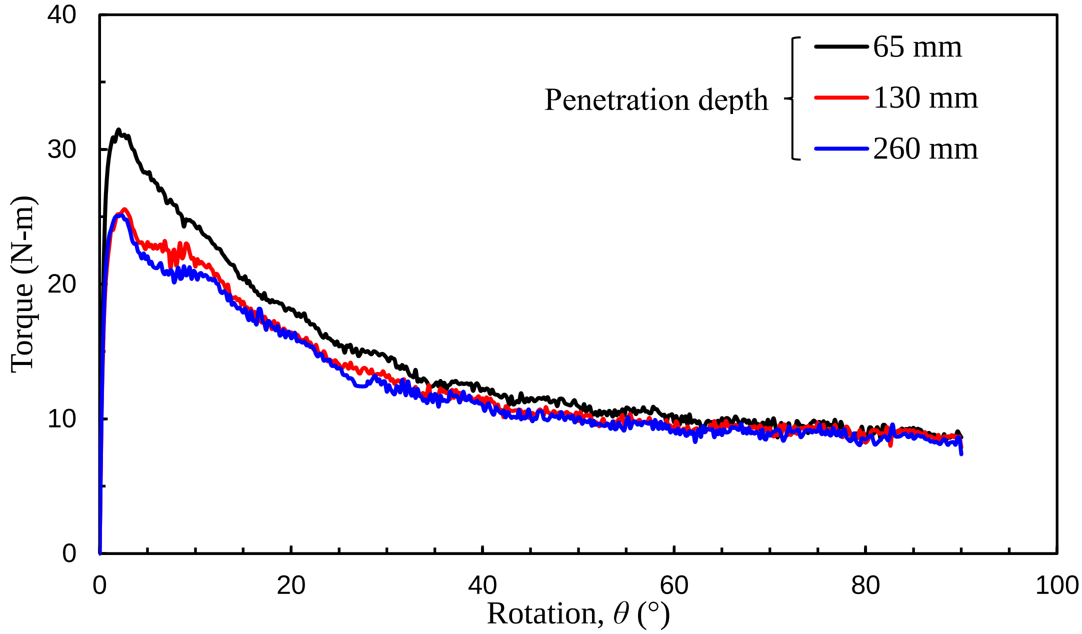

Figure 4.9: Effects of penetration depth prior to rotation on torque

Figure 4.10 shows the equivalent plastic shear strain ($\varepsilon_{\mathrm{q}}^{\mathrm{p}}$) at the end of penetration at three different sections of vane: top, middle, and bottom. For the case of 65-mm penetration depth, $\varepsilon_{\mathrm{q}}^{\mathrm{p}}$ is not well developed around the top section of the vane because the vane is not penetrating through this section. However, in the case of 130-mm penetration, $\varepsilon_{\mathrm{q}}^{\mathrm{p}}$ is fully developed throughout the depth of the vane. Also, no significant difference is found for a larger penetration depth (260-mm), because, starting from 130-mm to a larger penetration depth, the soil contributing to the torque is disturbed throughout the depth of the vane.

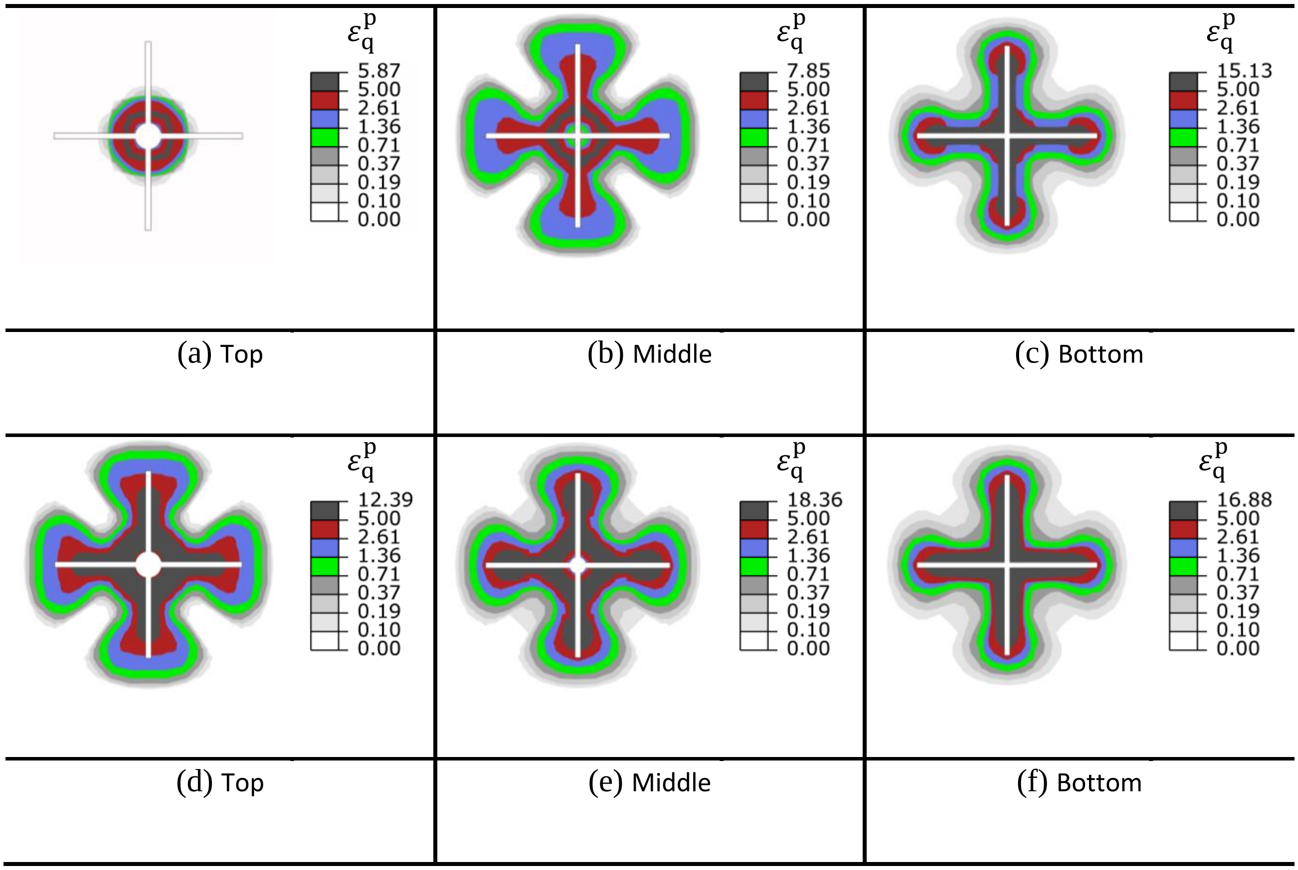

Figure 4.10: Equivalent plastic shear strain for different penetration depths: (a–c) for 65 mm and (d–f) for 130 mm

4.6.6 Stress distribution on the vertical plane

Figure 4.11 shows the variation of normalized von Mises stress (σ_e/σ_{y0}) along a vertical path at 45º from the blade in the soil domain, as indicated by a red dotted line in Fig.4.11. This figure shows the variation of stress for an elastic perfectly plastic soil model for different rotations. As shown, the stress is maximum at the top and bottom corners of the vane. That means the shear stress is higher at the ends than in the middle. At peak and post-peak conditions, a uniform shear stress distribution along the edge of the vane is found. Also, on the cylindrical surface, full shear strength is mobilized. Note that the distribution of shear stress on the horizontal plane has been discussed in Chapter 3 from two-dimensional simulations.

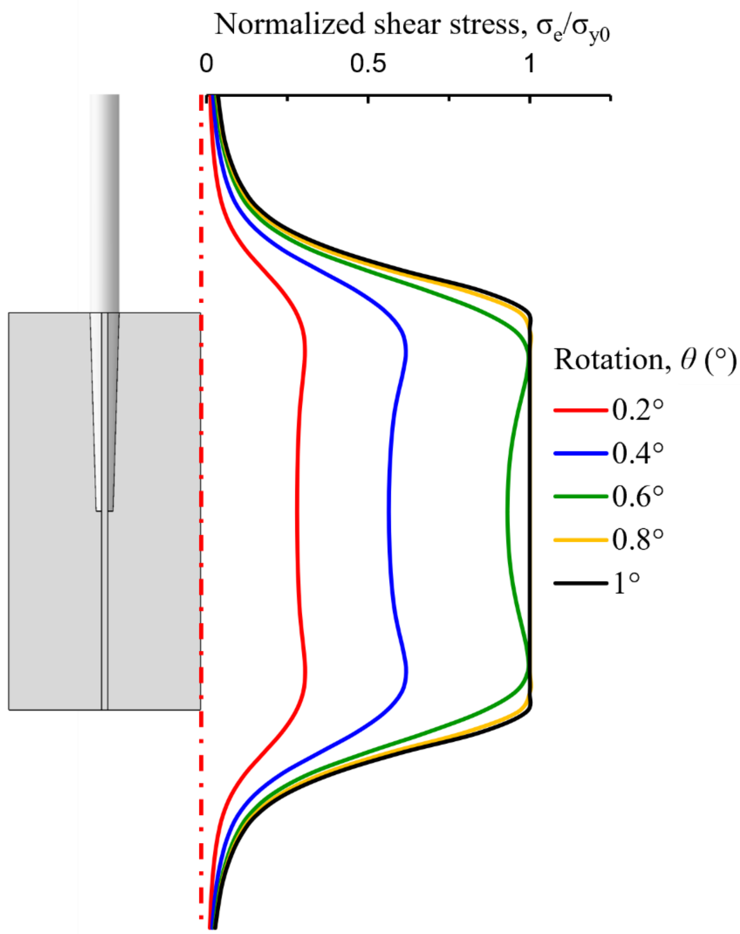

Figure 4.11: Shear stress distribution on the vertical plane for elastic perfectly plastic soil model

Figure 4.12 shows the variation of normalized von Mises stress (σ_e/σ_{y0}) for sensitive clay. From the start of rotation up to the maximum torque, it follows the same pattern as shown above (Fig. 4.11) for the elastic perfectly plastic soil model. At the post-peak region, stress starts to decrease because of the strain-softening behaviour of the soil. The decrease in σ_e/σ_{y0} is initially higher at the middle of the vane than at the top and bottom corners, and at remolded conditions, the distribution is uniform throughout the height of the vane.

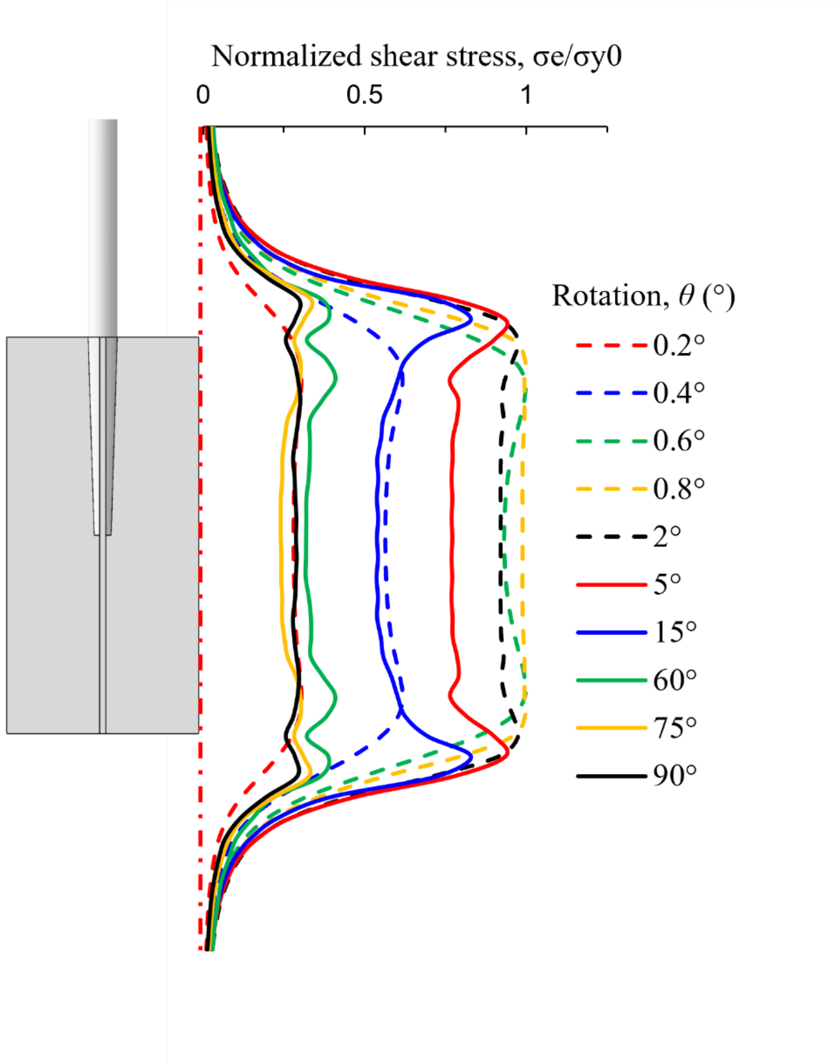

Figure 4.12: Shear stress distribution on a vertical plane for soil model with strain rate and strain softening effects (δ_{95} = 0.03 m)

4.6.7 Effect of post-peak strength degradation parameter (δ_{95})

In addition to s_{u0}/s_{uR}, the parameter δ_{95} in Eq. (4.5) controls the softening rate—the higher the δ_{95}, the slower the post-peak shear strength degradation rate. Figure 4.13 shows the simulation results of a set of analyses with δ_{95} = 0.1 m, 0.03 m, and 0.01 m. For the only rotation model, all the values of δ_{95} give the same maximum torque, and the torque decreases with rotation. The smaller the value of δ_{95}, the faster the reduction of torque. In the full models, the peak strength is also less for smaller values of δ_{95}, which is because of higher disturbance during penetration, as discussed in previous sections. At large rotations ($\theta > 80°$), the calculated torque is almost the same for δ_{95} = 0.03 m and 0.01 m because of sufficient remoulding of soil. However, the shear strength degrades slowly for δ_{95} = 0.1 m; therefore, it gives slightly higher torque even at this level of rotation.

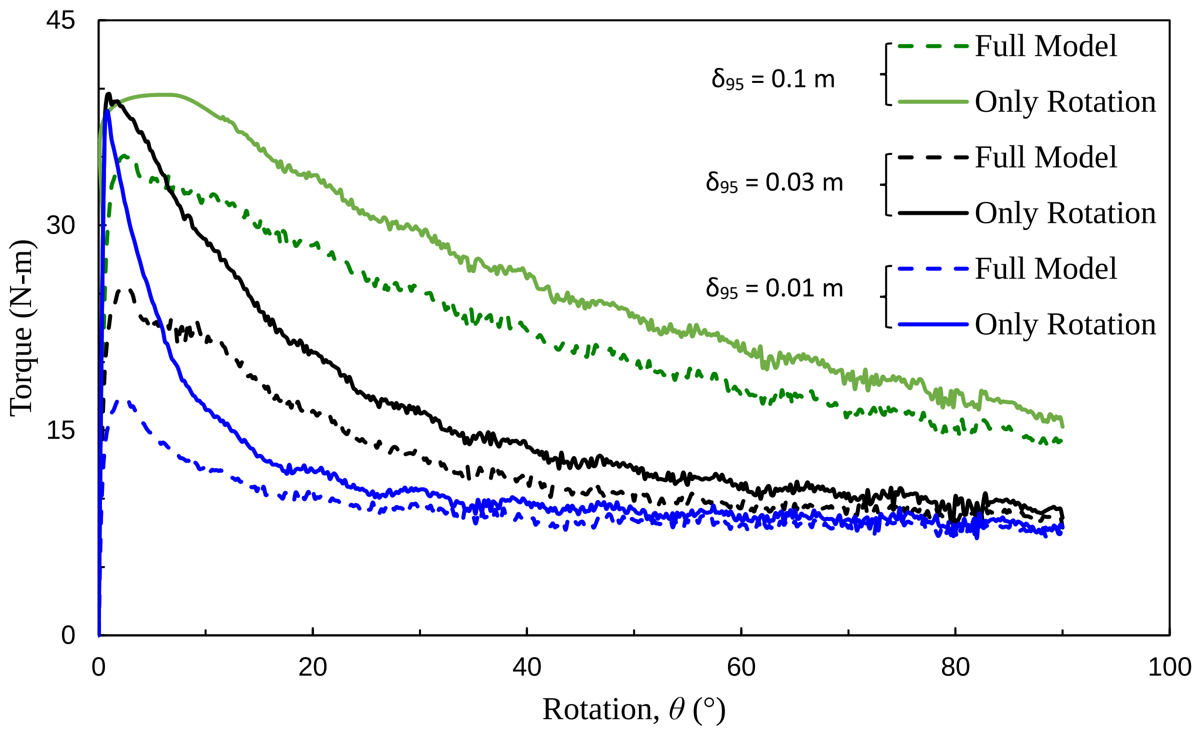

Figure 4.13: Effect of post-peak strength degradation parameter (δ_{95})

4.6.8 Velocity profile

Figures 4.14 and 4.15 show the instantaneous velocity vectors of soil elements for different soil properties and at different times for the only rotation model and full model, respectively. For the only rotation model, the instantaneous velocity vectors of soil particles are always on a circular path and independent of soil properties. Figure 4.14 shows the velocity vectors of soil elements when the maximum torque is mobilized for different soil models and only rotation cases.

In the case of the full model, the instantaneous velocity vectors of soil particles depend on soil properties. The instantaneous velocity vectors are almost circular for the elastic perfectly plastic soil model (Fig. 4.15(a)). However, the scenario is very different with an increase in s_{u0}/s_{uR}. For sensitive soil, due to the penetration of the vane, soil close to the vane gets disturbed, and the disturbance is more for a larger s_{u0}/s_{uR}. For soil with $s_{u0}/s_{uR} = 2.5$, no significant difference is found, compared with the elastic perfectly plastic soil model. However, for $s_{u0}/s_{uR} = 5$, there is a tendency of diagonal movement of some soil elements; in fact, some soil elements move inward. The instantaneous velocity of the soil is in a circular path when the rotation is around 45º. The soil around the vane gets more disturbed due to penetration for higher s_{u0}/s_{uR}. For $s_{u0}/s_{uR} = 10$, some soil elements show inward instantaneous velocity, and after rotation to ~45º, the velocity profile is almost circular.

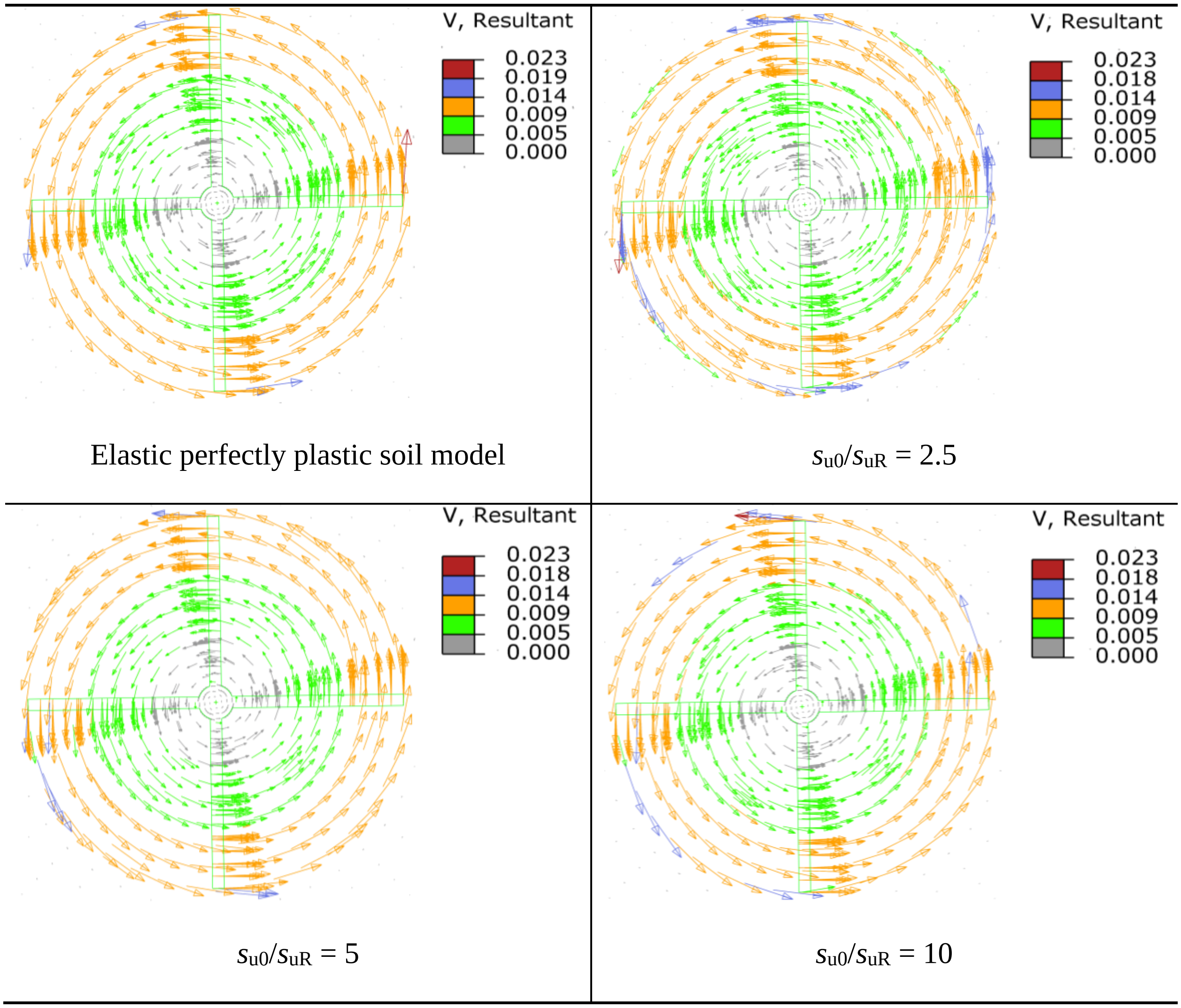

Figure 4.14: Velocity vectors of soil elements for only rotation model

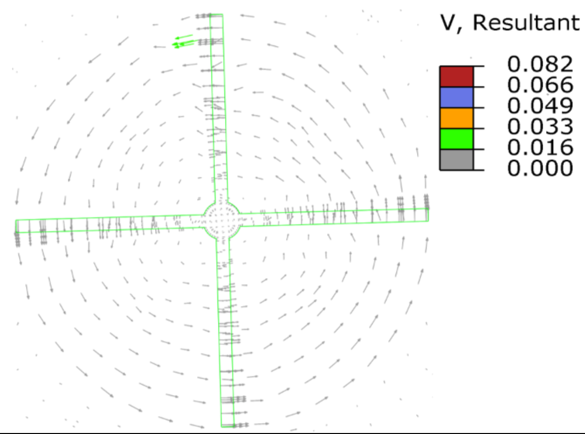

(a) Elastic perfectly plastic soil model

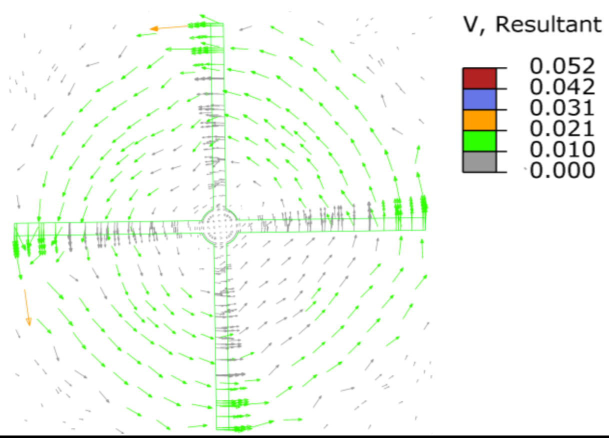

(b) pre peak

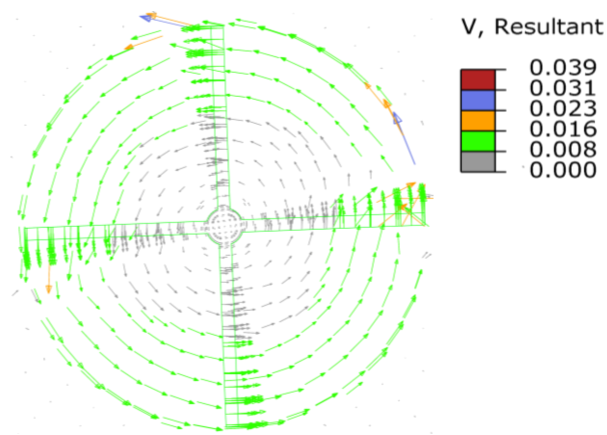

(c) peak

s_{u0}/s_{uR} = 2.5

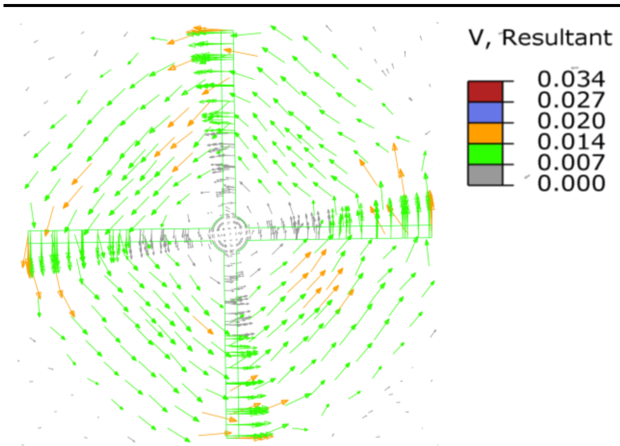

(d) pre peak

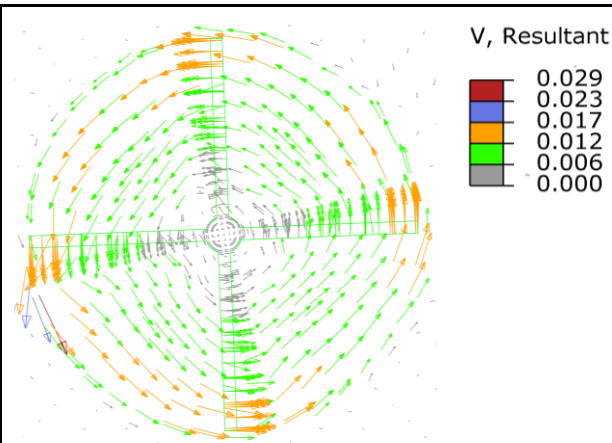

(e) peak

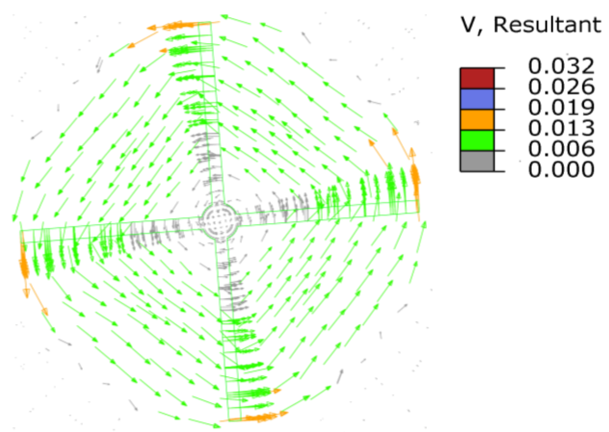

(f) post peak

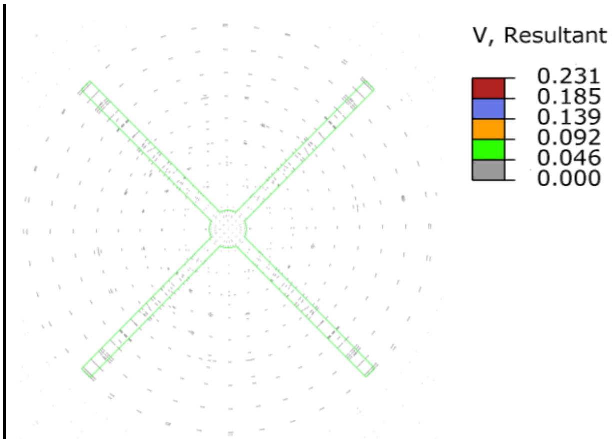

(g) post peak (45°)

$s_{u0}/s_{uR} = 5$

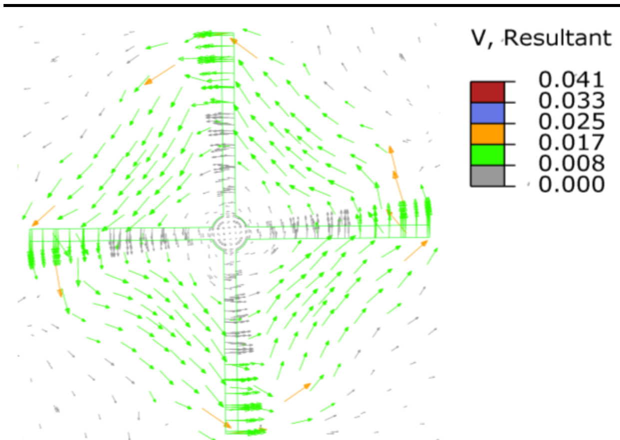

(h) pre peak

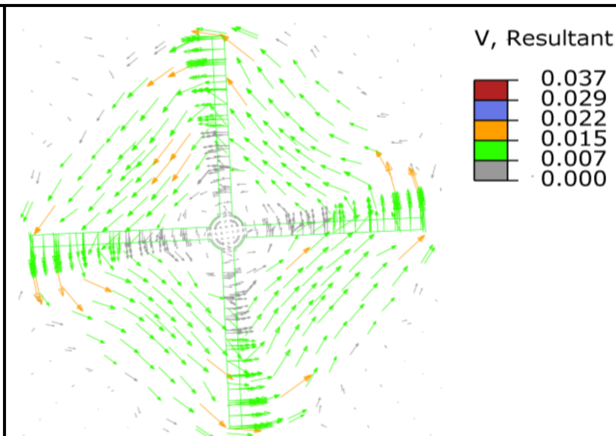

(i) peak

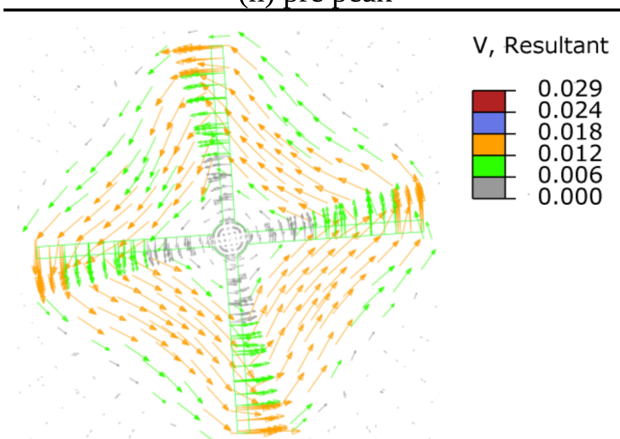

(j) post peak

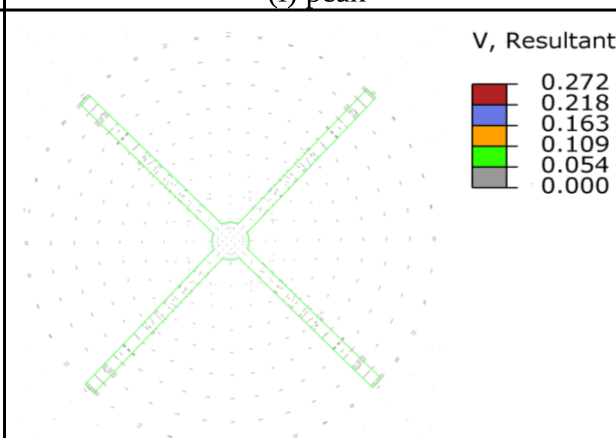

(k) post peak (45°)

$s_{u0}/s_{uR} = 10$

Figure 4.15: Velocity vectors of soil elements for full model

4.6.9 Normalized penetration resistance

During penetration, soil gets disturbed, and the disturbance depends on several factors. The amount of disturbance affects the response in subsequent rotation. In this section, the discussion is focused primarily on normalized penetration resistance (N) versus penetration depth, the effect of blade thickness (e), and post-peak shear strength degradation parameters (s_{u0}/s_{uR} and δ_{95}).

In the undrained analysis, if a body is penetrated into the soil, the penetration resistance comes from two sources: resistance due to the shear strength of the soil (F_s) and self-weight. Self-weight is like buoyancy force (F_b). The resistance provided by soil is obtained as $F_s = F - F_b$, where F is the total resistance. F_b is calculated by multiplying the vane volume with the unit weight of the soil. Then, the normalized penetration resistance is calculated as $N = F_s/s_u A_v$, where A_v is the cross-sectional area of the vane. Here, only the cross-sectional area of the vane is used to calculate N.

Figures 4.16(a)–4.16(c) show the normalized penetration resistance for different e, $s_{u0}/s_{uR,}$ and $\delta_{95,}$ respectively. An increase in blade thickness decreases the normalized penetration resistance because the larger blade thickness causes more disturbance of the soil, resulting in lower normalized penetration resistance (Fig. 4.16(a)) (when the values of s_{u0}/s_{uR} = 5 and δ_{95} = 0.03 m are kept the same for all the cases). Figure 4.16(b) shows the comparison between penetration resistances for an elastic perfectly plastic soil and sensitive clays (s_{u0}/s_{uR} = 2.5, 5 and 10) when blade thickness, e = 2 mm and δ_{95} = 0.03 m, are kept constant. For the elastic perfectly plastic soil, the normalized penetration resistance is higher, and it remains constant after the maximum value, as there is no degradation of shear strength. However, the normalized penetration resistance decreases in sensitive clays, and the decrease is higher for larger s_{u0}/s_{uR}. Figure 4.16(c) shows the effect of δ_{95} on normalized penetration resistance when blade thickness, e = 2 mm and s_{u0}/s_{uR} = 5 are kept constant. A lower value of δ_{95} means the undrained shear strength degrades quickly, resulting in lower normalized penetration resistance.

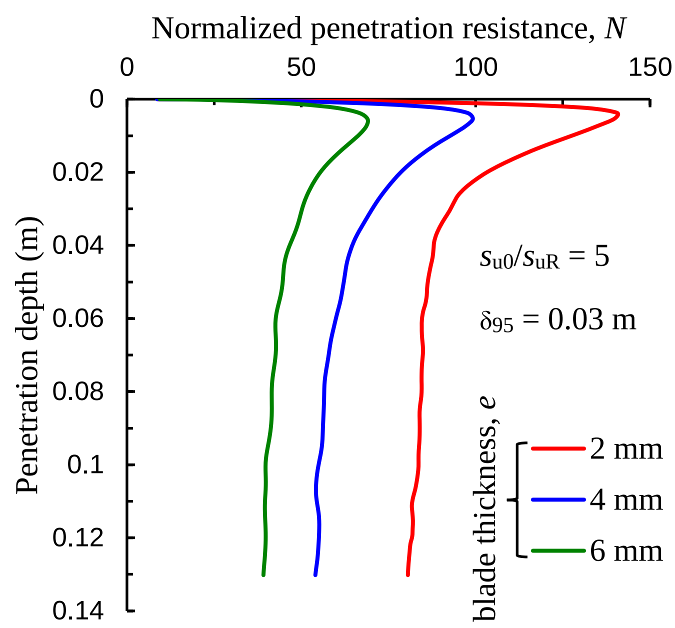

(a)

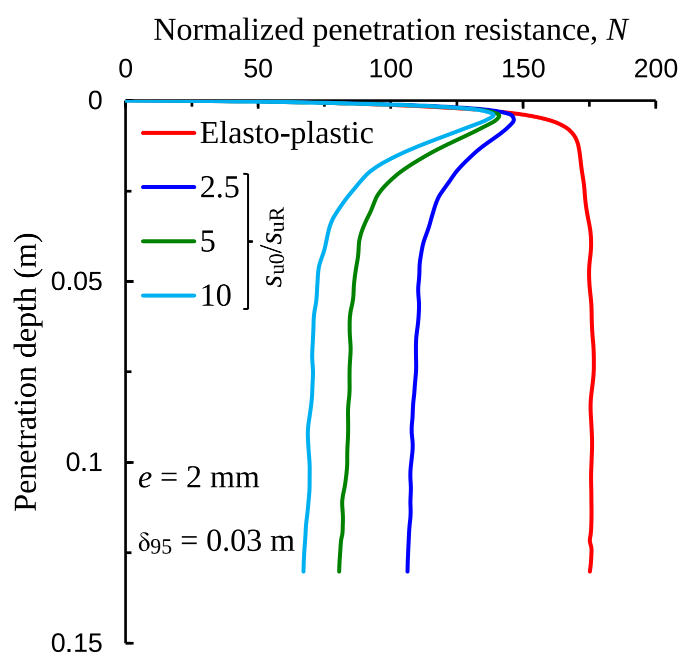

(b)

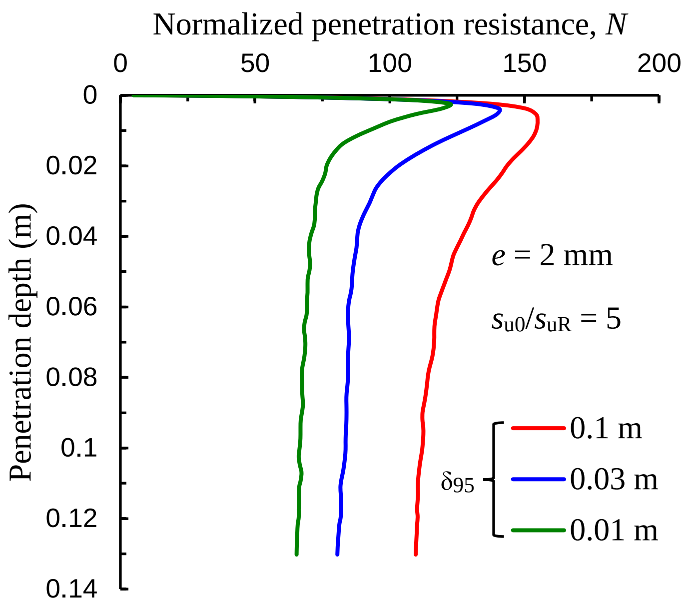

(c)

Figure 4.16: Normalized penetration resistance: (a) effect of blade thickness (e) (b) effects of s_{u0}/s_{uR}; and (c) effects of δ_{95}

The amount of disturbance during vane penetration also affects the response in subsequent rotation. In other words, penetration plays a very significant role in vane shear tests. In the present study, it is also found that after a certain level of penetration, there is no significant change in normalized penetration resistance, and that is why further penetration is not considered in this study, to save the computational cost. However, to check if there is any effect of larger penetration depth, one analysis is performed where the vane is penetrated to 260 mm prior to rotation (as discussed above); however, no significant change in torque–rotation response is found.

4.6.10 Effect of tapering

The ends of the vane may be flat or tapered. The taper angle is usually 0º for a rectangular vane and 45º for the typical tapered vane. The tapering can be on both ends or only at the bottom of the vane. The upper tapered vane has the advantage during withdrawal, and the bottom tapered vane can be used to facilitate penetration into the soil (ASTM D2573, 2018). The tapered vane is also used for measuring the anisotropic effect. Silvestri and Aubertin (1988) used both rectangular-shaped and diamond-shaped vanes to study the effect of anisotropy on undrained shear strength, though anisotropy is beyond the scope of the present study. Only a bottom tapered vane is used in the present study, to investigate the effect of penetration on isotropic soil.

The general expression for calculating the undrained shear strength from the measured torque for different types of vanes (such as rectangular, only bottom taper, and both ends taper, as shown in Fig. 4.17), is (ASTM D2573, 2018):

$$s_{\mathrm{u0}} = \frac{12\, T_{\max}}{\pi D^2 \left(\frac{D}{cos(i_{\mathrm{T}})} + \frac{D}{cos(i_{\mathrm{B}})} + 6H\right)} \times K \tag{4.7}$$

where s_{u0} = peak undrained shear strength (kPa or lb/ft^2); $T_{\max}$ = measured maximum torque from the field (N-m or lb-ft); D = diameter of vane (mm or in); H = height of vane (mm or in); i_{T} = angle of taper at the top of the vane; i_{B} = angle of taper at the bottom of the vane; K = 10^6 for the SI units and 1728 for the FPS unit.

In this section, analysis is performed for a rectangular and a bottom taper vane for both the full model and only rotation model. Figure 4.18 shows the torque–rotation relation up to a rotation of 90º. No significant effect of tapering is found. The calculation of peak undrained shear strength based on Eq. (4.7) is given in Table 4.3. However, it should be noted that the results might vary for anisotropic soil, which has not been investigated here.

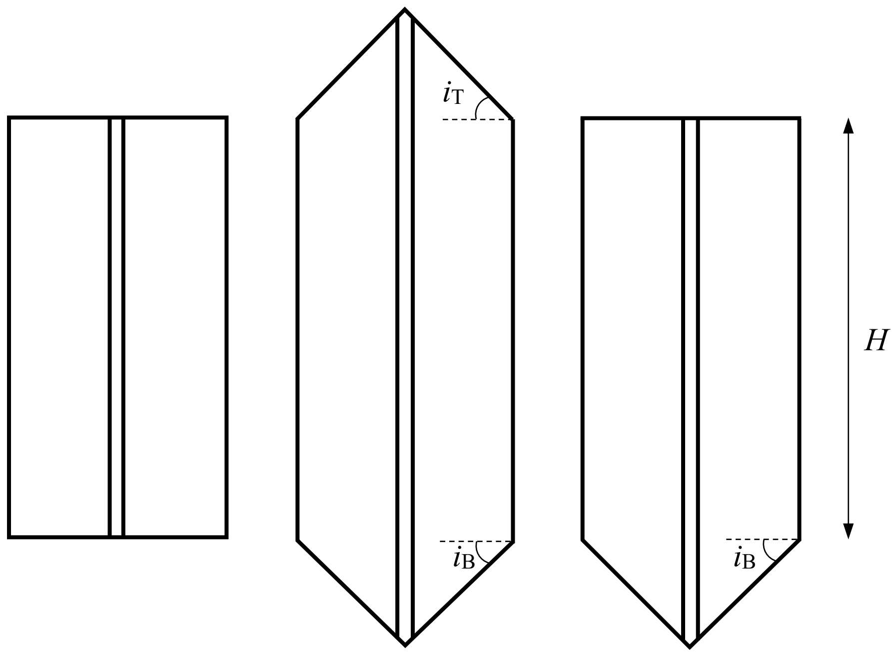

Figure 4.17: Different geometry of field vanes (after ASTM D2573 2018)

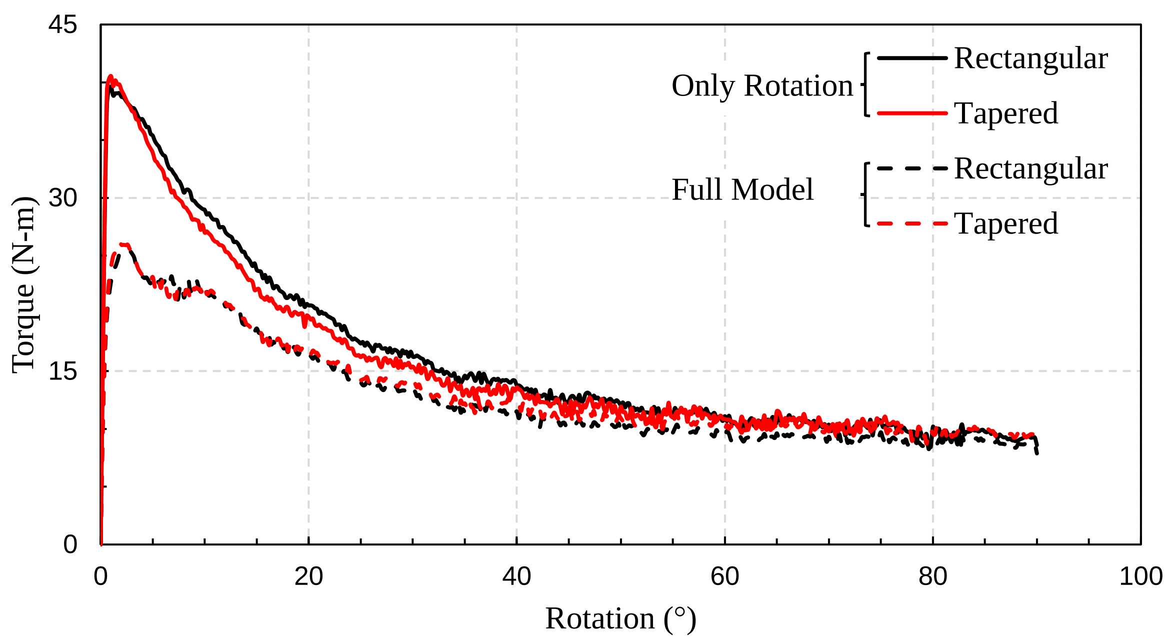

Figure 4.18: Effect of vane tapering on torque–rotation relation

Table 4.3: Peak undrained shear strength for rectangular and tapered vanes

Parameters	Rectangular vane	Bottom taper vane
T_{max} **(maximum torque) (N-m)**	39.60	40.53
D **(mm)**	65	65
H **(mm)**	130	130
i_T **(º)**	0	0
i_B **(º)**	0	45
s_{u0} **(kPa)**	39.34	39.11

Figure 4.19 shows the result of penetration resistance for rectangular and tapered vanes. Again, no significant difference in penetration resistance due to tapering is found.

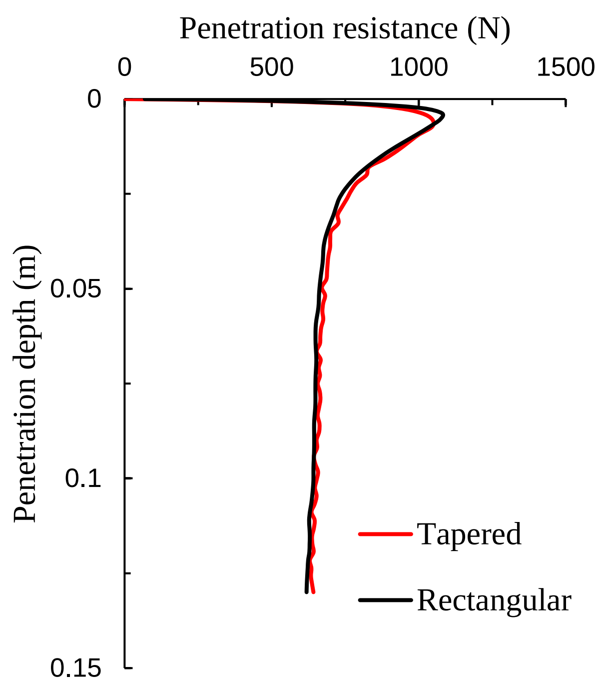

Figure 4.19: Effect of vane tapering on penetration resistance

4.6.11 Mesh sensitivity

Analysis is also performed with a smaller mesh to investigate the effects on normalized penetration resistance (*N*) and equivalent plastic shear strains' ($\varepsilon_{\mathrm{q}}^{\mathrm{p}}$) propagation during vane penetration. The larger mesh (see inset of Fig. 4.20) is used for all the analysis in this chapter, and the smaller mesh (see inset of Fig. 4.20) is used only for the mesh sensitivity analysis. The analysis is performed with a simple elastic perfectly plastic soil model, and the normalized penetration resistance is shown in Fig. 4.20; no significant difference in penetration resistance is found in the result. Figure 4.21 shows the $\varepsilon_{\mathrm{q}}^{\mathrm{p}}$ for the smaller and larger mesh during penetration. Figures 4.21(a)–4.21(c) are for the fine mesh and Figs 4.21(d)–4.21(f) are for the coarse mesh. Firstly, the strain initiates from the face of the vane blade, then it increases continuously in the radial direction, and the strain distribution pattern is quite similar for different mesh sizes. The dense mesh is computationally very expensive. The simulation with the finer mesh took 157 hours, whereas the coarser mesh took 9 hours for 130-mm penetration with a 3.4 GHz Intel Core i7 processor and 16 GB RAM, and was not feasible. That is why a slightly larger mesh is used for all the analysis.

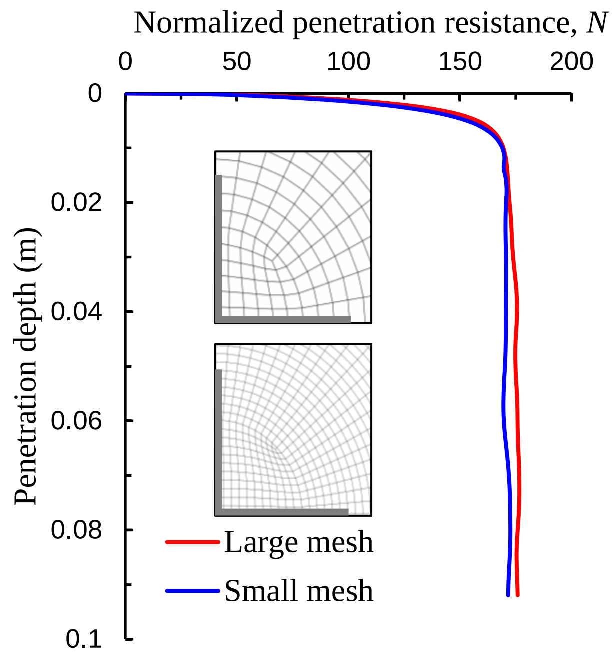

(a)

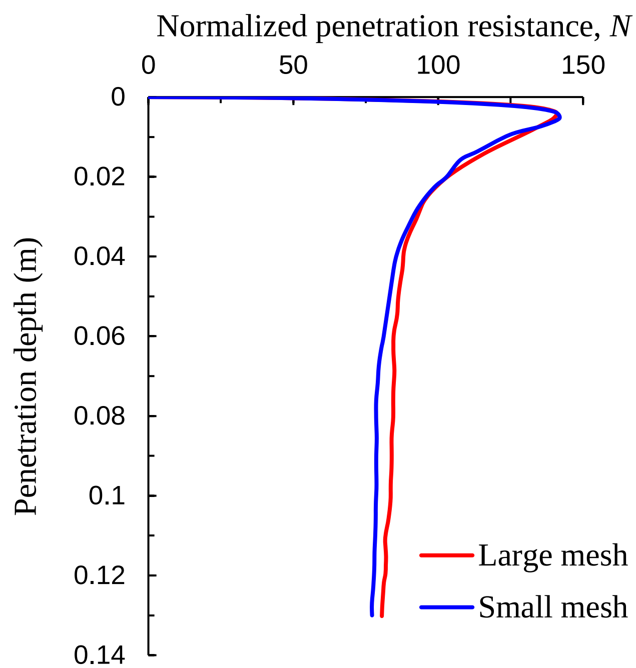

(b)

Figure 4.20: Mesh sensitivity analysis for normalized penetration resistance (a) for elastic perfectly plastic soil model (b) for soil model with strain rate and strain softening effects

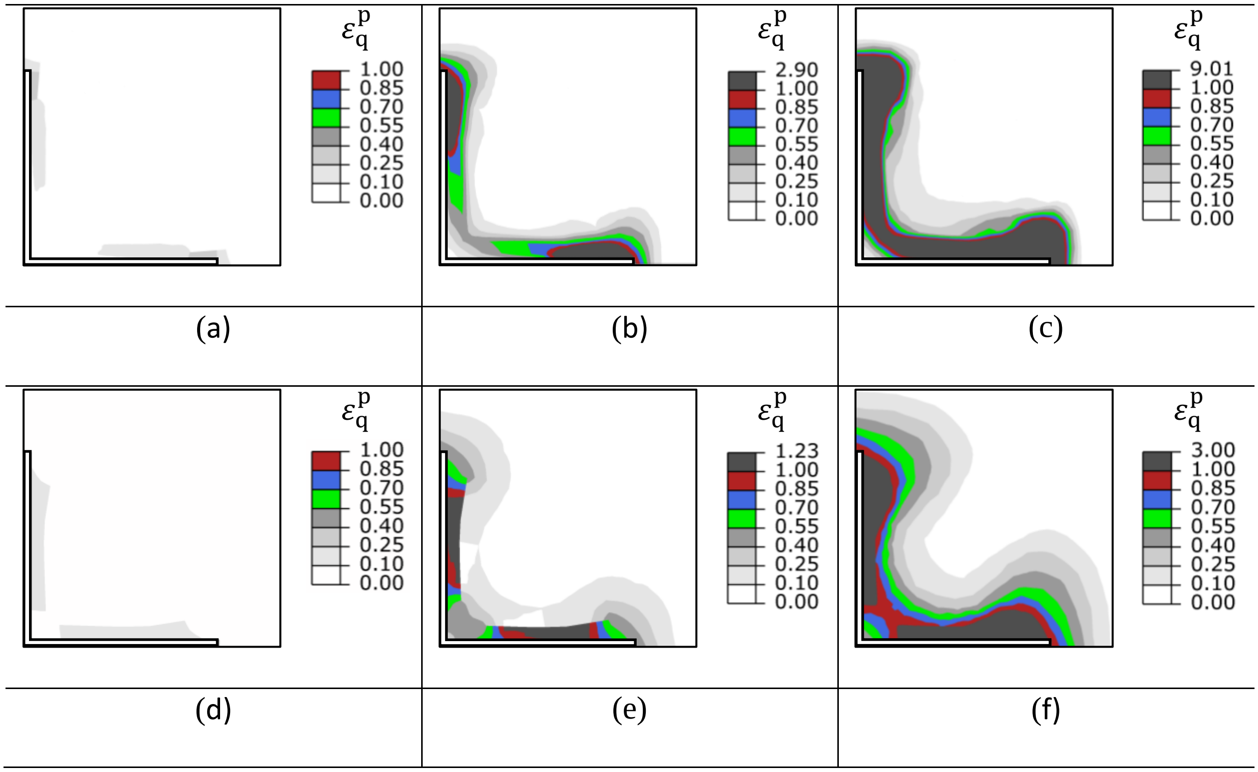

Figure 4.21: Effects of mesh size on strain propagation during vane penetration: (a–c) for fine mesh and (d–f) for coarse mesh

4.6.12 Energy verification

The analysis in the present study has been done using explicit analysis. The solution from the explicit analysis is conditionally stable, so it is recommended to check the relevant energy to ensure the quasi-static condition. In the present study, all the analyses are performed for a quasi-static condition. The penetration velocity (v_p) and rotation rate of the vane should be sufficiently small to minimize the inertia effects. Therefore, considering the computational cost and by ensuring a quasi-static condition to minimize the inertia effects, all the analyses presented in the study are conducted with v_p = 0.15 m/s and 24°/s rotation rate. The rotation rate is a 240 times faster rate than the standard field vane rotation rate 0.1°/s. Therefore, the $\dot{\gamma}$ obtained from FE is divided by 240 to calculate f_2 using Eq. (4.6). All the analysis has been done considering smooth interface conditions. Analysis has also been done with lower penetration velocity and rotation rate, but no significant change is found in the result. So, the penetration and rotation rate have been chosen accordingly to reduce the computational cost without hampering the result. In general, for a quasi-static analysis, the model's kinetic energy should not exceed 5%–10% of its internal energy throughout the simulation (Robert et al. 2020). The internal and kinetic energy variation for the analysis with soil property shown in Table 4.2 is shown in Fig. 4.22, which clearly shows that the quasi-static condition has been satisfied.

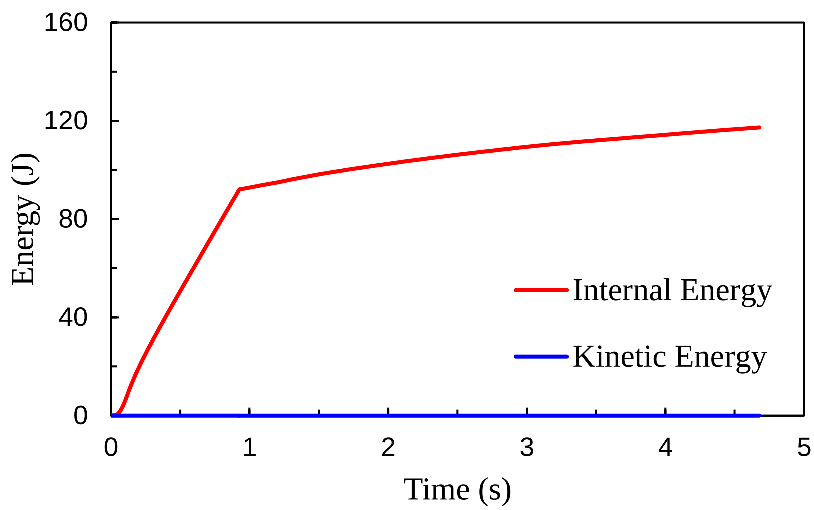

Figure 4.22: Energy variation of the analyses

4.7 Summary

This chapter presents three-dimensional large deformation FE modelling of vane shear tests in soft sensitive clay. Both penetration and subsequent rotation are simulated. Some simulations are performed only for rotation to investigate the effects of penetration. It is found that large deformation FE simulation is needed to understand different aspects affecting the vane shear test results. The penetration of the vane prior to rotation could cause disturbance of the surrounding soil and result in lower undrained shear strength, and the disturbance is more for sensitive clays.

Different factors such as the post-peak strength degradation parameter (δ_{95}), blade thickness (e), and sensitivity contribute to the extent of disturbance caused during vane penetration.

Chapter 5: Conclusions and Future Recommendations

5.1 Conclusions

Proper estimation of soil parameters is necessary for safe and economical geotechnical engineering design. The undrained shear strength of soil is one of the critical design parameters, which can be obtained from field and laboratory tests. Among different field tests, the vane shear test has been widely used for characterizing soft and sensitive clays. Although the test is relatively simple, the interpretation of the results is difficult, as some assumptions have to be made to calculate the undrained shear strength, and several factors influence the results. The interpretation is more complex for highly sensitive clays because of the strain-softening behaviour of the soil. The mechanisms involved and potential sources of uncertainties can be evaluated through numerical modelling.

The present study investigates the soil failure mechanisms during the vane shear test and the factors affecting the test results through large deformation finite element modelling. The Coupled Eulerian-Lagrangian (CEL) approach available in Abaqus FE software is used for numerical simulations. A strain-softening and strain-rate dependent undrained shear strength model is implemented. Analyses are performed for two- and three-dimensional conditions. A set of analyses involves penetration of the vane prior to the rotation, to identify the effects of soil disturbance due to penetration on the measured torque. A comprehensive parametric study is performed to show the effects of key factors. The following conclusions can be drawn from this study:

i) Abaqus CEL can model the complete phenomena involved in the vane shear test, including the progressive formation of failure planes and strain localization.

ii) Failure initiates from the tip of the vane blade where the shear stress is maximum. For sensitive clays, the initially developed failure surfaces form a rounded square-shaped soil block; however, with further rotation, the failure block becomes a circular one after mobilization of peak torque.

iii) Two-dimensional analysis shows a parabolic distribution of shear stress on the horizontal plane. The shear stress distribution remains the same after mobilization of the maximum torque for the elastic perfectly plastic soil model. However, for sensitive clays, further rotation after the peak torque results in a reduction of shear stress distribution.

iv) Three-dimensional analysis shows higher shear stress at the ends than in the middle of the vane at the pre-peak condition and a uniform shear stress distribution at peak and post-peak conditions for the elastic perfectly plastic soil model. However, for sensitive clays, further rotation after the peak results in a reduction of shear stress. The decrease is initially higher at the middle of the vane than at the top and bottom corners, and at remolded conditions, a uniform distribution is observed throughout the height of the vane.

v) Penetration of the vane could significantly disturb the surrounding sensitive clays and thereby reduce the maximum torque during rotation. For the cases analyzed, the penetration-induced disturbance can reduce the maximum torque up to 35% of that obtained without considering penetration effects.

vi) The extent of disturbance due to penetration of the vane depends on several factors. Thicker blades, higher sensitivity, and a faster rate of post-peak strength degradation increase the disturbance of surrounding soil.

5.2 Future recommendations

The numerical analyses presented in this thesis shows some important features that should be taken care of while designing geotechnical structures based on the undrained shear strength measured by the field vane shear test. However, there are some limitations, which may be addressed in future studies.

i) Although the element size scaling rule is used to minimize the mesh size-dependency of the solution, further studies could be performed to develop a better approach.
ii) The effects of anisotropy are not considered in the present study, which could be significant in sensitive clays.
iii) Some advanced experimental study could be performed to quantify the effects of penetration disturbance and the development of a better strain-softening model.
iv) The analyses presented in this thesis are performed for a fixed vane dimension (65-mm diameter and 130-mm height). Analyses could be performed for varying vane dimensions.

References

Aas, G. 1965. "A study of the effect of vane shape and rate of strain on the measured values of in-situ shear strength of clays". *Proceedings, 6th International Conference on Soil Mechanics and Foundation Engineering*, Montreal, 1: 141–145.

Aas, G. 1967. "Vane tests for investigation of anisotropy of undrained shear strength of clays." *Proceedings of the Geotechnical Conference*, Oslo, 1: 3–8.

Ansari, Y., Pineda, J., Kouretzis, G. and Sheng, D. 2014. "Experimental and numerical investigation of rate and softening effects on the undrained shear strength of ballina clay." *Australian Geomechanics Journal*, 49(4): 51–57.

Arman, A., Poplin, J.K. and Ahmad, N. 1975. "Study of the vane shear." In *Proc. of ASCE on In Situ Measurement of Soil Properties*, Raleigh, 1: 93–120.

ASTM D2573 2018. Standard test method for field vane shear test in saturated fine-grained soils. West Conshohocken, Pennsylvania, USA.

Baligh, M. M., Azzouz, A. S. and Chin, C. T. 1987. "Disturbances due to "ideal" tube sampling." *Journal of geotechnical engineering*, 113(7): 739–757.

Benson, D. J. 1992. "Computational methods in lagrangian and eulerian hydrocodes." Comput. Method Appl. M. **99**, No. 2–3, 235–394.

Biscontin, G. and Pestana, J.M. 2001. "Influence of peripheral velocity on vane shear strength of an artificial clay." *Geotechnical Testing Journal*, 24(4): 423–429.

Bjerrum, L. 1972. “Embankments on soft ground.” *Proceedings, ASCE Specialty Conference on Performance of Earth and Earth Supported Structures*, Purdue University, Lafayette, Ind., 1–54.

Boukpeti, N., White, D.J., Randolph, M.F. and Low, H.E. 2012. “Strength of fine-grained soils at the solid–fluid transition.” *Géotechnique*, 62(3): 213–226.

Cadling, L. and Odenstad, S. 1950. “The vane borer-An apparatus for determining the shear strength of clay soils directly in the ground.” *Royal Swedish Geotechnical Institute Proc*, No. 2.

Cerato, A.B., and Lutenegger, A.J. 2004. “Disturbance effects of field vane tests in a varved clay.” In *Proceedings of the 2nd International Conference on Site Characterisation*, Porto, Portugal. Millpress, Rotterdam, the Netherlands. 1: 861–867.

Chandler, R.J. 1988. “The in-situ measurement of the undrained shear strength of clays using the field vane.” In *Vane Shear Strength Testing in Soils: Field and Laboratory Studies*, ASTM STP 1014, A.F. Richards Ed., Philadelphia, 13–44.

Cheng, R. Y. K. 1981. “Effect of shearing strain-rate on the undrained strength of clay.” *Laboratory Shear Strength of Soil*, ASTM STP 740. R. N. Yong and F. C. Townsend, Eds., American Society for Testing and Materials, 243–253.

Chini, M., Wallace, J. F., Rutherford, C. J. and Peschel, J. M. 2015. “Shearing failure visualization via particle tracking in soft clay using transparent soil.” *Geotechnical Testing Journal*., 38, No. 5, 708–724.

Crawford, C. B. (1959). The influence of rate of strain on effective stresses in sensitive clay. In Papers on Soils 1959 Meetings. ASTM International.

Crawford, C. B. (1963). Cohesion in an undisturbed sensitive clay. *Géotechnique*, 13(2), 132–146.

Crawford, C. B. (1965). The resistance of soil structure to consolidation. *Canadian Geotechnical Journal*, 2(2), 90–97.

De Alencar, J.A., Chan, D.H. and Morgenstern, N.R. 1988. “Progressive failure in the vane test.” In *Vane Shear Strength Testing in Soils: Field and laboratory Studies*, ASTM, STP 1014, A.F. Richards Ed., Philadelphia, 150–165.

D’Elia, B., Picarelli, L., Leroueil, S., and Vaunat, J. 1998. “Geotechnical Characterisation of Slope Movements in Structurally Complex Clay-soils and Stiff Jointed Clays.” *Italian Geotechnical Journal*, 32(3): 5–32.

DeGroot, D. J., DeJong, J. T., Yafrate, N. J., Landon, M. M., and Sheahan, T. C. 2007. “Application of recent developments in terrestrial soft sediment characterization methods to offshore environments.” *Offshore Tech. Conf.* Texas. Paper OTC 18737.

Dey, R., Hawlader, B., Phillips, R. and Soga, K. 2015. “Large deformation finite-element modelling of progressive failure leading to spread in sensitive clay slopes.” *Géotechnique*, 65(8): 657–668.

Dey, R., Hawlader, B., Phillips, R. and Soga, K. 2016. “Modeling of large-deformation behaviour of marine sensitive clays and its application to submarine slope stability analysis.” *Canadian Geotechnical Journal*, 53(7): 1138–1155.

Donald, I.B., Jordan, D.O., Parker, R.J. and Toh, C.T 1977. “The vane test–a critical appraisal.” *Proc. 9th Int. Conf. Soil Mech. Found. Enng.*, Tokyo, 1: 81–88.

Dutta, S., Hawlader, B. and Phillips, R. 2015. “Finite element modeling of partially embedded pipelines in clay seabed using coupled eulerian–lagrangian method.” *Canadian* Geotech. J. **52**, No. 1, 58–72.

Einav, I. and Randolph, M. F. 2005. “Combining upper bound and strain path methods for evaluating penetration resistance.” *Int. J. Num. Methods Engineering*, 63(14): 1991–2016.

Einav, I. and Randolph, M. F. 2006. “Effect of strain rate on mobilised strength and thickness of curved shear bands.” *Géotechnique,* 56(7): 501–504.

Flaate, K. 1966. “Factors influencing the results of vane tests.” *Canadian Geotechnical Journal,* 3(1): 18–31.

Fornes, P. and Jostad, H. P. 2017. “Correction factors for undrained LE analyses of sensitive clays.” Landslides in Sensitive Clays, Springer, V. Thakur et al., Eds., 225–235.

Graham, J., Crooks, J. H. A. and Bell, A. L. 1983. “Time effects on the stress–strain behaviour of natural soft clays.” *Géotechnique* 33, No. 3, 327–340.

Griffiths, D. V. and Lane, P. A. 1990. “Finite element analysis of the shear vane test.” *Computers and Structures,* 37(6): 1105–1116.

Griffiths, D. V. and Lane, P. A. 1999. “Slope stability analysis by finite elements.” *Géotechnique*, 49(3): 387–403.

Gupta, T., Chakraborty, T., Abdel-Rahman, K. and Achmus, M. 2016. “Large deformation finite element analysis of vane shear tests.” *Geotechnical and Geological Engineering,* 34(5): 1669–1676.

Gylland, A. S., Jostad, H. P. and Nordal, S. 2012. “Failure geometry around a shear vane in sensitive clays.” In *Proceedings of the 16th Nordic geotechnical meeting,* Copenhagen, 1: 103–110.

Gylland, A. S. 2012. “Material and slope failure in sensitive clays.” PhD thesis, NTNU, Norway.

Gylland, A. S., Jostad, H.P., Nordal, S. and Emdal, A. 2013. "Micro-level Investigation of the in Situ Shear Vane Failure Geometry in Sensitive Clay." *Géotechnique,* 63(14): 1264–1270.

Gylland, A. S., Thakur ,V. and Emdal, A. 2016. "Extended interpretation basis for the vane shear test." In *Proc., 17th Nordic Geotechnical Meeting, Challenges in Nordic Geotechnic* 25–28 May, 233–240. Reykjavik, Iceland: Icelandic Geotechnical Society

Henneseid, O. 2018. "A numerical investigation of strain-softening in soft clay for a modelled shear vane." Master's thesis, NTNU, Norway.

Hvorslev, M. J. 1949. "Subsurface exploration and sampling of soils for civil engineering purposes." Waterways Experimental Station, Vicksburg, Miss., USA.

Islam, N., Hawlader, B., Wang, C. and Soga, K. 2019. "Large deformation finite element modelling of earthquake-induced landslides considering strain-softening behaviour of sensitive clay." *Canadian* Geotech. J. **56**: 1003–1018.

Karlsrud, K. and Hernandez-Martinez, F. G. 2013. "Strength and deformation properties of Norwegian clays from laboratory tests on high-quality block samples." *Canadian Geotechnical Journal,* 50(12): 1273–1293.

Karmaker, R. and Hawlader, B. 2018. "Modeling of pile stabilized clay slopes using a large deformation finite-element method." *7th Canadian Geohazards Conference,* paper no-155.

Karmaker, R., Hawlader, B. and Wang, C. 2019. "Finite element modeling of jacked piles in clay and loose sand." *72nd Canadian Geotechnical Conference,* St. John's, NL, Canada, paper no-436.

Keentok, M., Milthorpe, JF. And O'Donovan, E. 1985. "On the shearing zone around rotating vanes in plastic liquids: theory and experiment." *Journal of Non-Newtonian Fluid Mech.,* 17: 23–35

Kimura, T. and Saitoh, K. 1983. “Effect of disturbance due to insertion on vane shear strength of normally consolidated cohesive soils.” *Soils and Foundations*, 23(2): 113–124.

Kouretzis, G., Pineda, J., Krabbenhøft, K. and Wilson, L. 2017. “Interpretation of vane shear tests for geotechnical stability calculations.” *Canadian Geotechnical Journal*, 54(12): 1775–1780.

Kvalstad, T.J., Andresen, L., Forsberg, C.F., Berg, K., and Bryn, P. 2005. “The Storegga slide: evaluation of triggering sources and slide mechanisms.” *Marine and Petroleum Geology*, 22(1-2): 245–256.

Ladd, C. C. 1991. “Stability evaluation during staged construction.” *J. Geotech. Engrg.*, 117(4): 540–615.

La Rochelle, P. and Lefebvre, G. 1971. “Sampling disturbance in champlain clays.” In *Sampling of Soil and Rock*, ASTM STP 483, American Society for Testing and Materials, 143–163

La Rochelle, P., Roy, M. and Tavenas, F. 1973. “Field measurements of cohesion in champlain clays.” *Proceedings of the 8th International Conference on Soil Mechanics and Foundation Engineering*, Moscow, 1: 229–236.

Locat, A., Jostad, H.P. and Leroueil, S. 2013. “Numerical modeling of progressive failure and its implications for spreads in sensitive clays.” *Canadian Geotechnical Journal*, 50(9): 961–978.

Locat, A., Leroueil, S., Fortin, A., Demers, D., and Jostad, H. P. 2015. “The 1994 landslide at Sainte-Monique, Quebec: geotechnical investigation and application of progressive failure analysis.” *Canadian Geotechnical Journal*, 52: 490–504.

Lunne, T., Berre, T., Andersen, K.H., Strandvik, S., and Sjursen, M. 2006. “Effect of sample disturbance and consolidation procedures on measured shear strength of soft marine Norwegian clays.” *Canadian Geotechnical Journal*, 43(7): 726–750.

Lunne, T., and Andersen, K. H. 2007. “Soft clay shear strength parameters for deepwater geotechnical design.” In *Proc. of the 6th Int. Off. Site Investigations and Geotechnics Conf*., London, UK., 151–176.

Martinez, A., and Frost, J. D. 2017. “Numerical comparison of vane shear and torsional interface shear test.” In *Proc., 19th Int. Conf. Soil Mechanics and Geotechnical Engineering*, London: International Society for Soil Mechanics and Geotechnical Engineering.

Matsui, T. and Abe, N. 1981. “Shear mechanisms of vane test in soft clays.” *Soils and Foundations*, 21(4): 69–80.

Menzies, B.K. and Merrifield, C.M. 1980. “Measurements of shear stress distribution on the edges of a shear vane blade.” *Géotechnique*, 30(3): 314–318.

Ortigão, J. A. R. and Collet, H. B. 1988. “Errors caused by friction in field vane tests.” In *Vane Shear Strength Testing in Soils: Field and Laboratory Studies*, ASTM STP 1014, A.F. Richards Ed., Philadelphia, 104–116.

Pérez-Foguet, A., Ledesma, A. and Huerta, A. 1999. “Analysis of the vane test considering size and time effects.” *International Journal for Numerical and Analytical Methods in Geomechanics*, 23(5): 383–412.

Qiu, G. and Grabe, J. 2012. “Numerical investigation of bearing capacity due to spudcan penetration in sand overlying clay.” *Canadian Geotechnical Journal*, **49**, No. 12, 1393–1407.

Quinn, P. E., Diederichs, M. S., Rowe, R. K., and Hutchinson, D. J. 2011. “A new model for large landslides in sensitive clay using a fracture mechanics approach.” *Canadian Geotechnical Journal*, 48(8): 1151–1162.

Randolph, M.F., White, D.J. and Yan, Y. 2012. “Modelling the axial soil resistance on deep-water pipelines.” *Géotechnique*, 62(9): 837–846.

Rismyhr, K. 2017. “Effect of anisotropy, strain rate and progressive failure in numerical simulations of the shear vane test.” Master's thesis, NTNU, Norway.

Robert, D. J., Britto, A. and Setunge, S. 2020. “Efficient approach to simulate soil-pipeline interaction.” *J. Pipeline Syst. Eng. Pract*. 11 (1): 04019046.

Roy, M. and Leblanc, A. 1988. “Factors affecting the measurements and interpretation of the vane strength in soft sensitive clays.” In *Vane Shear Strength Testing in Soils: Field and Laboratory Studies,* ASTM STP 1014, A.F. Richards Ed., Philadelphia, 117–128.

Selänpää, J., Di Buò, B., Länsivaara, T., and D’Ignazio, M. 2017. “Problems related to field vane testing in soft soil conditions and improved reliability of measurements using an innovative field vane device.” *In* Landslides in sensitive clays, Edited by Springer, the Netherlands, 109–119.

Silvestri, V., and Aubertin, M. 1988. “Anisotropy and in-situ vane field vane tests tests.” In *Vane Shear Strength Testing in Soils: Field and Laboratory Studies,* ASTM STP 1014, A.F. Richards Ed., Philadelphia, 88–103.

Skempton, A. W. 1948. “Vane tests in the alluvial plain of the River Forth near Grangemouth.” *Géotechnique,* Vol. 1, No. 2, 111–125.

Stark, T. D. and Eid, H. T. 1994. "Drained residual strength of cohesive soils." *J. Geotech. Engng Div.*, ASCE 120, No. 5, 856–871.

Stark, T., and Contreras, I.A. 1996. "Constant volume ring shear apparatus." *Geotechnical Testing Journal*, 19(1): 3–11.

Taiani, B., Ferlisi, S., and Gylland, A. S. 2016. "Numerical analyses of field vane tests on soft clays." 1st IMEKO TC-4 International Workshop on Metrology for Geotechnics Benevento, Italy.

Tavenas, F., Flon, P., Leroueil, S. and Lebuis, J. 1983. "Remolding energy and risk of slide retrogression in sensitive clays." In *Proc. of the Symposium on Slopes on Soft Clays*, J. Lindgren, Ed., Linköping, Sweden, 17: 423–454.

Thakur, V. 2007. "Strain localization in sensitive soft clays." Doctoral thesis, Norwegian University of Science and Technology, Trondheim, Norway.

Thakur, V., Jostad, H.P., Kornbrekke, H.A. and Degago, S.A. 2014. "How well do we understand the undrained strain softening response in soft sensitive clays?" In *Advances in natural and technological hazards research, landslides in sensitive clays* — from geosciences to risk management. Edited by J.-S. L'Heureux, A. Locat, S. Leroueil, D. Demers, and J. Locat. 36: 291–303.

Thakur, V., Gylland, A.S., Degago, S.A., Oset, F. and Sandven, R. 2015. "In-situ determination of disintegration energy for soft sensitive clays." *Proc. of GEOQuébec2015*, Québec, Canada.

Torstensson, B. A. 1977. "Time-dependent effects in the field vane test." *International Symposium on Soft Clay*, Bangkok, 387–397.

Veneman, P.L. and Edil, T.B. 1988. “Micromorphological aspects of the vane shear test.” In *Vane Shear Strength Testing in Soils: Field and Laboratory Studies*, ASTM STP 1014, A.F. Richards, Ed., ASTM, Philadelphia, 182–190.

Wang, C., Hawlader, B., Islam, N. and Soga, K. 2019. “Implementation of a large deformation finite element modeling technique for seismic slope stability analyses.” *Soil Dyn. Earthq. Eng*. 127, 105824.

Wang, C., Hawlader, B., Perret, D. and Soga, K. 2020. “Effects of geometry and soil properties on type and retrogression of landslides in sensitive clays.” *Géotechnique*, 1–15.

Wiesel, C. E. 1973. “Some factors influencing in situ test results.” *Proceedings, 8th International Conference on Soil Mechanics and Foundation Engineering*, Moscow, U.S.S.R., 2: 475–479.

Wilson, N. E. 1964. “Laboratory vane shear tests and the influence of pore-water stresses.” *Laboratory shear testing of soils*, ASTM SPT No. 361, 377–385.

Wroth, C.P. 1984. “The interpretation of in situ soil tests.” *Géotechnique*, 34(4): 449–489.

Yerro Colom, A. 2015. “MPM modelling of landslides in brittle and unsaturated soils.” PhD thesis, Polytechnic University of Catalonia.

Zhu, H. and Randolph, M. F. 2011. “Numerical Analysis of a Cylinder Moving Through Rate-dependent Undrained Soil.” *Ocean Engineering*, 38(7): 943–953.